

國立交通大學

光電工程研究所

博士論文

The logo of National Central University (NCTU) is a circular emblem with a gear-like border. Inside the circle, there is a stylized figure holding a torch, and the year '1896' is inscribed at the bottom. The text '國立中央大學' is written around the top inner edge of the circle.

液晶透鏡於行動裝置之成像應用研究
**Liquid Crystal Lenses for Imaging Application in
Mobile Devices**

研究生：廖凌嶢

指導教授：黃乙白

中華民國一百年九月

液晶透鏡於行動裝置之成像應用研究

**Liquid Crystal Lenses for Imaging Application in
Mobile Devices**

研究生：廖凌曉

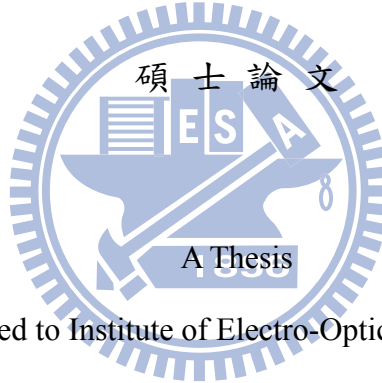
Student : Lin-Yao Liao

指導教授：黃乙白

Advisor : Yi-Pai Huang

國立交通大學

資訊科學系



Submitted to Institute of Electro-Optical Engineering
College of Electrical Engineering and Computer Engineering

National Chiao Tung University

for the Degree of

Doctor of Philosophy

in

Department of Photonics

September 2011

Hsinchu, Taiwan, Republic of China

中華民國一百年九月

液晶透鏡於行動裝置之成像應用研究

學生：廖凌嶢

指導教授：黃乙白

國立交通大學光電工程學系（研究所）博士班

摘要

行動手持裝置已成為日常生活中不可缺少的電子用品，而手持裝置裝中的攝像鏡頭，往往成為在執行攝影、影像辨識、電腦視覺以及影像溝通時重要元件。在諸多的光學元件中，液晶透鏡由於擁有電控式變焦以及體積小等特點，泯除傳統機械式移動的特性，充分展現應用於體積輕巧的行動手持裝置優勢。然而，液晶透鏡目前仍無法克服的缺點，諸如較差的影像品質、反應速度過慢以及不切實際的高驅動電壓，都大大地降低液晶透鏡的實用性。

在本論文中，我們首先針對液晶轉角不易精準控制的問題，提出多電及控制結構，藉由多電擊的高控制自由度，可更精準控制液晶層轉角分布，以提高聚焦品質。在此項研究項目中，我們也實現了針對不同焦距給定不同電壓組的最佳化控制。第二，我們提出突破性的液晶透鏡控制結構—漸變式驅動液晶透鏡，在此項目中，我們應用高電阻層做為控制電極，不但能夠充分利用施加之電場，亦可創造出漸變性的電壓分布，一方面大大將控制電壓從原本的幾十伏特甚至上百伏特降低至五伏特以內，搭配爾後本團隊發展出來針對液晶透鏡的加強驅動方式，將原本大於三十秒以上的反應速度將低至六百毫秒內，這對液晶透鏡發展領域無疑是突破性的發展，再者，由於電阻及液晶層猶如一層 RC 電路，所以頻率上的可控制性，亦延續了先前多電極控制這種高自由度的控制概念，來提升聚焦品質。在論文最後，我們展示了結合所有成果於手機鏡頭的成像應用，實現了快速、低電壓驅動的液晶透鏡之近距離攝影(近拍)成果。

Liquid Crystal Lenses for Imaging Application in Mobile Devices

Doctoral Student: Lin-Yao Liao

Advisor: Dr. Yi-Pai Huang

Institute of Electro-Optical Engineering

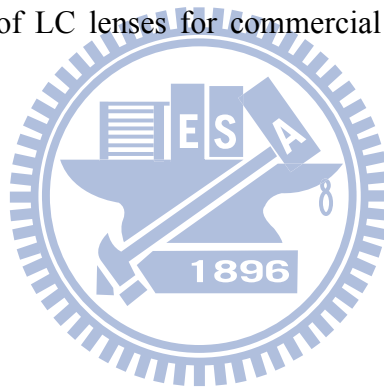
National Chiao Tung University

Abstract

Mobile devices become necessary products for daily life's use in recent years. When perform functions of photography, phantom identification, computer vision, and image communications, lens-heads play an important role to deal with the basic function of imaging. Liquid crystal (LC) lens has unique properties such as electrically tunable focal length. Since there are no moving mechanical parts, LC lens is smaller and lighter than conventional tunable glass lenses. In mobile devices, LC lens can directly combine with mobile lens-module in front of the lens-head, and easily perform auto-focusing (AF) function by driving appropriate voltage to focus objects at different distances. However, inferior optical quality, slow focusing time, and high driving voltage are current major issues of LC lenses' study. These drawbacks make LC lenses unpractical and unfeasible in real usage for mobile devices.

In this thesis, we first started from Multi-electrode Driven LC lens (MeDLC lens) to precisely control profiles of LC lens for different focal length. By the multi-electrode, we demonstrate highly controlled freedom for modifying the index distributions for each focal length to obtain similar and superior focusing profiles. In the second part, Gradient-driven LC lens (GDLC lens) was proposed to intrinsically improve the driving efficiency. We utilized a

resistance layer connected with electrodes as the control layer. The benefit of this structure is that the applied electric field can be efficiently employed and a gradient distribution in voltage can be produced. By GD-LC lens, the driving voltage typically higher than tens root-mean-square voltages was reduced down to less than $5V_{\text{rms}}$ for imaging 6cm closed objects. In the third part, Over-drive (OD) method for LC lenses was proposed to investigate focusing behavior. A switching operation in this method according to the focusing profile was used to reduce the focusing time. Performing with GDLC lens, we yielded 600msec focusing time by a LC lens with 60um cell gap and 2mm aperture size for capturing the 6cm objects. By combining these results, we not only dramatically improved the performance for current LC lenses but also to break through the issues of the current studies. Our outcome, furthermore, make the use of LC lenses for commercial mobile devices more feasible and practical.



誌 謝

回想起第一次與指導教授 黃乙白老師會面，約的居然是在 田仲豪老師的辦公室，當時黃老師還是新進教師，沒有自己的地盤，只能在下班後趕往交大與我面談，也因此展開了研究所的生涯。但回顧起博士班的開始，應該是剛到實驗室的第一天，當初黃老師詳盡地介紹實驗室，也見識到了 謝漢萍老師不怒而威的霸氣，而後從 韋安琪學姊口中知道 黃乙白老師也是實驗室直升的博班生，於是也動起了直升博班的念頭，但真正的臨門一腳，是在一次實驗室的 meeting 中見到 楊柏儒學長以流利的英語跟大夥報告著他的研究成果，心中驚嘆：哇～博士班果然要接受不同於凡人的訓練啊。抱持著”吃得苦中苦”的心態，於是踏入了博士班這趟旅程。

剛進入這個大家庭，起初跟著 林芳正學長學習做 HDR 的相關題目，回想起那段成天跑 AUO 開會，開完會連同 廖振宇學長到附近的麵館吃麵的日子，已腸腸伴隨著 汪德美主管給予的壓迫帶來的愁容，雖是研究生卻有如工程師一般。最後，大夥的成果發表成了論文，也因為這篇論文，我第一次到了美國，到了洛杉磯，到了拉斯維加斯，研究所的初體驗是如此精彩而充實。

正式進入博士班以後，著手於液晶透鏡的研究，這是個有趣而不那麼容易的的題目。我開始進到無塵室，展開沒日沒夜的製程工作，泛黃的燈光灑在冰冷的機台，靜默的工作區偶爾夾雜著擾人的機器聲響，心裡想著，這彷彿不是我想像中的博士生涯，抗拒的心理也隨之而來。就在萬念俱灰之際，慶幸地，許多努力的學弟妹們一起加入奮鬥，讓我們困難的工作出現了轉機，無論是李俊賢學弟、陳致維學弟、沈拓江學弟、以及後來紛紛加入的林裕閔學弟、黃怡菁學妹、陳博詮學弟等，都努力的投入，沒有你們，也許我早早就撐不下去了。

但最讓我嘗到研究的甜美成果的，無非是和謝博元(博六)學弟以及陳禹辰(小發特)學弟所組成的三人 Group 的研究期間吧，博六的細心謹慎加上小發特的大鳴大放，著實讓我們的研究成果產生了極大的火花，短短幾年的研究，成果已經趕上了國際知名團隊，

甚至超越。永遠忘不了第一片鍍上高阻層液晶透鏡聚焦成像的那一天，也忘不了大夥常常準備到半夜，為了隔天某某國際大咖將親臨觀賞我們的展示，諸多人的努力與配合，成就了那不到 1 秒的快速聚焦！

如今我在亞利桑那光學中心，寫下這份誌謝，心中萬分的感激與感嘆，就是這四五年之間，讓身邊的人事物以及所見所聞如此不同，感謝奶奶以及家人們長期的支持，感謝我的未婚妻朱苑爾的陪伴，感謝好友林柏瑋一起到香港看 coldplay，學姊 蔡韻竹、學長 許精益常在 meeting 時一起嘴砲，以及資格考三人組的另外兩員猛將簡上杰、蔡武衛的一起衝刺並在資格考結束當天衝去吃羊肉爐，學長 林淇文在實驗上的大力幫忙，更要感謝實驗室所有學長姐、學弟妹的指教，沒有你們的幫忙，我無法完成這本論文，最最最重要的，要感謝我的指導教授黃老師，感謝您在背後無限的奧援、信任與支持。謝謝！！



常常懷念起謝老師說的：「技術方面的學習都不是大問題，重要的是要把英文學好。」現在真的深深體會這句話，也唯有充分的溝通，才能讓自己”Presentable”吧！

Contents

CHAPTER 1. INTRODUCTION	1
1.1 TUNABLE-FOCUS LENSES	1
1.2 LC LENSES.....	3
1.3 COMPARISON OF SINGLE-TUNABLE LENSES	7
1.4 LENS-HEADS IN MOBILE DEVICES.....	8
1.4.1 Auto-focusing (AF)	9
1.4.1.1 Voice Coil Motor (VCM)	9
1.4.1.2 Extended Depth-of-field (EDoF)	11
1.4.1.3 LC Lenses	12
1.4.2 Optical Zoom	13
1.5 MOTIVATION AND OBJECTIVE OF THIS THESIS.....	15
CHAPTER 2. THEORY AND PRINCIPLE OF LC LENSES	17
2.1 INTRODUCTION TO LIQUID CRYSTALS	17
2.2 ENERGIES IN LC CELLS.....	18
Elastic Energy	19
Electric Field.....	20
Anchoring Effect	21
2.3 OPTICAL PRINCIPLE OF LC LENSES.....	22
CHAPTER 3. MULTI-ELECTRODE DRIVEN LC LENS	26
3.1 INTRODUCTION	26
3.2 MULTI-ELECTRICALLY DRIVEN LIQUID CRYSTAL LENS (MEDLC LENS).....	27
3.2.1 MeDLC Lens.....	27
3.2.2 Optimization	28
3.3 EXPERIMENTAL RESULTS	31
3.4 DISCUSSION - GRATING STRUCTURE OF MED-LC LENS.....	34
3.5 CONCLUSION.....	36
CHAPTER 4. GRADIENT DRIVEN LIQUID CRYSTAL LENS EXHIBITING ULTRA-LOW OPERATING VOLTAGES	37
4.1 INTRODUCTION	37
4.2 GRADIENT DRIVEN LIQUID CRYSTAL LENS (GD-LC LENS)	40
4.2.1 Concept.....	40
4.2.2 Structure and Principles.....	41

4.3	EXPERIMENTAL RESULTS	46
4.4	PHASE RETARDATION OF CONVEX AND CONCAVE MODES	49
4.5	CONCLUSION.....	52
CHAPTER 5. OVER-DRIVE METHOD FOR FAST FOCUSING LIQUID CRYSTAL LENS.....		53
5.1	INTRODUCTION	53
5.2	OVER-DRIVE METHOD FOR LC LENS	54
5.3	3-DIMENSIONAL IMAGING AND ANALYSIS FOR LC LENSES BY FLUORESCENCE CONFOCAL POLARIZING MICROSCOPY.....	58
5.3.1	3-D Imaging of LC lenses.....	59
5.3.2	Phase retardation	63
5.4	EXPERIMENTS AND OPTIMIZATION OF OVER-DRIVING VOLTAGES	66
5.5	CONCLUSION.....	69
CHAPTER 6. AF IMAGING WITH SPHERICAL GD-LC LENS.....		70
6.1	INTRODUCTION	70
6.2	FABRICATION.....	70
6.3	OPTICAL PROPERTIES OF SGD-LC LENS.....	72
6.4	AF EXPERIMENT WITH SGD-LC LENS.....	75
6.4.1	Experimental Principle.....	75
6.4.2	Results	79
	Resolution Test Chart for different focal length.....	79
	AF test	81
	MTF measurement.....	82
6.5	CONCLUSION.....	84
CHAPTER 7. CONCLUSION AND FUTURE WORK.....		85
7.1	CONCLUSION.....	85
7.1.1	Multi-electrode Driven LC Lens (MeDLC Lens).....	85
7.1.2	Over-driving (OD) Method for LC lenses.....	86
7.1.3	Gradient Driven Liquid Crystal Lens (GD-LC lens).....	87
7.2	FUTURE WORK	89
7.2.1	Optical design for LC lens.....	89
7.2.2	Polarizer free LC lens.....	90
7.2.3	Optical Zoom.....	91
REFERENCE.....		94

Figure Captions

Figure 1-1 (a)The liquid lens employs the oil-water surface and electrically control the surface shape. (b) The liquid lens mechanically controlled the membrane shape to focus the light.	2
Figure 1-2 The world first LC lens proposed by Prof. Susumu Sato.....	3
Figure 1-3 The typical structures controlled by inhomogeneous field with an inhomogeneous layer on (a) short focusing state, and (b) long focusing state.	4
Figure 1-4 The typical structures controlled by inhomogeneous field with an homogeneous LC layer.	4
Figure 1-5 Two of the most general homogeneous LC Lenses, (a) the structure with external electrodes, and (b) the structure with internal electrodes utilizing electrical fringe field of the electrodes to generate a gradient variation in phase retardation. The low freedom of electrical control limits the range of focusing.	6
Figure 1-6 Structure of conventional VCM actuator.	10
Figure 1-7 The focusing mechanism of VCM approach.	10
Figure 1-8 The principle of EDoF method.	12
Figure 1-9 The mechanism of LC lens used for AF function in mobile device.	13
Figure 1-10 The structure of LC zoom lens and conventional zoom lens.	15
Figure 2-1 The phases of LCs under different range of temperature	18
Figure 2-2 The three possible forms of deformation, (a) splay, (b) twist, and (c) bend, of nematic LCs.....	19
Figure 2-3 LC directors, n , which indicates the directions of LC molecules in Cartesian coordinate	20
Figure 2-4 The field was decomposed into two perpendicular directions along n and perpendicular to n	21
Figure 2-5 Three of the common alignment methods, (a)perpendicular, (b)anti-parallel, and (c)parallel alignments for LC cells.....	22
Figure 2-6 The ordinary and extraordinary lights travelling in the LC material and extraordinary lights see the different indices which are dependent to the included angles between the incident light and the optical axis of LC molecules.	23
Figure 2-7 The wavefront focusing of LC lens.	24
Figure 2-8 The diagram of LC lens considered as a GRIN lens for analyzing the focusing.....	25
Figure 3-1 The focusing profile of the homogeneous LC lens with different	

focal length, 4cm and 10cm. The focusing profiles are different.....	27
Figure 3-2 MeD-LC Lens with large number of electrodes. MeD-LC Lens utilized the arrangements of driving voltages to finely control the LC orientation, and yielded a wide range of superior focusing.....	28
Figure 3-3 The profile of Δn_l generated by MeD-LC Lens and an ideal lens for around 3.5cm focal length. The ideal lens represented by a parabolic curve is compared with that of MeD-LC, presenting a deviation from the ideal case.	30
Figure 3-4 The quantified errors, E , representing the deviation of the results of MeD-LC from the parabolic curve, is utilized to optimize the number of electrodes for MeD-LC Lenses.	30
Figure 3-5 The optimized driving voltages for 9-electrode MeD-LC Lens in convex applications. The symmetrical arrangement of each driving voltage was adjusted for particular focal length. In convex MeD-LC Lens, marginal voltages are higher than central voltages to form convex-like phase retardation.....	32
Figure 3-6(a) Cylindrical MeDLC Lens measured by CCD sensor at a distance of corresponding focal length (EF), and (b) the focusing profile were compared with two conventional LC lens. As the results shows, two conventional LC lenses only yielded a particular range of focusing. On the other hand, the multi-electrode of MeDLC Lens served the LC layer optimized phase retardation for each focal length and a wide range of focusing.....	33
Figure 3-7(a) The focusing profile of MeD-LC Lens without coating PMMA and (b) coating with PMMA for suppressing the intensity of side lobes. The large side lobes of focusing profile due to the grating structure of MeD-LC raised undesired cross-talk effect. The coating material with approximate reflective index can effectively reduce the side lobes.....	35
Figure 4-1 The simulations of electric field for four kinds of homogeneous LC lenses including internal and external electrodes with two and multi controls.	39
Figure 4-2 The structure of internal continuous electrode performs a smooth gradient electrical field and can conserve the electrical energy inside the LC layer. The simulation work was done by using 2DimMOS.	40
Figure 4-3 The testing device of LC cell with high resistance layer connected by two controlling electrodes.	41
Figure 4-4 The results of interference pattern of the testing device driven by different operating voltages, (a) $\Delta V=3$ Vrms, (b) $\Delta V=3.6$ Vrms, and (c)	

$\Delta V=5V_{rms}$. The LC cell was design by 60 μm cell gap driven by the two controllable electrodes with 2mm separation.	41
Figure 4-5 The configuration of GD-LC Lens. The structure with 2mm lens aperture and 60 μm anti-parallel LC cell gap was constructed by combining triple internal electrodes with the high resistance layer.....	42
Figure 4-6 The schematic of resistance of the controlled high R layer.	43
Figure 4-7 The schematic of induced polarizations by z direction electric field.	44
Figure 4-8 The simulated voltage distribution and corresponding phase retardations, the region which applying voltage under threshold value cannot distorted the LC directions. In other words, the model only considering the configuration as transmission line and driven by uniform electric may miss the accuracy of complete electrical field simulations.	45
Figure 4-9 The focusing profile of GD-LC Lens driven at (a) $V=0$, and (b) $V=2.35V_{rms}@2.4kHz$ for 5cm focal length.	47
Figure 4-10 The relationship of focal length to operating voltage and frequency of GD-LC Lens.	48
Figure 4-11 The focusing profiles of GD-LC lens at different focal length from 2.5cm to 10cm controlled by voltage and frequency.	49
Figure 4-12 The phase retardation of GD-LC Lens operated in (a) convex, and (b) concave modes. By the different operating arrangement, both convex and concave lenses were achieved.	51
Figure 5-1 (a) General structure of homogeneous LC Lens driven by marginal over-drive voltages, and (b) The curve of focusing response time to normalized intensity on CCD sensor for a particular focal length. The over-drive voltages yielded a initial focusing as shown the first peak.	55
Figure 5-2 The variation of focusing intensity with time driven by OD method and general driving was measured by CCD sensor.	57
Figure 5-3 The results of OD method by different switching time. The switching at the time approximated to the initial focusing can obtained the shortest focusing time.	57
Figure 5-4 The diagram of the fluorescence confocal polarizing microscopy system.	59
Figure 5-5 The setup of measure by FCPM.	60
Figure 5-6 (a) The scanned result before applying driving voltage, and (b) ~ (d) that of scanned layers after driving.	60
Figure 5-7 The contours indicating the refractive index and LC tilt angle of each layer.	62

Figure 5-8 The 3D diagram of LC profile.	63
Figure 5-9 The phase retardation calculated by (a) FCPM method and (b) measured by fringing pattern approach.....	65
Figure 5-10 The cross sections of phase retardation for 5 cm focal length by FCPM method and fringing pattern approach, as well as the ideal curve.	66
Figure 5-11 The result of relation between focusing time and OD voltages. Improvement was saturated as the voltage was larger than 65Vrms.	67
Figure 5-12 (a)The structure of GD LC lens with multi-electrically control, and (b) the relation of response time to over-drive voltages.	69
Figure 6-1 The electrode patterns of (a) cylindrical and (b) spherical GD-LC lens.	71
Figure 6-2 The double-layer electrode structure of sGD-LC lens employing an insulator to separate the electrode layers.	72
Figure 6-3 The structure of GD-LC lens.	72
Figure 6-4 The focusing profile of sGD-LC lens driven by 3.3Vrms at 4.22 kHz.	73
Figure 6-5 The focusing profiles of sGD-LC lens from focal length, 7cm~15cm.	74
Figure 6-6 The relationship between of focal length to operating voltage and frequency of sGD-LC Lens.	74
Figure 6-7 The schematic of lens-system with and without LC lens.	76
Figure 6-8 (a)The setup of lens-system and (b) the experimental arrangement.	77
Figure 6-9 (a)The function of control signal and (b) the equipmet.	78
Figure 6-10 The test chart placed in front of sGD-LC lens at the distance corresponding to the focal length.	79
Figure 6-11 The results of test chart for different focal length.....	80
Figure 6-12 The AF experiment and the toys placed at different distances. ...	81
Figure 6-13 (Video) The AF result of four toys at different distances, and OD result focusing from the farrest toy to the nearest one.	82
Figure 6-14 MTF of sGD-LC lens measured by ImageMaster® HR, Trioptics.	83
Figure 7-1 The relations of the topics for each issue	85
Figure 7-2 The change of LC lens structure from conventional single control to multi-control freedom.	86
Figure 7-3 (a) The operation of OD method and (b) the focusing transition by OD method.	87

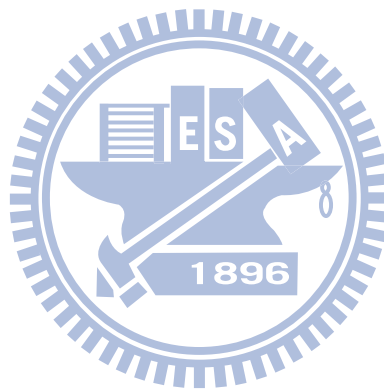
Figure 7-4 The dramatic improvement in driving voltage and focusing time with GD-LC lens combined with the volt. & freq. dual-control and OD method.88

Figure 7-5 The relation of lens design tool for LC lens design90

Figure 7-6 The concept of DIP for polarizer free LC lens.....91

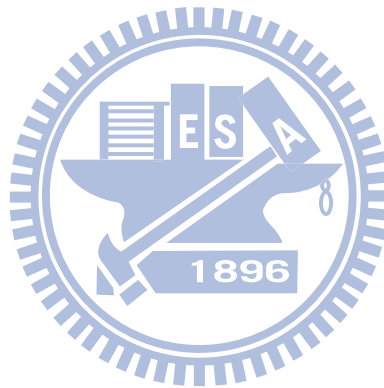
Figure 7-7 The schematic of LC zoom lens92

Figure 7-8 The variation of lens power, K , changed by LC lens power, K_1 and K_2 93



List of Tables

Table 1 The comparison of LC lenses proposed by the world leading groups.	7
Table 2 The spec. list of conventional VCM.....	11
Table 3 The comparison of three AF solution for mobile devices.....	16
Table 4 The comparison of focusing time and corresponding operating voltage. The result shows GD-LC Lens significantly improved driving voltage and only can be only driven by less than 5Vrms.	52
Table 5 The results and comparisons of two main structures of LC lenses driven by OD method. In the internal structure part, focusing response time was reduced to 0.2sec by 15Vrms over-drive voltage.....	68
Table 6 The comparisons of single tunable lenses.....	89
Table 7 The comparison of the AF solutions after the improvements of our group for LC lens.....	89



Chapter 1.

Introduction

1.1 Tunable-focus Lenses

Lenses are key elements of optical systems. Most of the conventional lenses are made of glass, polymer, or other transparent solid materials, which exhibits fixed focal length. A lens system with tunable-focus can be achieved by adjusting the distance of two or more lenses. This approach for Auto-focusing, or Zoom function in imaging systems has been widely utilized, and the theory for optimization of imaging aberrations are also developed. Zoom Lenses, for example, adjust the positions of lens groups to varied the effective focal length and simultaneously compensate the deviation of imaging plane to the position of image sensor. Another option in actuator technology, voice-coil motor (VCM) [1-5], is used combining with lens-head for the auto-focusing in cellphones. The motor controls the position of whole lens module to image objects at different positions, but the lens groups is difficult to be individually controlled duo to the size and tolerance limitation. Therefore, these approaches either make the devices bulky and heavy or only can perform simple functions due to the spacing or a number of components. In many consumer products, slim and light would be the key concern, especially in mobile devices.

Single tunable lens already exist in nature. Human eye is one of the single-lens systems with a tremendously wide tunable focal range. The primary tuning mechanism is shape change, as controlled by the muscles in the eye. To mimic the fovea imaging of the human eye, similar technologies was proposed to change the material's shape, including liquid lenses [6-13], or microfluidics lenses [14-18]. General liquid lenses are constructed by an interface between two different materials. These materials can be air-to-water or two different liquid materials (water-to-oil, for example) [19-24]. Electrically or mechanically control the shape of

the interface; we can vary the lens power, and shown in Figure 1-1(a) (b). The issues of this technology are the environmental limitations, such as gravity or low feasible range of temperature.

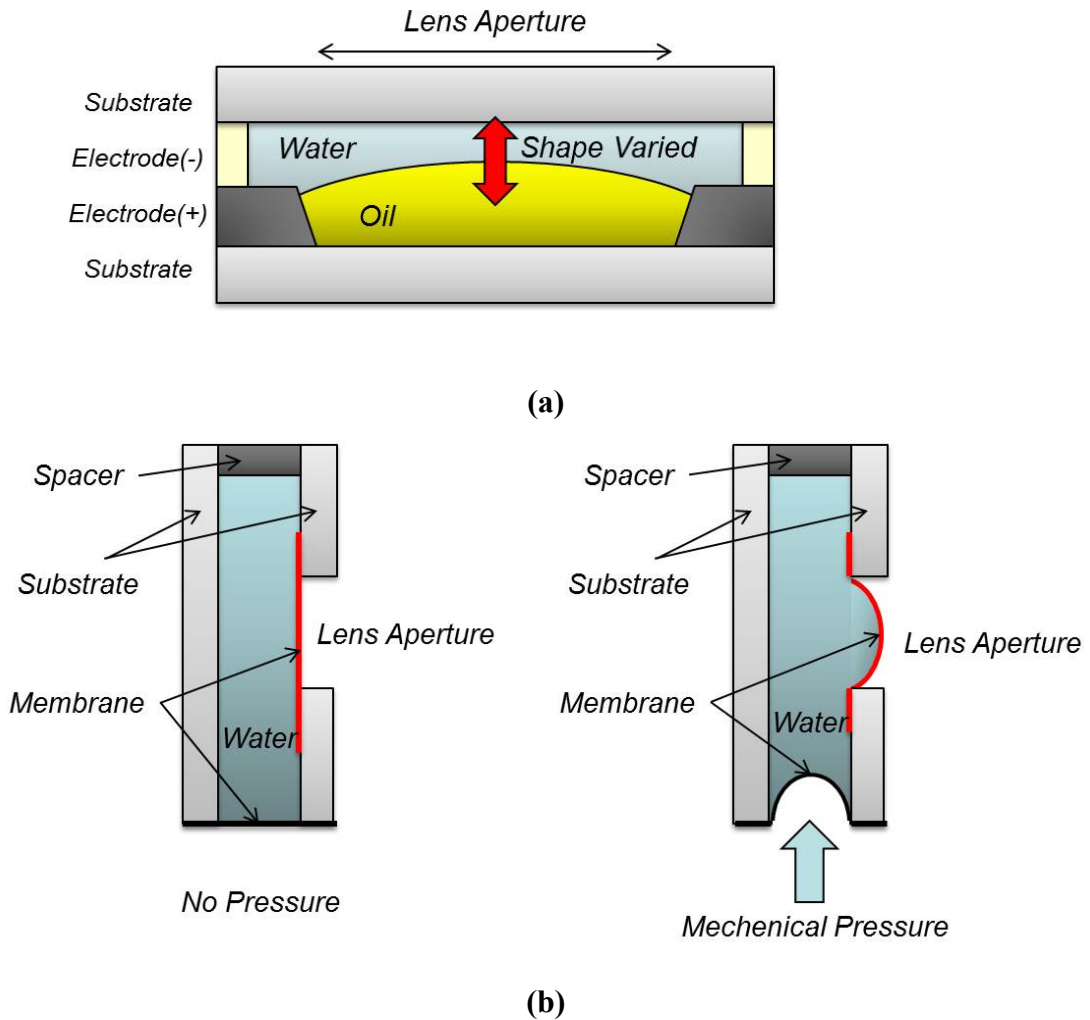


Figure 1-1 (a)The liquid lens employs the oil-water surface and electrically control the surface shape. (b) The liquid lens mechanically controlled the membrane shape to focus the light.

Polymer and liquid crystal (LC) are also material for single tunable lens. Instead of the shape changing, stressed polymers and LC are examples of using refractive index change. For current applications, LC is widely utilized for Spatial Light Modulators (SLMs) [25-34], one of which is Liquid Crystal Displays (LCDs) [35, 36]. The most important property of LC is

that the refractive index is sensitive to electrical control. Its stability also favors the industrial fabrications. Therefore, LCs is a unique and suitable material for single tunable lenses.

1.2 LC Lenses

LC employed for lens application was firstly proposed in 1979 [37]. Prof. Susumu Sato prepared the concave and convex glass lenses covered by the transparent substrate, and injected Liquid crystal into the cavity, as shown in Figure 1-2. By the electrical control, the optical power can be changed without shape changing. In the both cases, the refractive index of glasses was well-chosen, and the operating voltage can change the orientation of LC to control the incident light. Of course, polarizers in front of the lenses are necessary to yield polarized light.

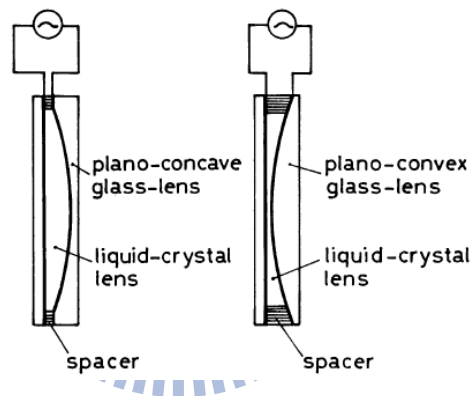


Figure 1-2 The world first LC lens proposed by Prof. Susumu Sato

Prof. Shin-Tson Wu further classified LC lenses into the structures of inhomogeneous and homogeneous LC layer controlled by inhomogeneous or homogeneous electrical field respectively [38-41]. Two of the typical structures controlled by inhomogeneous field are shown in Figure 1-3 and Figure 1-4. In the inhomogeneous layer, the LC are sandwiched between substrates, one of which are a concave substrate deposited an indium-tin-oxide (ITO) electrode. In the voltage-off state, the effective refractive index of LC material is driven as n_e . By a well-chosen n_g of the glass which is smaller than n_e , the LC lens is driven to a convex lens with a shorter focal length. Compared to the mode of voltage-on state the index of LC material is driven as n_o which is similar to n_g for a longer focal length.

On the other hand, the homogeneous layer, LC is sandwiched between a flat bottom substrate and a top planar-concave glass. To fabricate such an LC lens, the plano-concave glass is prepared with an appropriate curvature. The concave surface is coated with ITO as the control electrode, as shown in Figure 1-4. The bottom substrate, as well as, is coated with ITO layer to form the inhomogeneous electrical field. Two of the driving voltage applied on the ITO electrodes can generate different orientation of LC.

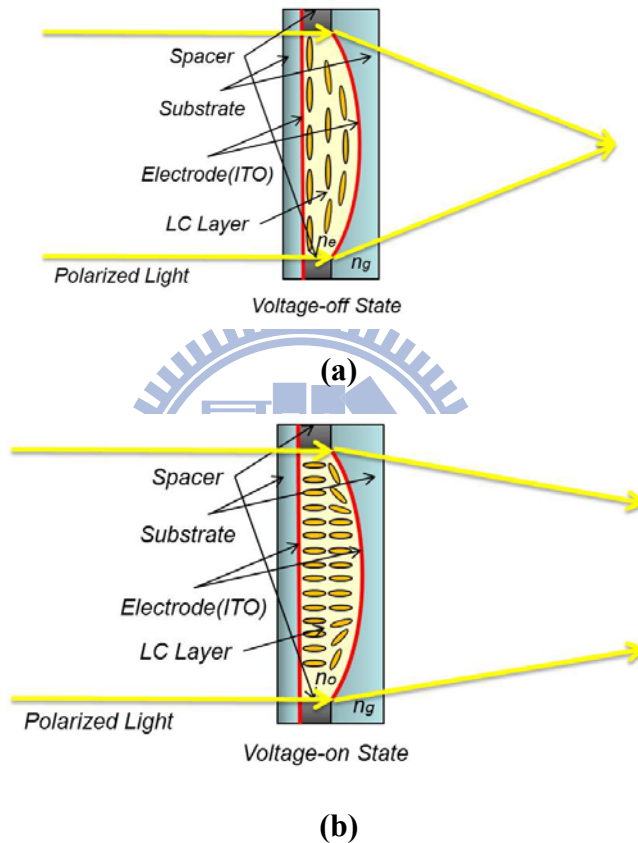


Figure 1-3 The typical structures controlled by inhomogeneous field with an inhomogeneous layer on (a) short focusing state, and (b) long focusing state.

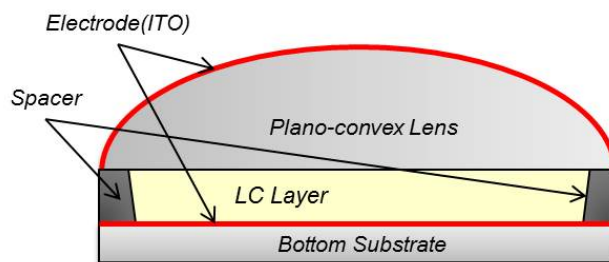


Figure 1-4 The typical structures controlled by inhomogeneous field with an homogeneous LC layer.

There are also combined structures which including the homogeneous LC layer and inhomogeneous structure to yield non-uniform electrical field [42]. It utilizes an inhomogeneous glass lens sandwiched between two homogeneous electrodes, the gradient electrical field can be generated, although the flat structure of ITO and LC layers. Other approaches for LC lenses were also proposed, such as polymer type and other novel approaches [43-51].

A simplest structure of LC Lenses is utilizing the electrical fringe field to control the orientation of LC. This structure is typically constructed by two flat substrates clipping a homogeneous LC layer. The ITO electrodes on the substrates can be patterned to yield the fringing field. Prof. Shin-Tson Wu also discussed eight different types of this kind of LC Lenses [52]. In this kind of homogeneous LC Lens, the patterns of electrodes and electrical control are critical for yielding the desired phase retardation on uniform LC layer. Two of the homogeneous LC Lenses are shown in Figure 1-5 (a) (b), structures with external and internal electrodes, both of which utilize the fringe field of the electrodes to control the phase retardation of the LC layer. The electrodes are typically constructed of ITO. The difference of these two structures is the insertion of high K material (i.e. the substrate) between two ITO layer, which the function is to smooth electric field communicated to the LC layer. This kind of structure is effective, simple, and also easy for realizing spherical and cylindrical LC Lenses. In order to have the benefit of simple structure and more flexible for applications, our studies focused on this kind of LC lenses.

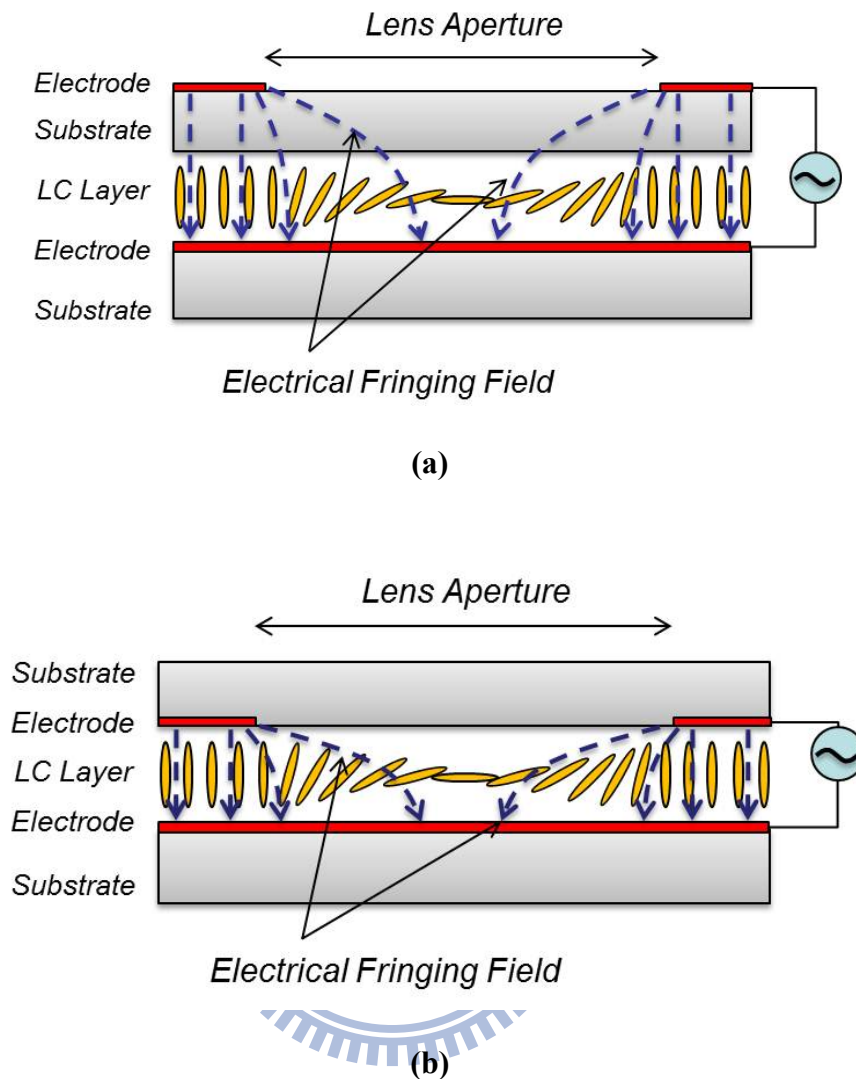


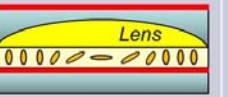



Figure 1-5 Two of the most general homogeneous LC Lenses, (a) the structure with external electrodes, and (b) the structure with internal electrodes utilizing electrical fringe field of the electrodes to generate a gradient variation in phase retardation. The low freedom of electrical control limits the range of focusing.

To summarize these structures for LC lens, a comparison lists the representative structures, as in Table 1. Typically, the principle of these types is employing the inhomogeneous LC layer or non-uniform electric field to yield lens-shape gradient index distributions.

Table 1 The comparison of LC lenses proposed by the world leading groups.

	Inhomogeneous LC Layer	Homogeneous LC layer	Combined Structure	Polymer Type
Structure				
Principle	Lens shape + Index difference	Fringing field	Lens substrate varies the field	Lens shape + Index difference
Features	The 1 st proposed structure	The simplest LC lens	Well controlled by shape of the lens	Shorter focusing time
Group	Prof. Sato	Prof. S.T. Wu	LensVector	Prof. S.T. Wu

1.3 Comparison of Single-tunable Lenses

In the previous sections, two kinds of single-tunable lens, liquid and LC lens were discussed. In the liquid lens part, it is a shape changed system to control the incoming light, which also means the requirement of more complicate structure for controlling the surface between two liquid materials. As the result, the structure is relatively bulky than that of LC lens. Furthermore, from the reports of newly papers, the shape of liquid is usually difficult to be changed. For example, the variation of the surface requires ultra-high voltage. Besides, issue of gravity also results in lateral deviation of its optical axis. On the other hand, LCs has the unique feature which is sensitive to electric field. LCs can be driven by low driving voltage and the orientation can be easy controlled to change the phase retardation. This feature is also the reason LCs have been wildly used in LCD industry. Therefore, the easy driving and simpler structure is the why we choose LC lens as the device for imaging application in mobile devices. However, the optical property and the use of polarizer make LC lens have intrinsic limitation for lens applications. For the optical property part, the inhomogeneous refractive index of LCs results in difficulty for optical analysis. Therefore, LC lens cannot be

analyzed by the shape of a lens which is principle of optimizations for conventional lens-head and also is feasible for liquid lenses. This also means we cannot use available lens design tool for the optimization of LC lens. On the other hand, the use of polarizer in LC lens reduces a half of incoming light efficiency. The loss of light efficiency changes cognition of f-number (F/#) which is used to describe light efficiency of a lens-head, and may result in requirement for larger aperture size for keep the same efficiency.

To summarize the above comparison, Table 2 lists the advantages and disadvantages of liquid and LC lens. LC lens shows the intrinsic benefit, such as easy control, simple structure, and no gravity issues, which are more convenient for fabrication and applications in mobile devices. For the last to issue, optical analysis and use of polarizer, these can be overcome by linking simulation tools for LC cell and lens-head design and utilize image processing to eliminate information from ordinary-ray, which will be discussed in last part of the thesis.

Table 2 The comparison of two single-tunable lens, liquid and LC lens.

	Liquid lens	Liquid Crystal Lens
Driving	Difficult	Easy
Structure	Complicate, Bulky	Simple, Slim
Gravity Issue	Yes	No
Optical Analysis	Easy	Difficult
Polarizer	No	Required

1.4 Lens-heads in Mobile Devices

Mobile devices become the necessary produces for daily life's usage in recent years, especially when communication technology is growing up fast. Lens-heads are key components in the devices, such as cellphones, laptops, and tablet PCs. When performing functions of photography, phantom identification, computer vision, and image communications through these devices, lens-heads always play an important role to deal with the basic function of imaging. For this essential function, image quality of the lens-heads is improved to satisfy the rapid growing-up pixel numbers. Furthermore, optical designers also

face the challenge to minimize the thickness of lens modules as these devices are required to be slimmer and slimmer. Not only the simple imaging function, but also technologies of auto-focusing (AF) and optical-zoom are also diligent directions for improving the image quality. For the improvement of image quality, tree of the AF technologies for imaging objects at different distances are developed.

1.4.1 Auto-focusing (AF)

1.4.1.1 Voice Coil Motor (VCM)

Voice Coil Motor (VCM), as mentioned in section 1.1, is one of the approaches to perform AF in mobile devices. The principle of VCM is the same as a loudspeaker exciting its voice coil with a controlled current to vibrate its diaphragm. In the application of AF, the VCM actuator consists of two main parts, the fixed permanent magnets and the moving lens-holder coiled coil, as shown in Figure 1-6. To actuate a lens-head, the positive and negative Lorentz force can be yielded by different direction of driven currents. The equation illustrates the relation following:

$$\vec{F} = N \cdot l \cdot \vec{i} \times \vec{B} \quad (1-1)$$

where \vec{F} , N , l , \vec{i} , and \vec{B} indicate Lorentz force, the number of coil, the length of coil vertical to direction of magnetic field, driven current, and magnetic flux density respectively. Moving the lens-head, VCM method can shift the image plane to the position of image sensor for focusing objects at a finite distance, as shown in Figure 1-7. Therefore, it is an effective approach to perform AF in such a limited space of mobile devices, and one of the mainstreams for current solutions for AF. However, the size of VCMs is generally larger than that of lens-heads for embedding the lens-heads, as Table 3 shows the fundamental spec. and appearance of VCM products of TDK Xiamen CO., LTD [53]. Cost is also increased due to the additional VCM module and the integrations. Furthermore, for such a limited space (generally required to less than 5mm) in mobile devices, only one VCM is usually used to actuate the whole lens-head instead of the individual lenses. As a result, only one variable can

be changed to perform AF by adjusting the relative distances of object and image, not mention to other functions such as zoom.

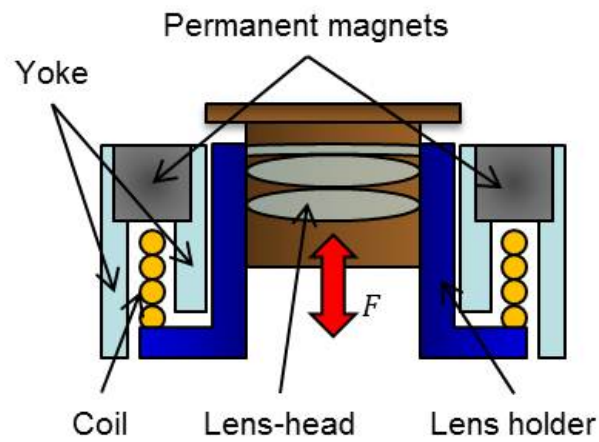


Figure 1-6 Structure of conventional VCM actuator.

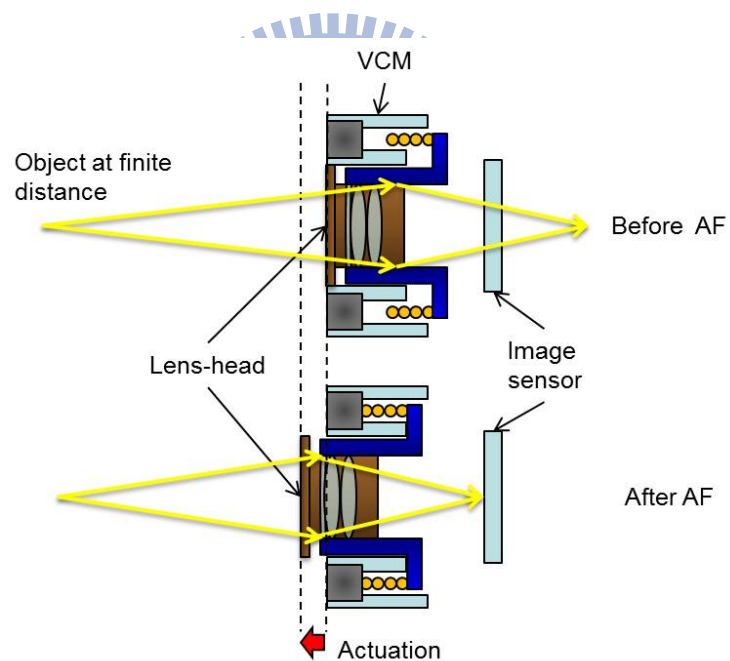


Figure 1-7 The focusing mechanism of VCM approach.

Table 3 The spec. list of conventional VCM.

Product Appearance	Model	Specifications
	TVF-810	Dimension:14mm x 14mm x 10.5mm Lens barrel:M8 x 0.35 Lens weight:<0.9g Lens motion range:0.33mm
	TVF-750	Dimension:10mm x 10mm x 4.6mm Lens barrel:M7 x 0.35 Lens weight:<0.2g Lens motion range:0.3mm
	TVF-752	Dimension:10mm x 10mm x 6.3mm Lens barrel:M7 x 0.35 Lens weight:<0.2g Lens motion range:0.3mm
	TVF-550	Dimension:8.5mm x 8.5mm x 4.2mm Lens barrel:M5.5 x 0.35 Lens weight:<0.08g Lens motion range:0.3mm
	TVF-651	Dimension:8.5mm x 8.5mm x 4.7mm Lens barrel:M6 x 0.35 Lens weight:<0.1g Lens motion range:0.25mm

1.4.1.2 *Extended Depth-of-field (EDoF)*

Another technology, Extended Depth-of-field (EDoF) a novel computational imaging approach for extending the Depth-of-field (or Depth-of-focus) of fixed-focus mobile lens [54-59]. Utilizing a phase mask combined with lens-head, the system can generate similar Point Spreading Functions (PSFs) from object points within a wide range. By digital image processing (DIP), the object points can be reconstructed and imaged clearly, as the schematic shown in Figure 1-8. The PSFs captured from different distances are similar which means the field exhibiting clear images can be extended. However, EDoF method is not really AF, while it applies computational photography [60] to perform digital-auto-focus. Furthermore, the computational complexity would be an issue as the rapid increasing of pixel numbers.

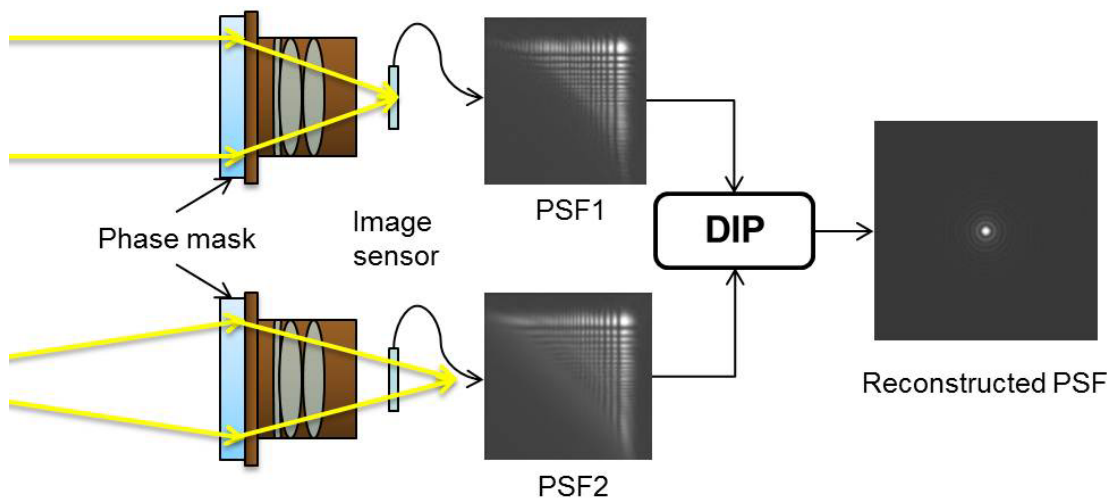


Figure 1-8 The principle of EDoF method.

1.4.1.3 LC Lenses

The LC lens has unique properties such as electrically tunable focal length. Since there are no moving mechanical parts, the LC lens can be smaller and lighter than conventional tunable glass lenses. In mobile devices, the LC lens can directly combine with mobile lens-module in front of the lens-head, and easily perform AF function by driving appropriate voltage to focus objects at different distances. For example, as illustrated in Figure 1-9, a conventional lens-head focuses object at infinite distance, and utilizes the LC lens applied by driving voltage to increase lens power for imaging the objects at finite distance. Rays from the object point can be parallel and inputted to the lens-head through the LC lens. There is no difference for the lens-head to image the object at infinity and finite distance, if the LC lens can image the finite one well. However, the major technical challenge of LC lens is to generate desired gradient refractive index to optimize the imaging. In generally, the imaging performance of conventional lens-heads is better than that of LC-combined lenses, because the adjustment of lens power would damage the optimized aberrations and yielded worse image quality. Actually, it is difficult to generate diffraction-limit performance by the LC lens in the structure for the following imaging. Furthermore, the PSFs of those focal lengths driven by different voltages would also be different which results in unstable image quality for objects

at different distance. To optimize this part, we need to minimize the spot size of the PSFs for the LC lens.

On the other hand, the long focusing time is one of the serious issues in the study of LC lenses. How to instantaneously focus after applying voltages is important to perform AF. The cell gap of LCs is usually much thicker than that of LCDs for yielding large optical power. This requires very high operating voltage to shorten the focusing time. In many studies, the focusing time is typically larger than 10 sec or up to 1 min for cell gaps which are larger than 60um. The driving voltage was usually higher than 30Vrms. In some reports, it was even higher than 100Vrms. As a result, this situation makes the application unpractical and unfeasible for commercial products.

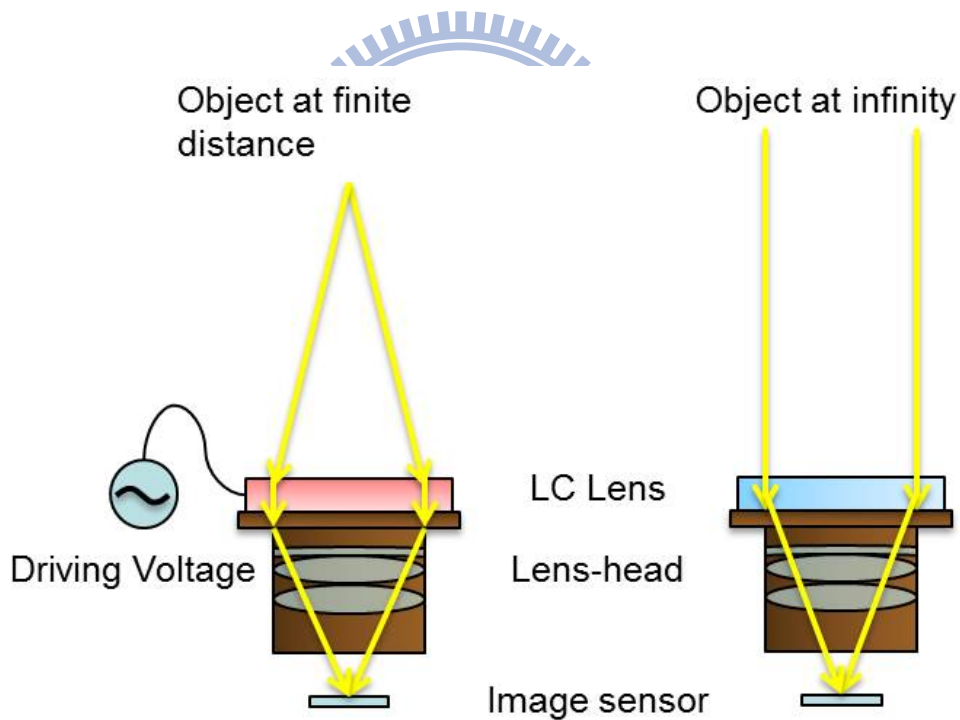


Figure 1-9 The mechanism of LC lens used for AF function in mobile device.

1.4.2 Optical Zoom

Optical zoom is usually performed in imaging systems to zoom the captured images in and out. By changing the effective focal length (EFL) of the imaging system, the zoom ratio can

be adjusted. However, zoom lens is usually a bulky system due to the requirement of spacing for moving the lens groups. Especially in mobile devices, the space and tolerance are much critical for adding this function. Therefore, digital zoom is widely adopted for magnifying images, although it cannot provide adequate image performance. In VCM approach, as mentioned in section 1.4.1.1, it actuates the whole lens-head rather than the individual lenses, so the EFL cannot be changed to adjust the zoom ration. On the other hand, EDoF performed digital AF for a wild field to obtain the clear images from objects at different distance, but this technology also cannot change EFL of optical systems.

LC lenses have the ability to change the focal length electrically without the mechanical moving. That means the optical system embedded LC Lenses can change its EFL to achieving optical zoom within a constant thickness. In other words, LC lens is distinguished from the other methods which not only can perform AF but also has the potential for optical zoom simultaneously within the small spacing. The simplest approach is to utilize double LC lenses to simulate the variator and compensator of conventional zoom lenses respectively, as Figure 1-10 shows. By adjusting the focal lengths, f_1 and f_2 , of each LC lens. The EFL of the system are varied for corresponding zoom ratio. Rather than modifying the spacing, D1 and D2, the LC zoom lens can maintain the minimized total thickness of the system and increase tolerance of integrations.

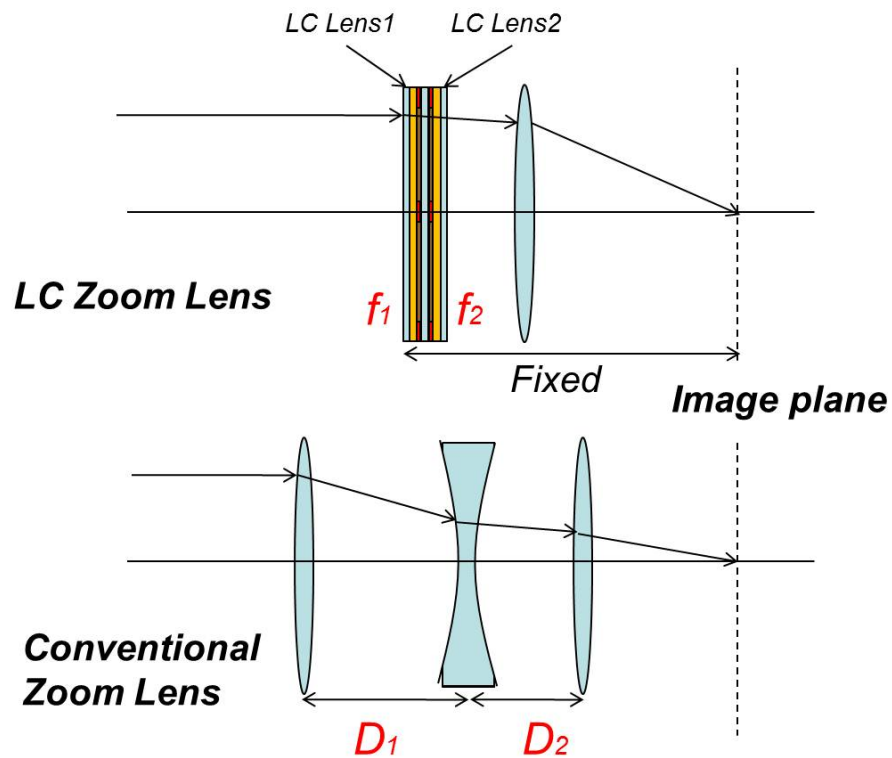


Figure 1-10 The structure of LC zoom lens and conventional zoom lens.

1.5 Motivation and Objective of This Thesis

To summarize the discussion in section 1.1 to 1.3, we know that LC lenses have the potential to perform the imaging functions for mobile devices in limited spaces. The most unique characteristic of LC lenses is the electrically tunable focal length without the mechanical movement, which can fix the total thickness of the lens system and reduce the integration cost. Furthermore, AF and optical zoom can be performed simultaneously by the simple structure, as shown in Figure 1-10. As Table 4 summarized, the most competitive advantage of LC lenses are the small dimension and self-tunable focusing. Without complicate integrations, AF and optical zoom can be performed. However, the issues as mentioned, inferior optical performance, slow focusing time, and high driving voltage, are the practical problems which governs LC lens can be commercialized or not.

Therefore, in this thesis, we want to overcome these issues. In the part of optical performance, we try to increase the range to obtain superior focusing. On the other hand, the

focusing time and driving voltage actually indicate the same work to improve the efficiency of driving. In typically, AF should be completed in one second for most mobile phones. This illustrates the focusing time should be reduced down to 200ms, if we perform several times of focusing in one AF. The improvement of focusing time can be achieved by increasing the driving efficiency. That means the same performance should be generated by lower driving voltage. In mobile devices, the driving voltage less than 15V or 10V could be an acceptable range.

Table 4 The comparison of three AF solution for mobile devices.

	Size	Integration	Driving	Speed	Image Quality
Voice Coil Motor (VCM)	✗	✗	△	○	○
Extend Depth of Focus (EDoF)	○	○	△	△	✗
Liquid Crystal Lens (LC Lens)	○	○	✗	✗	✗

○ :Better △ :Adequate ✗ :Worse



Chapter 2.

Theory and Principle of LC Lenses

The basic mechanical theories of LC molecular and optical properties of LC lenses are introduced in this chapter. In the mechanical description, the orientations of LC molecules are usually calculated by the total free energy in a LC cell. This energy is induced by the elastic properties of LC material and effects of electric field on LC, as well as anchoring force on the boundary. In order to search for the director configuration, the total free energy is minimized to obtain the certain state. Response time is also introduced in this chapter. In the part of optical properties, the basic principle of LC lenses is introduced by propagations of plane wavefronts.

2.1 Introduction to Liquid Crystals

Liquid Crystal (LC) is a material which the state can be varied between crystal solid and isotropic liquid. It is believed that LC was discovered in 1888 by Friedrich Reinitzer, an Austrian botanist. He found the phases of LC were changed from a thick and turbid shape to a pure liquid when increased the temperatures. Following, Lehmann, a Germany physicist, further proved the state of crystalline liquid of LC utilizing polarizing microscope, and started the research of LC.

Typically, the phases of LC can be classified into crystal solid, *smectic*, *nematic*, and isotropic liquid under different range of temperature, as shown in Figure 2-1. At low temperature, the LC is in crystal solid state and the molecules have very high order in positions and orientations. When the temperature is increased, the state becomes to smectic phase. In this state, not only the orientations but also the positions of LCs become more random, and form a layered structure. Generally, LC in smectic phase higher viscosity and slower response time to applied electric field compared to nematic phase. When the temperature further increased, LC

is transformed to nematic phase, which is the most common state. In this phase, the LC molecules have partial orientation and aligned in one-dimension space. Nematic phase has the advantage of low viscosity and faster response time. Therefore, it is widely employed in many applications, such as LCD and other kind of displays. In this thesis, we also focus on this advantage, and utilized it for our research. At high temperature, the LC material becomes isotropic phase, which the orientations and positions of molecules are totally random. In this state, LC has no birefringence.

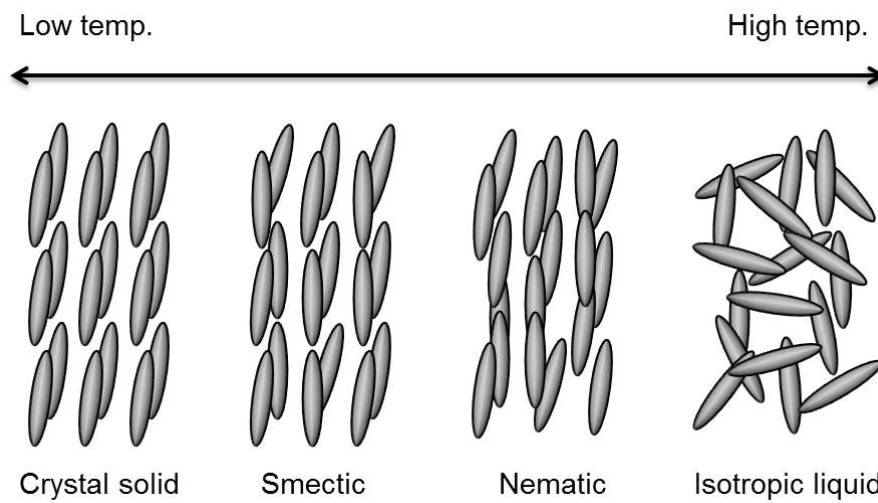


Figure 2-1 The phases of LCs under different range of temperature

2.2 Energies in LC Cells

Direction of LCs is uniform in the LC cell when there is no external energy or confinement. If there is applied energy or other limited conditions, the spatial directions of LCs will be re-orientated, and this change was named the deformation. To investigate and calculate the change of directors, continuum theory is well-used in calculating the equilibrium of energies in LC cells. Generally, these energies are considered including free energy density on uniform state (f_0), elastic energy (f_{ela}), electric or magnetic energy ($f_{electric}$), anchoring effect (f_s), and so on, as shown as Equation (2-1).

$$F = f_0 + f_{ela} + f_{electric} + f_s \quad (2-1)$$

Elastic Energy

In the nematic phase, there are three possible forms of deformation as shown in Figure 2-2. These forms were called splay, twist, and bend representing each specific variation of LC directors, \vec{n} , which indicates the directions of LC molecules, as shown in Figure 2-3. The general equation used to describe the energy stored by the three forms of deformations is

$$f_{ela} = \frac{1}{2}K_{11}(\nabla \cdot \vec{n})^2 + \frac{1}{2}K_{22}(\vec{n} \cdot \nabla \times \vec{n})^2 + \frac{1}{2}K_{33}(\vec{n} \times \nabla \times \vec{n})^2 \quad (2-2)$$

Each term in the left side indicates the deformation energy of the three forms. This equation is usually referred to as the *Ossen-frank energy*, and K_{11} , K_{22} , and K_{33} represent the splay twist, and bend elastic constant of LC material respectively.

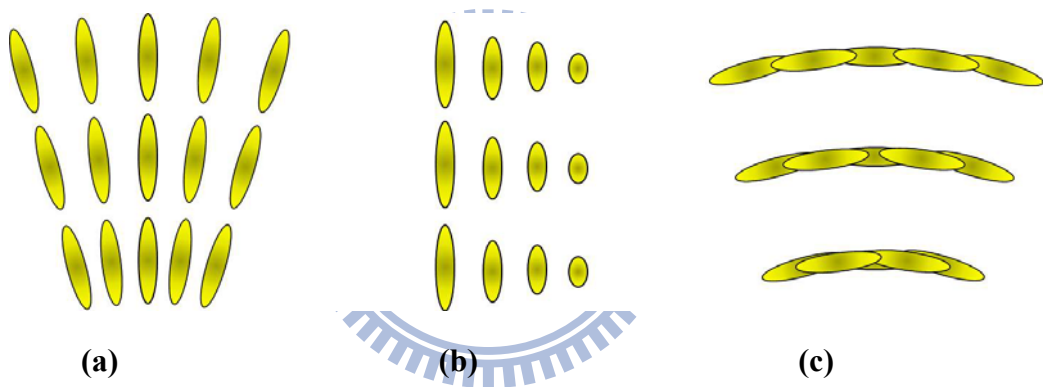


Figure 2-2 The three possible forms of deformation, (a) splay, (b) twist, and (c) bend, of nematic LCs.

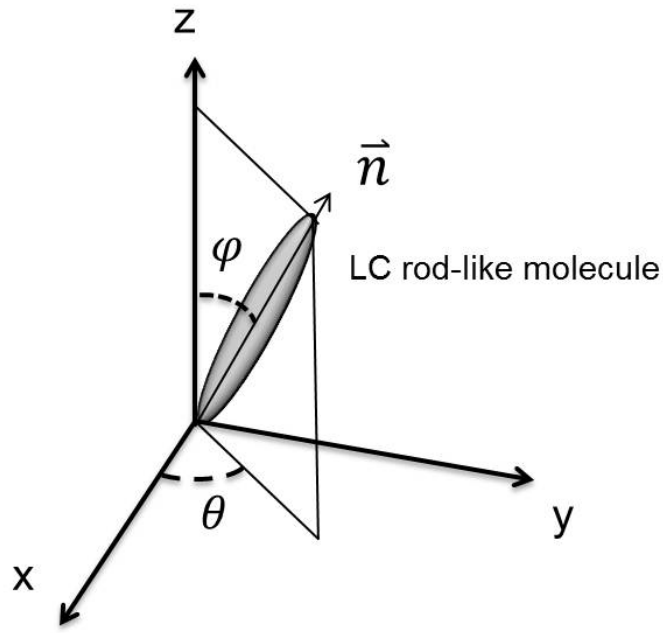


Figure 2-3 LC directors, \vec{n} , which indicates the directions of LC molecules in Cartesian coordinate

Electric Field

Electric field is considered to re-orientate LC directors because it induces polarization. While the permittivity of LC molecule in the direction parallel to \vec{n} , χ_{\parallel} , is different from that of perpendicular direction, χ_{\perp} , the polarization can be changed by applying different field. By decomposing the field into two perpendicular directions along \vec{n} and perpendicular to \vec{n} , as shown in Figure 2-4. The induced polarization can be analyzed by

$$\vec{P} = \varepsilon_0 [(\chi_{\parallel} - \chi_{\perp})(\vec{E} \cdot \vec{n})\vec{n} + \chi_{\perp}\vec{E}] \quad (2-3)$$

Thus, the electric energy of LC is derived as following:

$$f_{electric} = -\frac{1}{2}\vec{P} \cdot \vec{E} = -\frac{1}{2}\varepsilon_0(\chi_{\parallel} - \chi_{\perp})(\vec{E} \cdot \vec{n})^2 - \frac{1}{2}\varepsilon_0\chi_{\perp}E^2 \quad (2-4)$$

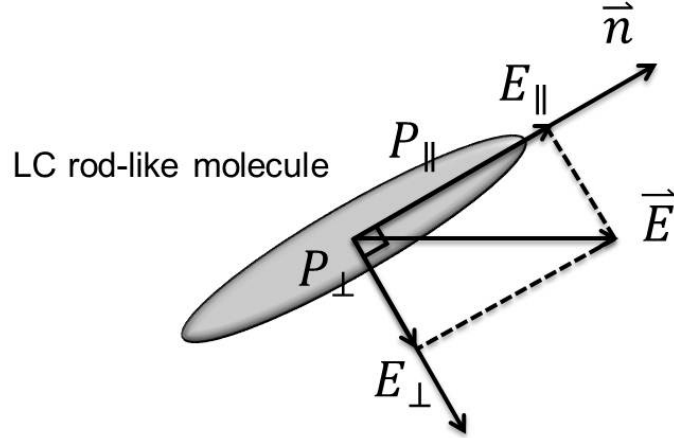


Figure 2-4 The field was decomposed into two perpendicular directions along \vec{n} and perpendicular to \vec{n} .

Anchoring Effect

In reality, to fabricate LC cells, the boundary forces of the substrates affect the equilibrium state. This force is usually achieved by coating an alignment layer on the substrates, and the directions of the layers can determine the initially configuration of LC directors. By arranging the directions of upper and lower substrates, stabilized LC profiles can be generated in specific types. Three of the common alignment methods are shown in Figure 2-5, the perpendicular, anti-parallel, and parallel alignments. Each of them is well-used for producing twist-nematic cell (TN), electrically controlled birefringence (ECB), and pi-cells, respectively. In the applications of LC lenses, ECB mode is widely used for simplifying the control and structures. The force describing the anchoring effect can be expressed by Rapini-Papoular approach as following:

$$f_s = f_\theta + f_\varphi \quad (2-5)$$

where

$$f_\theta = \frac{1}{2} W_\theta \sin^2(\theta - \theta_0) \quad (2-6)$$

$$f_\varphi = \frac{1}{2} W_\varphi \sin^2(\varphi - \varphi_0) \quad (2-7)$$

θ , and φ is the polar and azimuthal angles, as shown in Figure 2-3, which determine the

anchoring force of two components, f_θ , and f_φ respectively. W_θ and W_φ are the constant which are determined by interaction between the alignment layer and the LC molecules. θ_0 and φ_0 are the angles at which the interaction has minimum energy.

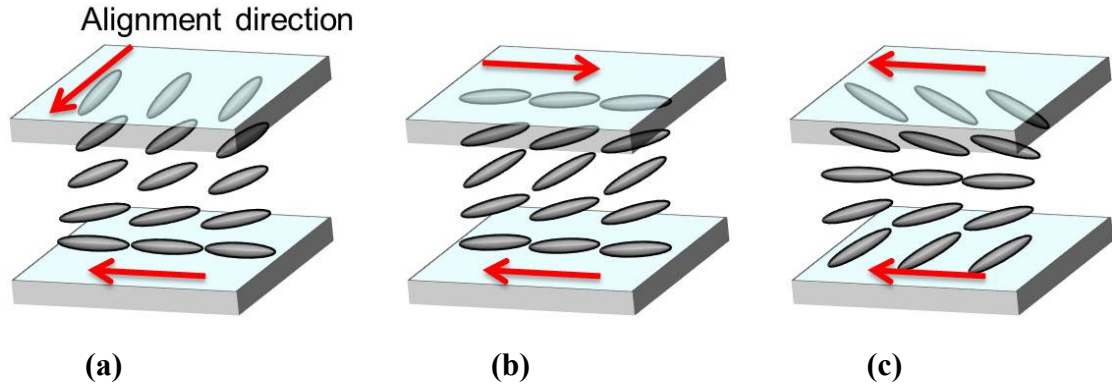


Figure 2-5 Three of the common alignment methods, (a)perpendicular, (b)anti-parallel, and (c)parallel alignments for LC cells.

2.3 Optical Principle of LC Lenses

LC is a material exhibiting birefringence. This property causes the incident light with different polarizations meet different refractive index. For analyzing the distribution of index, the light can be decomposed into two eigen-polarizations, one of which is parallel to the optical axis of the material and the other one is perpendicular to the plane of optical axis. The parallel one which is named ordinary light sees all the same index no matter how the included angle between the incident light and the optical axis, as shown in Figure 2-6. On the other hand, the polarization which is perpendicular to the plane of optical axis, named extraordinary light, sees the refractive index which is direction dependent. Although, the index would be varied by the included angles between the incident light and the optical axis, the effective index can be calculated by Equation (2-8).

$$n_{eff}(\theta) = \frac{n_o n_e}{\sqrt{n_o^2 \sin^2 \theta + n_e^2 \cos^2 \theta}} \quad (2-8)$$

where n_e and n_o are the extraordinary and ordinary refractive indices respectively. θ is the included angles between the incident light and the optical axis, as shown in Figure 2-6.

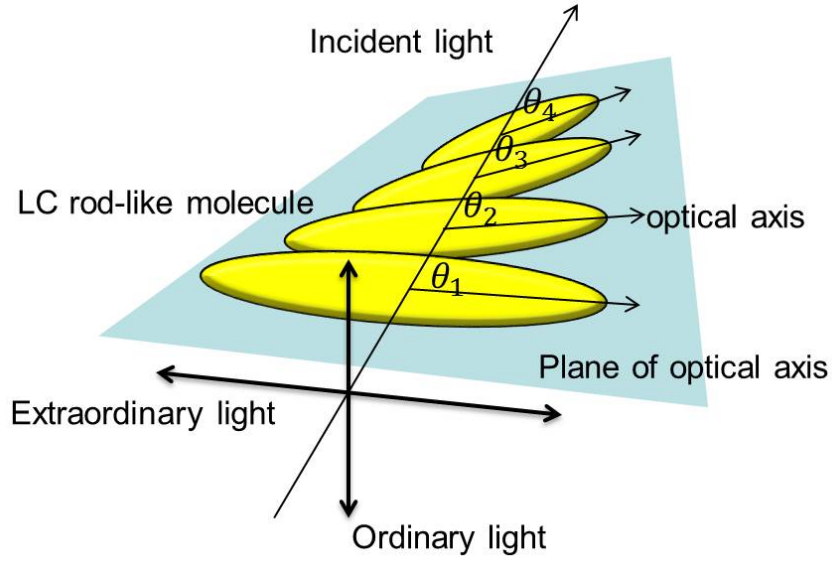


Figure 2-6 The ordinary and extraordinary lights travelling in the LC material and extraordinary lights see the different indices which are dependent to the included angles between the incident light and the optical axis of LC molecules.

LC lenses, as shown in Figure 2-7, employ the gradient electric field to control the LC layers. The distribution of the field is controlled by the applied voltages and generates phase retardation which is approximate to that of lenses to converge or diverge the incident extraordinary light. The schematic is shown in Figure 2-8. r , d , and f respectively represent the radius of lens aperture, thickness of LC layer, and the effective focal length. To derive the relation of these parameters, optical path length (OPL) of wavefront is used to explain. As shown in Figure 2-8, the LC layer of an LC lens can be considered as a GRIN Lens [61], thus the refractive index is a function of position \vec{r} . To simulate the focusing of the lens, we assume the rays of a plane wave passing the lens and arriving at point E have the same OPL. Therefore, the optical path difference (OPD) between ABE and CDE should be zero.

$$S_{AB} + n_0 \cdot \overline{BE} = S_{CD} + n_0 \cdot \overline{DE} \quad (2-9)$$

where S_{AB} , and S_{CD} are the OPL of ray AB and CD respectively, and n_0 is the refractive index in air. Generally, the lens power of LC lenses is relatively small, thus the refraction in the LC cell can be ignored. Therefore, Equation (2-9) is approximate as

$$\begin{aligned}
S_{AB} - S_{CD} &= n_0 \cdot (\overline{DE} - \overline{BE}) \\
\Rightarrow (n_1 - n_2) \cdot \overline{CD} &= n_0 \cdot (\overline{DE} - \sqrt{\overline{AB}^2 + \overline{DE}^2}) \\
\Rightarrow \Delta n \cdot \overline{CD} &\cong n_0 \cdot \left[\overline{DE} - \left(\overline{DE} + \frac{\overline{AB}^2}{2\overline{DE}} \right) \right] \\
\Rightarrow \Delta n \cdot \overline{CD} &\cong n_0 \cdot \frac{\overline{AB}^2}{2\overline{DE}} \\
\Rightarrow \overline{DE} &\cong n_0 \cdot \frac{\overline{AB}^2}{2\Delta n \cdot \overline{CD}}
\end{aligned} \tag{2-10}$$

where Δn indicate the difference of refractive index between border and center. By substituting r , d , and f for the length \overline{AB} , \overline{CD} , and \overline{DE} , Equation (2-10) can be rewrite as

$$f \cong n_0 \cdot \frac{r^2}{2\Delta n \cdot d} \tag{2-11}$$

In Equation (2-11), we have assumed the straight propagating of rays in LC layer, and the effective index, n_1 and n_2 at the border and center of the lens. To obtain a unique focal length, f , from the whole lens aperture, the distribution of Δn is

$$\Delta n \cong n_0 \cdot \frac{r^2}{2f \cdot d} = \kappa \cdot r^2 \tag{2-12}$$

which is a parabolic form of variable, r .

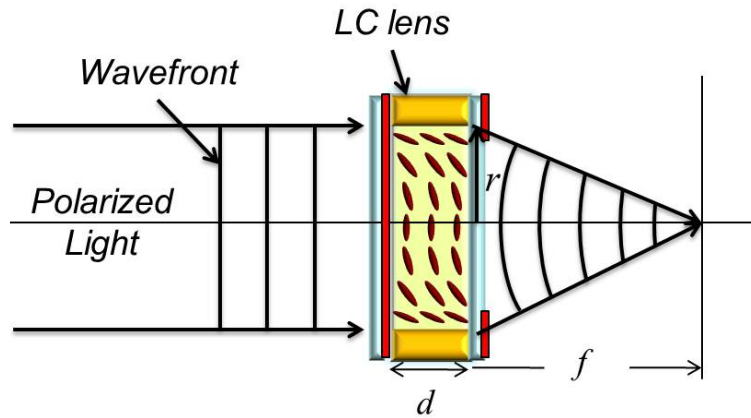


Figure 2-7 The wavefront focusing of LC lens.

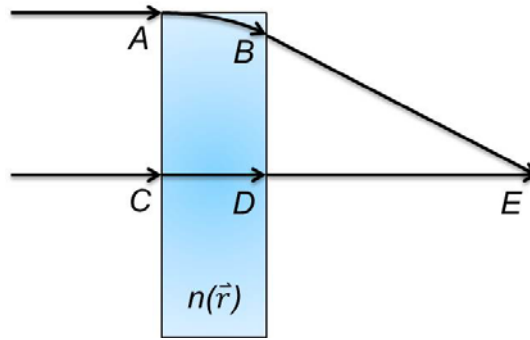
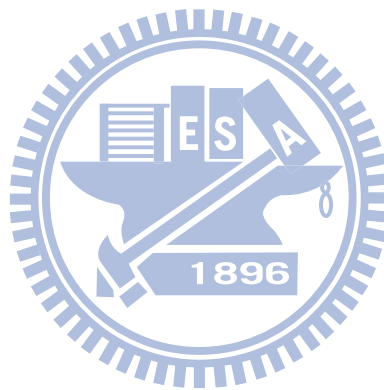


Figure 2-8 The diagram of LC lens considered as a GRIN lens for analyzing the focusing.



Chapter 3.

Multi-electrode Driven LC Lens

To have a tunable lens, the LC lenses were expected to produce superior focusing at each focal length, which can yield similar image quality for focusing objects at different position. Therefore, a well control for the electric field is required. In this chapter, we proposed Multi-electrode Driven LC Lens to have such high control freedom yielding superior focusing for each focal length by operating different sets of driving voltages.

3.1 Introduction

As mentioned in section 1.4.1.3, to achieve LC lenses exhibiting highly focusing ability, the spot size of PSF should be minimized for each focal length. However, the conventional structures with low control freedom, as introduced, are hard to significantly yield desired electrical field to control the LC orientation for wide range of focusing. Figure 3-1 shows a focusing example of the homogeneous LC lens with internal electrodes. When the higher driving voltage was applied, the higher focusing light intensity can be detected at focal length, 4cm, and the full width at half maximum (FWHM) of the spot size is 65um. When the driving voltage was decreased, however, the maximum light intensity was detected at focal length, 10cm, with a different beam profile from that of 4cm, whose FWHM increased to 121um. If we employed these results for AF, the image performances are different for objects at different distance. To finely control the phase retardation of LC layer, Multi-electrically Driven Liquid Crystal Lens (MeDLC Lens) was propose. MeDLC Lens utilized a large number of electrodes to significantly control the electrical field on LC layer. By optimizing the sets of driving voltages for different focal length, a wide range of superior focusing was yielded.

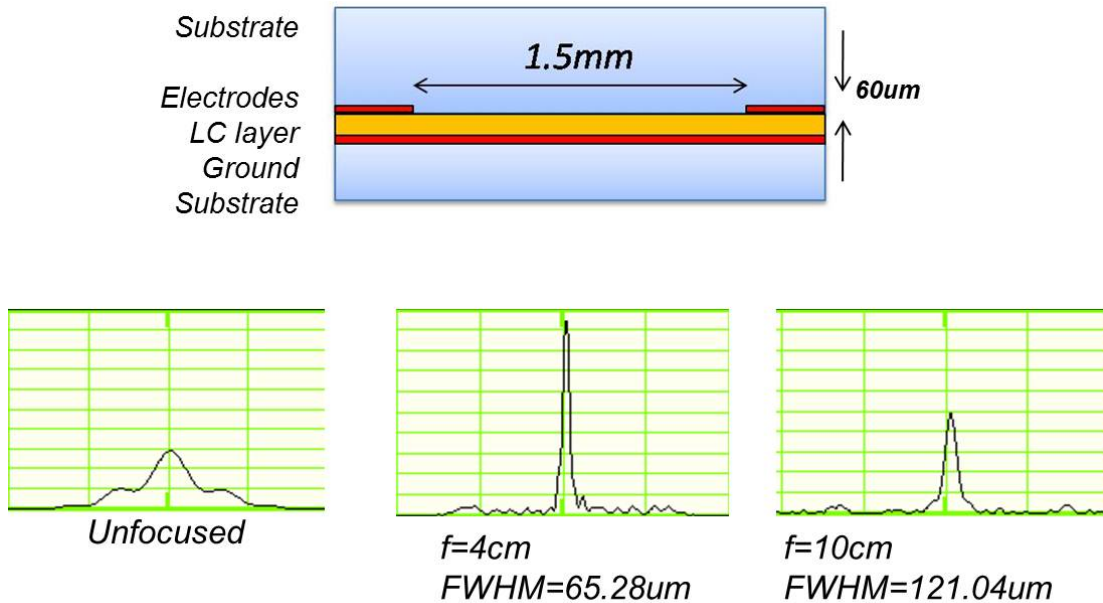


Figure 3-1 The focusing profile of the homogeneous LC lens with different focal length, 4cm and 10cm. The focusing profiles are different.

3.2 Multi-electrically Driven Liquid Crystal Lens (MeDLC Lens)

3.2.1 MeDLC Lens

The main concept of MeD-LC Lens is to utilize a large number of electrodes to finely control LC orientation, as the structure shown in Figure 3-2. To generate a smooth electrical field in LC layer, multi-electrode were constructed above a high K material (i.e. the glass). The number of electrodes and width of electrodes and slits, W_E and W_S , were designed for optimized the phase retardation by different aperture size, LC cell gap, and thickness of glass for different applications. By arrangement of driving voltages for each electrode, the phase retardation over the LC layer was optimized for particular focal length. Typically, the arrangement of driving voltages for MeD-LC Lens was correlated to the LC orientation. For a convex lens application, the driving voltages were higher at the marginal electrodes and decreased to the lowest voltage in the central region.

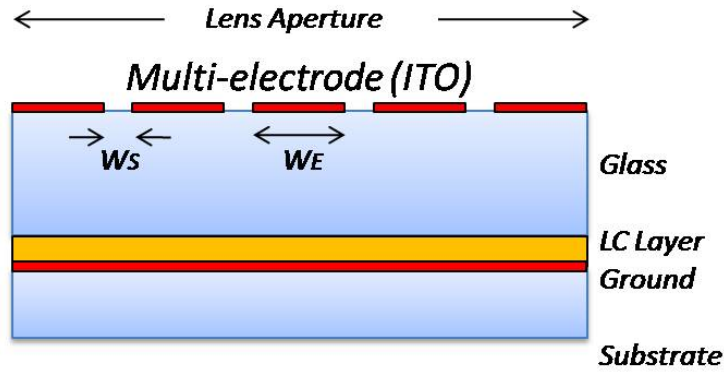


Figure 3-2 MeD-LC Lens with large number of electrodes. MeD-LC Lens utilized the arrangements of driving voltages to finely control the LC orientation, and yielded a wide range of superior focusing

3.2.2 Optimization

To optimize the number of electrodes, errors of phase retardation generated by MeD-LC Lens was quantified. The difference of reflective index of LC lenses is shown following:

$$\Delta n_l = \frac{r^2}{2 \cdot f(r) \cdot d} \quad (3-1)$$

where Δn_l donates the average difference of reflective index between border and center of the lens, r , $f(r)$, and d represent the aperture radius, focal length, and LC cell gap respectively. For an ideal case, a unique focal length for all lens apertures, the distribution of Δn_l is a parabolic curve and was used for analysis of phase retardation. As the phase retardation of MeD-LC Lens could be approximated to that of ideal one, which indicated MeD-LC Lens generates phase retardation with lower optical aberration and approaches to the lens with approximate unique focal length. So the optimization of MeD-LC Lens was focused on the design of the size of electrodes to match the ideal parabolic curve. To simplify the optimization, the ratio of W_E to W_S (W_E/W_S) was fixed to 1 for 1.5mm lens aperture. The LC cell gap and thickness of the glass were designed to 60um and 700um. LC material was chosen as Merck nematic LC (E7), which the intrinsic difference of reflective index between ordinary and extraordinary, Δn , is 0.22. Figure 3-3 shows Δn_l generated by MeD-LC Lens and an ideal lens for focal length of

approximate 3.5cm. As the number of electrodes increased, the curve of Δn_l generated by MeD-LC Lens approached to that of ideal one. In conventional LC lens design, the large marginal electrodes usually yielded flat electrical field in the border, and cannot generate lenses with full aperture size for lens array. On the other hand, MeD-LC Lens utilized the finer electrodes to yield the phase retardation which was much close to ideal parabolic curve and with full designed aperture size (1.5mm).

A merit function defined as following:

$$E = \sqrt{\frac{\sum_r [\Delta n_i(r) - \Delta n_{MeDLC}(r)]^2}{Aperture\ Size}} \quad (3-2)$$

was used to quantify the errors between ideal distribution of Δn_l and that generated by MeD-LC Lens, where Δn_i and Δn_{MeD-LC} represent Δn_l of ideal lens and MeD-LC Lens respectively. Through the result, as illustrated in Figure 3-4, the larger number of electrodes yielded smaller E -value, which means the curves was more approximate to the ideal parabolic one under electrical field of finely control. As the number of electrodes exceeded 9, E started to be saturate. In our study, 9 electrodes for MeD-LC Lens with 1.5mm aperture size would be a balance design.

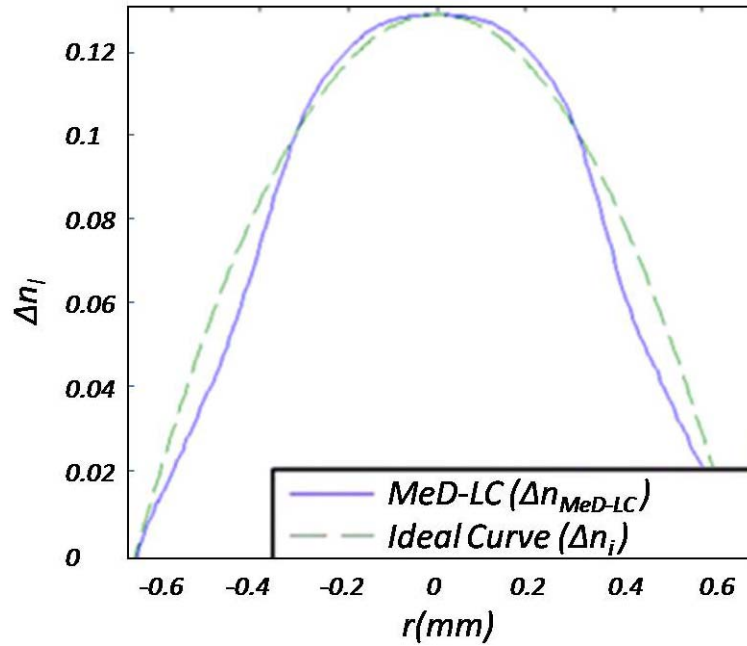


Figure 3-3 The profile of Δn_l generated by MeD-LC Lens and an ideal lens for around 3.5cm focal length. The ideal lens represented by a parabolic curve is compared with that of MeD-LC, presenting a deviation from the ideal case.

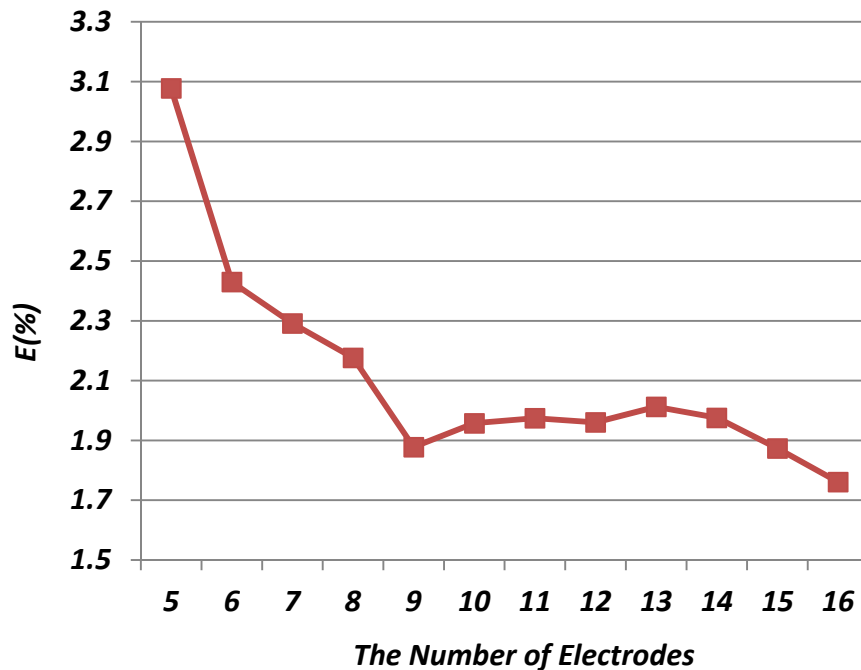


Figure 3-4 The quantified errors, E , representing the deviation of the results of MeD-LC from the parabolic curve, is utilized to optimize the number of electrodes for MeD-LC Lenses.

3.3 Experimental Results

Cylindrical MeD-LC Lens with 9-electrode and $W_E/W_S = 1$ for 1.5mm aperture size was investigated. For convex lens applications, the driving voltages of each electrode, as shown in Figure 3-5, were optimized for different focal length according to the focusing profile. The result showed a symmetrical arrangement. Each driving voltage was adjusted for particular focal length. In the convex MeD-LC Lens, marginal driving voltages are higher than central voltages to form convex-like phase retardation. As the total energy increased, the focal length was shortened. Figure 3-6 (a) and (b) illustrates the experimental setup and the comparison performed by the structures with external, internal electrodes mentioned above, and MeD-LC Lens. All of the structures with 60um LC cell gap, 1.5 mm aperture size and the same substrate were illuminated by 632.8nm Hi-Ne LASER and investigated the optimized focusing profile for focal length of 4cm, 7cm, and 10cm. The focusing profile was measured by GENTEC Beamage Series CCD sensor placed in front of the LC lenses by a distance of focal length. Corresponding cross-section (bottom right) and FWHM (bottom left) of the focusing profile are shown as well. For two of the conventional LC lenses, although the external structure generated acceptable focusing at focal length from 7cm to 10cm, the 4cm showed a broken result in beam profile. On the other hand, internal structure yielded adequate results from 4cm to 7cm, but the poor focusing at 10cm which the FWHM was much increased also indicated the limitation of low freedom of control. Comparing to the results, MeD-LC Lens yielded a wide range of superior focusing at all of 4cm, 7cm, and 10cm focal length that FWHM of focusing profile was maintained narrower.

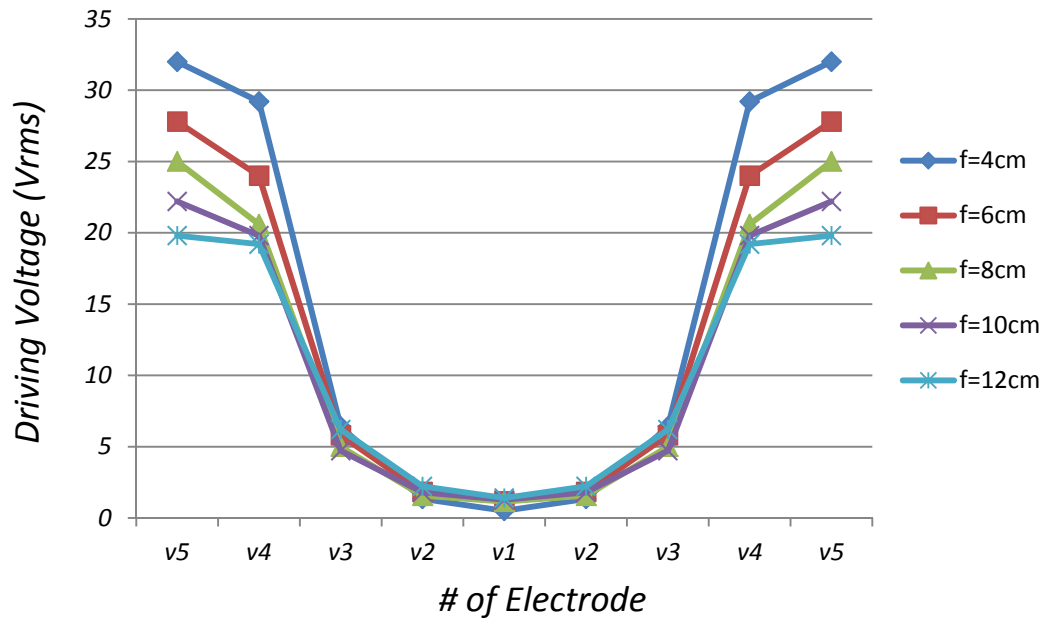
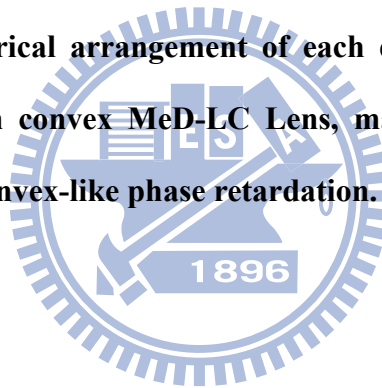
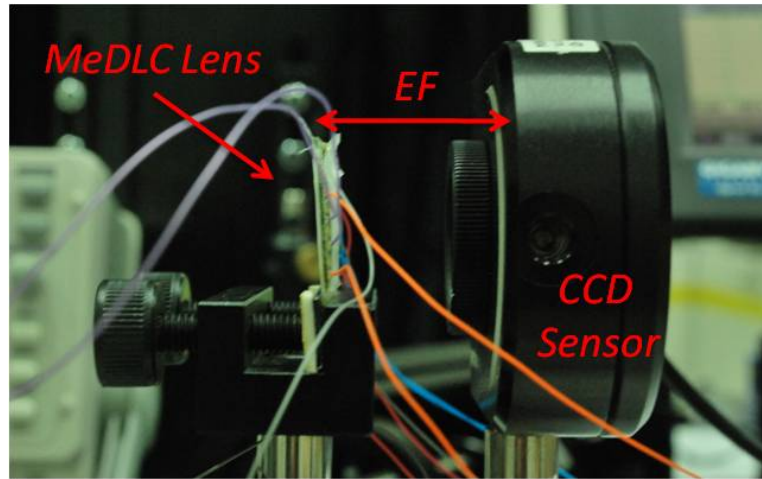
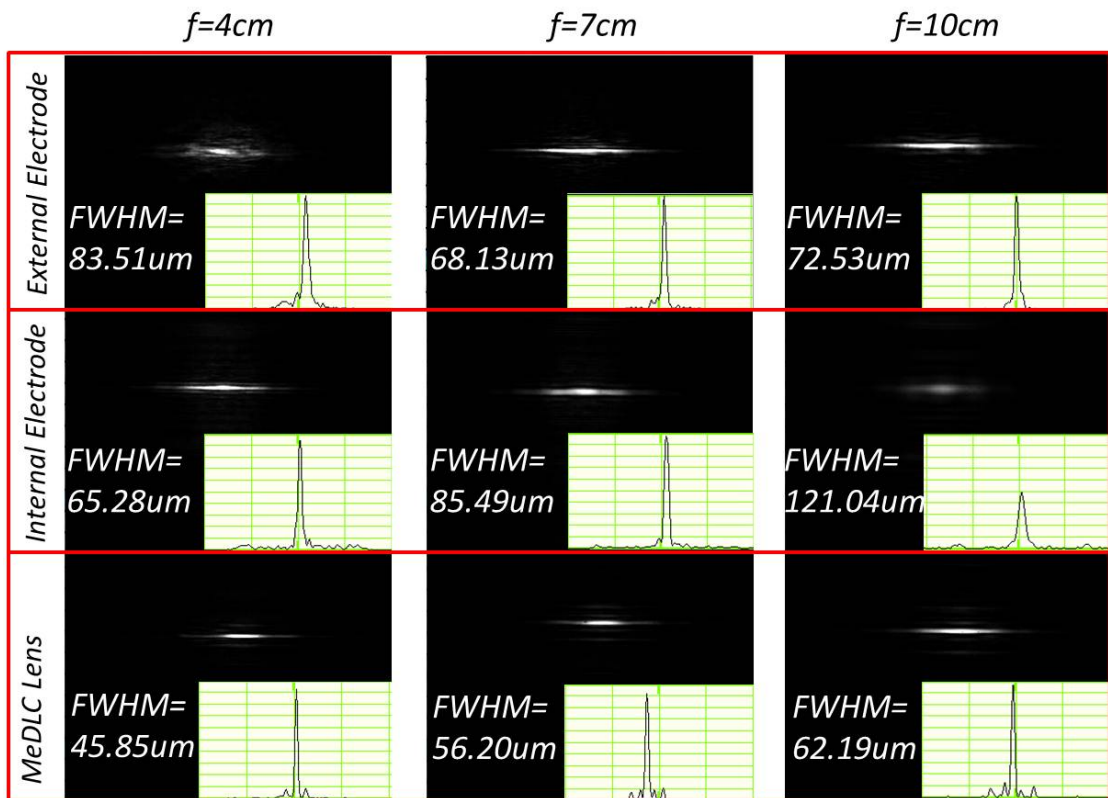


Figure 3-5 The optimized driving voltages for 9-electrode MeD-LC Lens in convex applications. The symmetrical arrangement of each driving voltage was adjusted for particular focal length. In convex MeD-LC Lens, marginal voltages are higher than central voltages to form convex-like phase retardation.





(a)



(b)

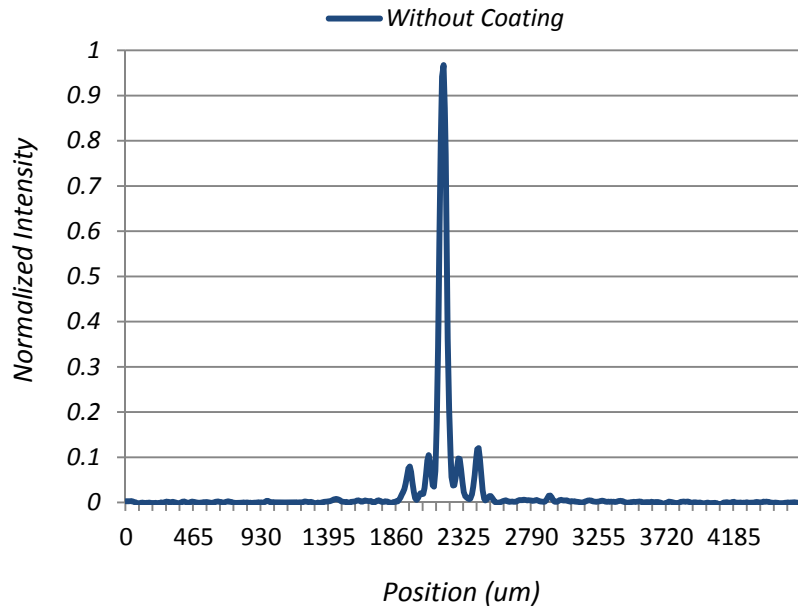
Figure 3-6(a) Cylindrical MeDLC Lens measured by CCD sensor at a distance of corresponding focal length (EF), and (b) the focusing profile were compared with two conventional LC lens. As the results shows, two conventional LC lenses only yielded a particular range of focusing. On the other hand, the multi-electrode of MeDLC Lens served the LC layer optimized phase retardation for each focal length and a wide range of focusing.

In our experiments, MeDLC Lens provided a smooth variance in focal length and maintained superior focusing profile. By the high freedom of multi-electrically driven, electrical field was significantly modified for different focal length from 3.5cm to infinity with 1.5mm aperture size and 60um LC cell gap. In the comparison, conventional LC lens with low control freedom only yielded focusing in a particular and narrow range. This phenomenon limits the applications for tunable lenses. MeDLC Lens provided stable performance in focusing for a wide range. This benefit can increase the feasibility for applications and achieve a highly tunable lens.

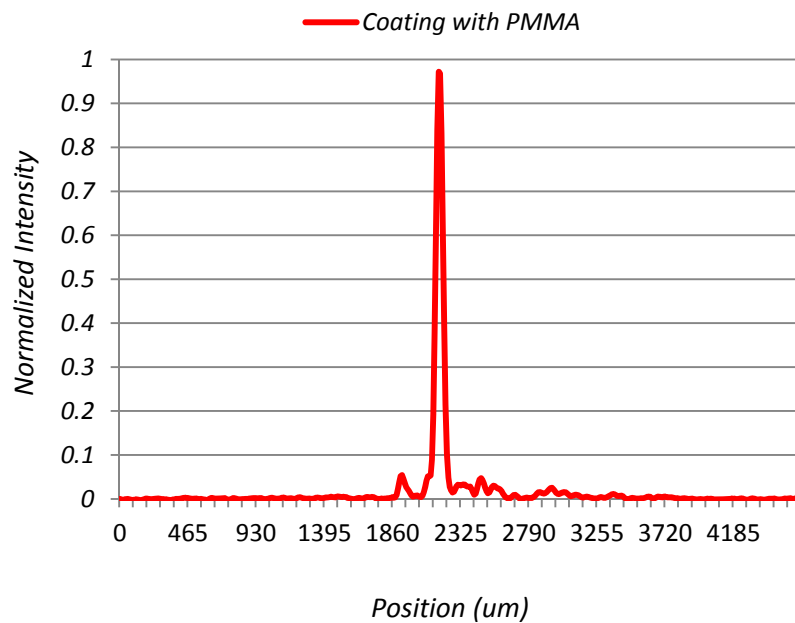
3.4 Discussion - Grating Structure of MeD-LC Lens

The electrodes of MeD-LC Lens, as shown in and the results are shown in Figure 3-2, generated obvious side lobes due to the particularly periodic grating structure. The side lobes may suppress image quality and increase the cross-talk effect. To reduce the side lobes, coating with material having high transmittance and approximate reflective index to ITO can effectively achieve. In our study, PMMA was utilized whose transmittance is larger than 90% with around 1.5 reflective index ($n_{\text{PMMA}} = 1.5$) for visible light. The result is illustrated in Figure 3-7. MeD-LC Lens coating with PMMA showed a suppression of intensity in the side lobes. Although this phenomenon cannot be totally eliminated due to mismatch of reflective index, through the coating method, this issue was much reduced.

Besides, different width of the control electrodes also yields different optical properties. For example, thinner width of the electrode at the border can further finely control the LC orientations, as Figure 3-8 shows. However, the thinner area of the electrode requires higher driving voltage to maintain the same electric energy, which may much increase the driving voltage.



(a)



(b)

Figure 3-7(a) The focusing profile of MeD-LC Lens without coating PMMA and (b) coating with PMMA for suppressing the intensity of side lobes. The large side lobes of focusing profile due to the grating structure of MeD-LC raised undesired cross-talk effect. The coating material with approximate reflective index can effectively reduce the side lobes.

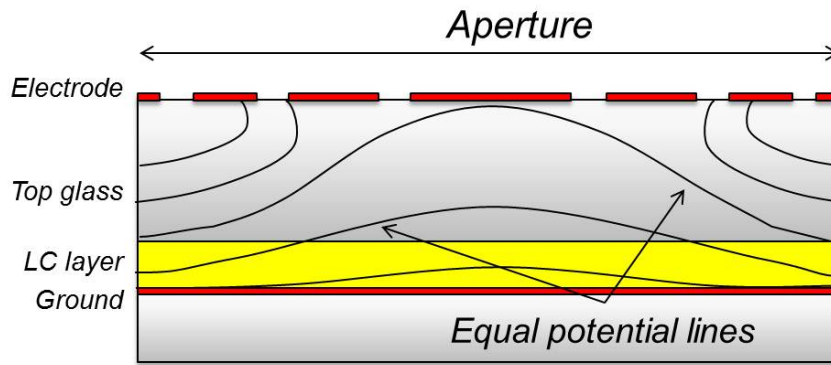


Figure 3-8 MeDLC lens with different width of electrodes to further finely control the LC orientations.

3.5 Conclusion

Multi-electrically Driven Liquid Crystal Lens (MeDLC Lens) was proposed to realize a highly tunable LC lens with wide range of superior focusing. Through high freedom of multi-electrically control, the phase retardation of LC layer was significantly optimized for different focal length. In the comparison, two of general homogeneous LC lenses with external and internal electrodes were investigated. The results showed conventional LC lenses with small number of driving electrodes limit the focusing range, and only can be apply to particular focal length for acceptable focusing performance. For cylindrical MeDCL Lens with 60um LC cell gap and 1.5mm aperture size, the focusing was tunable from 3.5cm to infinity. Furthermore, corresponding FWHM of focusing profile was maintained narrower. These results indicated MeDLC Lens increase the feasibility for tunable lenses. A smooth variance in focal length and stable focusing performance in wide range were also achieved.

Chapter 4.

Gradient Driven Liquid Crystal Lens Exhibiting

Ultra-low Operating Voltages

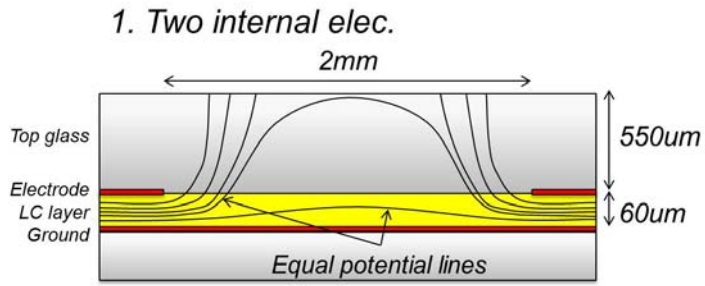
So far, although we applied the structure of MeDLC lens to improve the optical properties for each focal length, we can find the driving voltage of MeDLC lens is still high ($\sim 30V_{\text{rms}}$). Obviously, it is not only means the results are still unfeasible for general applications but also indicate the structures of LC lenses should be intrinsically innovated. In this chapter, a novel structure named Gradient Driven LC lens (GD-LC lens) was proposed. This structure intrinsically reduced the requirement for driving voltage down to few voltages. Combining with the concept of multi-control of MeDLC lens, GD-LC lens not only can be driven by operating voltage but also the driving frequency.

4.1 Introduction

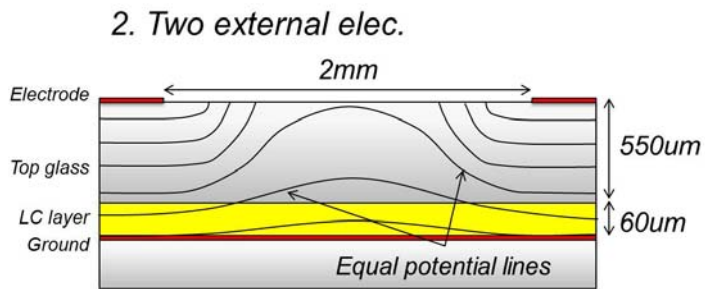
Before getting into GD-LC lens, we have to discuss why the conventional structures of LC lenses usually require high driving voltage and long focusing time. Figure 4-1 (a-d) shows four kinds of homogeneous LC lenses including internal and external electrodes with single control and multi-control. Each of them was simulated the distribution of electric field inside the LC cells, as the green line shows the equal potentials. For the first structure, two internal electrodes (Figure 4-1 (a)), as the driving voltage was applied, we can find the gradient variation of electric field was yielded. This kind of electric field can be used to generate a lens profiled of phase retardation in the aperture of the electrodes. However, ratio of the potential really applied to the LC cell to generate the LC effect was low (around 10% as indicated in the figure), which means as we applied $30V_{\text{rms}}$ to the electrodes, only around $3V_{\text{rms}}$ was used. In fact, the most of the electric field leaked outside of the LC cell. On the other hand, the structure with external electrodes, as shown in Figure 4-1 (b), although the insertion of high K

material (i.e. the glass) can smooth electric field communicated to the LC layer, the ratio of the potential really applied to the LC cell was low as well. Besides, the potential difference between the border and center was small. For the structure of MeDLC lens (Figure 4-1(c)), as discussed in Chapter 3, we can notice MeDLC lens has higher ability to control the electric field communicated to the LC layer than that of structure with only two electrodes, but it still had the drawback of low efficiency. Only around 10% voltage difference was really applied to the LC cell. Therefore, the driving voltage was required very high. The last structure, internal multi-electrode, as shown in Figure 4-1 (d), simulated discrete electric field in the LC cell due to the non-uniform arrangement of electrodes. This kind of electric field cannot generate lens profile which requires a smooth variation in the orientation of LC directors. Nevertheless, the potential applied to the LC cell can be totally fed to deform the LC molecules.

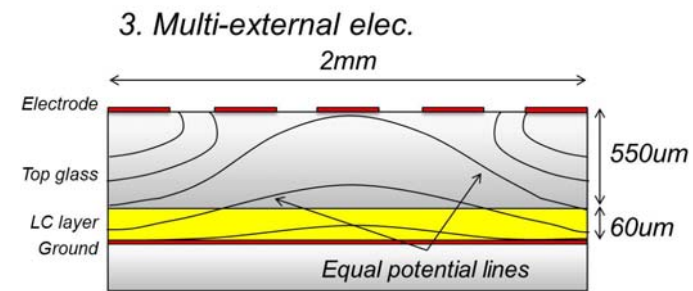
To summarize the above discussion, our previous simulation work indicated the configuration with internal continuous-distributed electrode has the ability to achieve gradient electrical field and maintain the energy inside the LC layer. These two features not only yielded the gradient phase retardation, but also sufficiently employed the applied energy. Figure 4-2 shows a structure for achieving these. Inside the LC layer, the applied energy is conserved by the covered continuous-distributed electrode, as the equal-potential lines show, which is distinguished from the conventional structures leaking out the electrical field. The generated gradient electrical field, as well, yielded gradient distribution of LC molecule to form lens-like phase retardation. Thus, the applying voltage can be reduced which also implied the focusing time can be improved.



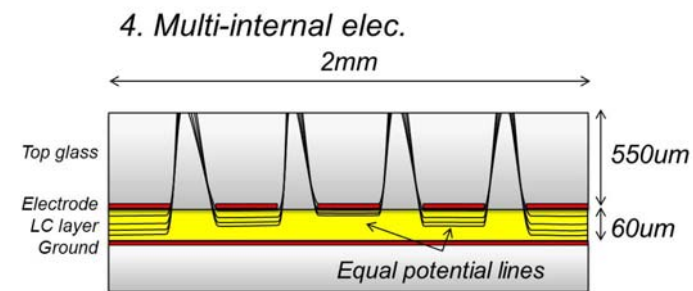
(a)



(b)



(c)



(d)

Figure 4-1 The simulations of electric field for four kinds of homogeneous LC lenses including (a) internal single control, (b) external signal control, (c) external multi-control, and (d) internal multi-controls.

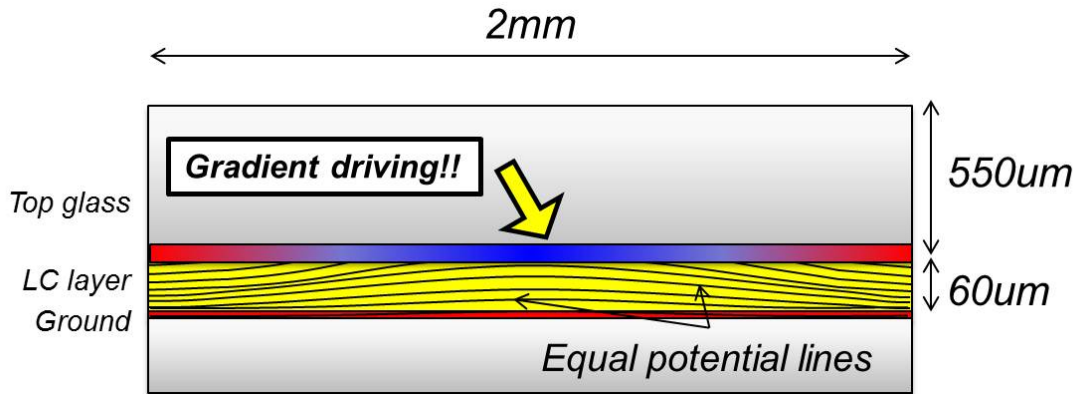


Figure 4-2 The structure of internal continuous electrode performs a smooth gradient electrical field and can conserve the electrical energy inside the LC layer.

4.2 Gradient Driven Liquid Crystal Lens (GD-LC Lens)

4.2.1 Concept

To achieve the configuration as shown in Figure 4-2, Gradient Driven Liquid Crystal Lens (GD-LC Lens) was proposed to intrinsically solve the issue of high driving voltage and slow focusing. GD-LC Lens utilized a high resistance layer (high R layer) to be the internal continuous-distributed electrode to achieve low operating voltage and improve the focusing time simultaneously. Experiments for testing the properties of the high R layer were investigated. The high R layer, which was spin coated on a substrate to connect two controlling electrodes. This structure generated gradient electrical distribution when applied two different operating voltages on each controlling electrode. Clevious P (sheet resistance $\sim 1M\Omega/\square$) from Baytron was chosen to be the high R layer. A $60\mu\text{m}$ cell gap of LC molecule, E7 ($\Delta n=0.2$) from Merck, was anti-parallel directed to controlling electrodes. Two of the controlling electrodes were separated by 2mm, as Figure 4-3 shows. In the investigation of spatial phase retardation, different operating voltages driven at 1 kHz were applied to the right side of controlling electrode. The left side electrode was grounded to yield an initial potential difference (ΔV) between two electrodes. Different interference pattern were observed by changing operating voltage. At $V=3V_{\text{rms}}$, the interference pattern was denser on the right side, as shown in Figure 4-4 (a). This pattern indicates a convex lens can be achieved

by symmetrically combining two identical structures with the same operating voltage. On the other hand, at $V=5V_{rms}$, the interference pattern was denser on the right side, as shown in Figure 4-4 (c). A concave lens also can be realized by the driving. Figure 4-4 (b) shows linear phase retardation between two electrodes which is unsuitable for lens applications.

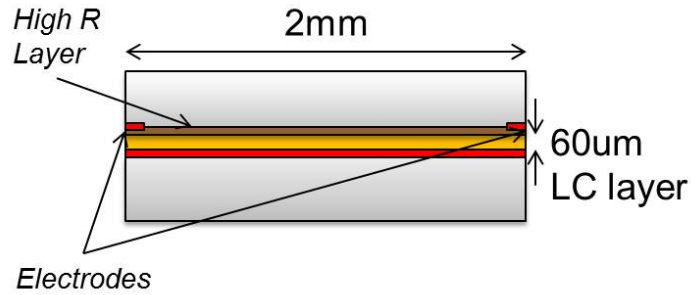


Figure 4-3 The testing device of LC cell with high resistance layer connected by two controlling electrodes.

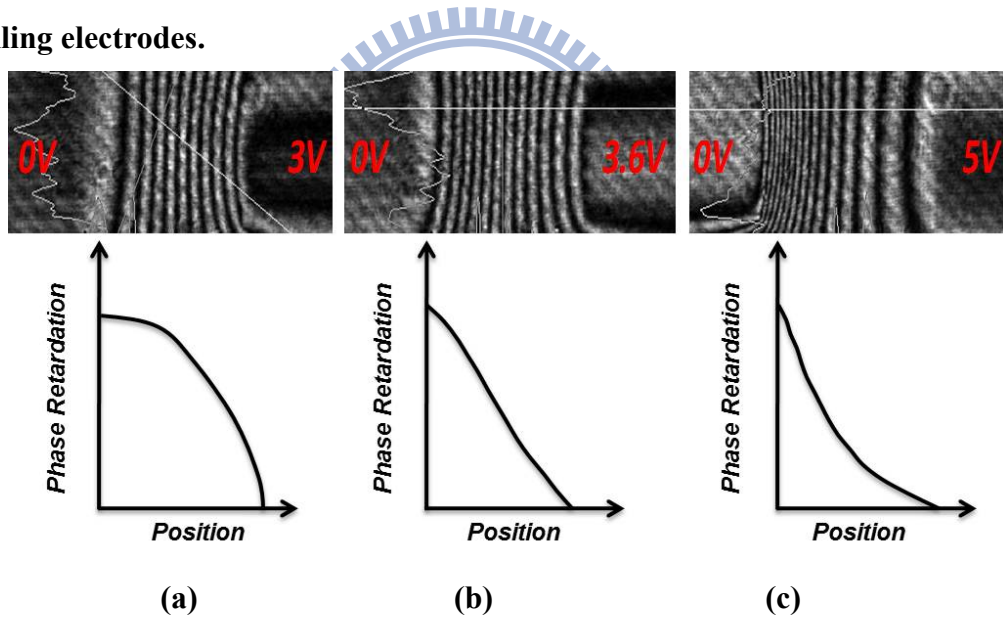


Figure 4-4 The results of interference pattern of the testing device driven by different operating voltages, (a) $\Delta V=3 V_{rms}$, (b) $\Delta V=3.6 V_{rms}$, and (c) $\Delta V=5V_{rms}$. The LC cell was design by $60\mu m$ cell gap driven by the two controlling electrodes with 2mm separation.

4.2.2 Structure and Principles

According to the testing results, the structure of GD-LC Lens was constructed by combining triple internal electrodes with the high resistance layer. Three controlling electrodes included two marginal controlling electrodes and a central controlling electrode. By applying the

voltage on the marginal electrodes and making the central electrode grounded, GD-LC Lens was driven in convex mode. Oppositely, concave mode can be achieved by the central controlling voltage with two grounded marginal electrodes. The arbitrary electric field gradient profile was achieved by adjusting driving voltages. The structure is shown as Figure 4-5.

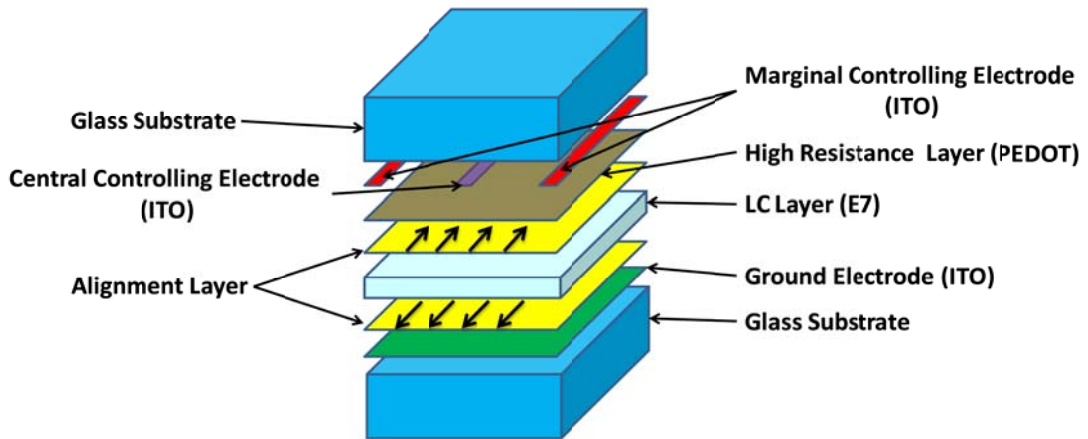


Figure 4-5 The configuration of GD-LC Lens. The structure with 2mm lens aperture and 60um anti-parallel LC cell gap was constructed by combining triple internal electrodes with the high resistance layer.

A similar concept, LC lens with Modal Control [62-65], was proposed by A. F. Naumov et al. In the research, a high resistance layer was utilized as the control electrode, and the thin LC layer was used to create a gradient electrical field. However, the numerical aperture (NA) was relatively low due to the controlling approach and the thin LC layer [66]. This situation limited the applications in cameras which may require short focal length and large F/# to perform AF for near object and have higher optical throughput.

In our simulation, voltage distribution of high resistance layer across the LC layer modeled by the transmission line

$$\nabla^2 V = \gamma^2 V \tag{4-1}$$

where

$$\gamma = \sqrt{(R + j\omega L) \cdot (G + j\omega C)} \quad (4-2)$$

indicates the basic parameters of transmission lines. The resistance R in Equation (4-2) is calculated as following

$$R = \frac{\rho_r}{A_r} l_r = \frac{\rho_r}{t_r \cdot w_r} l_r = R_s \frac{l_r}{w_r} \quad (4-3)$$

where ρ_r is the conductivity of the high R layer. A_r and l_r are the cross section and length of the resistance. R_s is equation (4-3) is the sheet resistance. The schematic is shown in Figure 4-6.

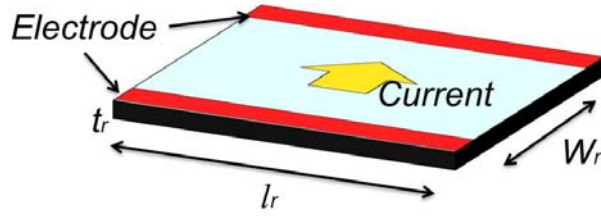


Figure 4-6 The schematic of resistance of the controlled high R layer.

To calculate the capacitance C in Equation (4-2), the structure was firstly considered to be controlled under uniform electrode field. The induced dipole moments of two directions parallel and perpendicular to LC direction, as shown in Figure 2-4, were used. The equivalent polarization is

$$\begin{aligned} P_z &= |\vec{P}_{\parallel}| \sin \theta + |\vec{P}_{\perp}| \cos \theta = \varepsilon_0 (\chi_{\parallel} \sin^2 \theta + \chi_{\perp} \cos^2 \theta) E \\ \Rightarrow \chi_z &= \frac{P_z}{\varepsilon_0 E} = \chi_{\parallel} \sin^2 \theta + \chi_{\perp} \cos^2 \theta \end{aligned} \quad (4-4)$$

The schematic is shown in Figure 4-7. The electric field was along the z direction which induced the polarization, \vec{P}_{\parallel} and \vec{P}_{\perp} . The equivalent capacitance, C , could be calculated by χ_z as

$$C = \frac{\varepsilon A}{d} = \frac{1 + \chi_z}{d} A \quad (4-5)$$

where d and A were the thickness and area of the meshed element respectively. The conductance, G , and inductance L , in Equation (4-2) were ignored for the calculations.

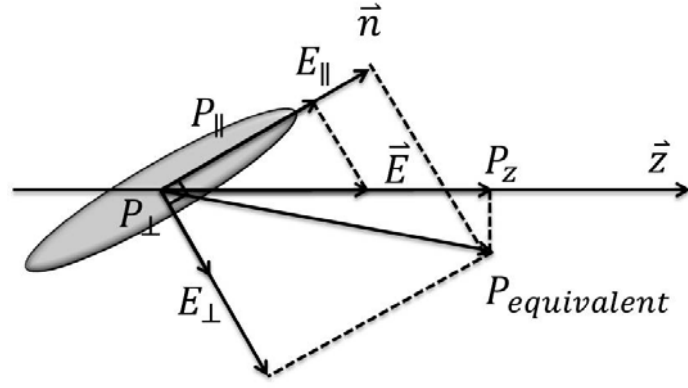


Figure 4-7 The schematic of induced polarizations by z direction electric field.

The LC direction, angle θ , of LC molecule over the cell gap derived by Euler-Lagrange method can be described by splay geometry driven by uniform electric field, E ,

$$\left(\frac{E}{E_c}\right)\left(\frac{z}{h}\right) = \frac{1}{\pi} \int_0^{\theta(z)} \left(\frac{\cos^2 \alpha + (K_{33}/K_{11}) \sin^2 \alpha}{\sin^2 \theta_m - \sin^2 \alpha}\right)^{1/2} d\alpha \quad (4-6)$$

where K_{11} , and K_{33} represent the splay and bend of Frank elastic constants respectively. θ_m is the maximum angle in the middle plane of LC layer which can be numerically calculated by replacing z by half thickness of the LC layer, $h/2$. The threshold field E_c is

$$E_c = \frac{\pi}{h} \sqrt{\frac{K_{11}}{\epsilon_0 \Delta \epsilon}} \quad (4-7)$$

which indicates there is a minimum voltage to distort the LC directions. By interacted calculations, Figure 4-8 shows the simulation result, which the solid line and dotted line means the voltage distribution and the corresponding phase retardation, respectively. Although the gradient voltage distribution was simulated, the phase retardation was unpredicted in the low voltage region from the model only considering the configuration as transmission line and driven by uniform electric. The complete electrical field should be considered in simulations.

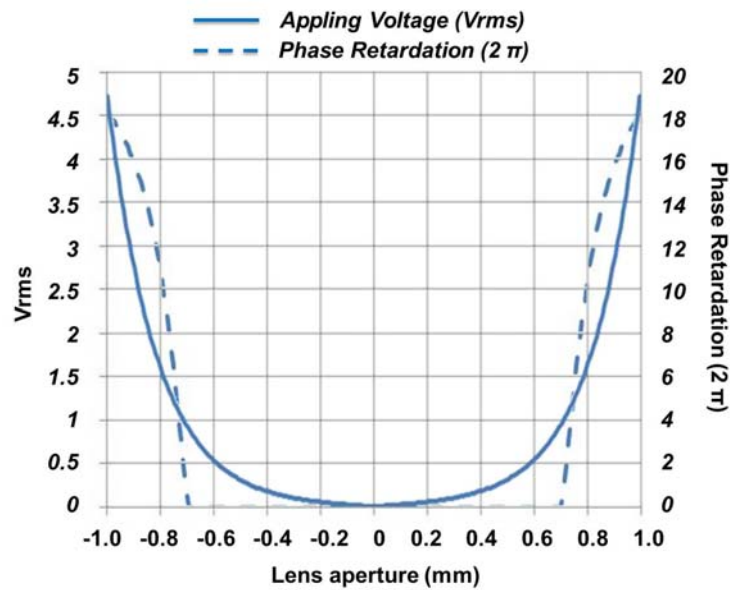


Figure 4-8 The simulated voltage distribution and corresponding phase retardations, the region which applying voltage under threshold value cannot distorted the LC directions. In other words, the model only considering the configuration as transmission line and driven by uniform electric may miss the accuracy of complete electrical field simulations.

Although the simulation work cannot obtain information for analyzing of GD-LC lens, an R-C circuit can be used to model this structure, as show in Figure 4-9. From the circuit, following principles could be observed.

- GD-LC lens can be voltage and frequency driving.
- The resistance of the high R layer should be control in a proper range. If the resistance is chosen too low. The resistance from the hetero junction will occupied large ratio of applied voltage. On the other hand, as the resistance of the high R layer is too large, only a small ratio of current can achieve the center area if V_1 is higher than V_0 . These two situations all result in no phase retardation in the central area.
- Extremely high frequency operation will result in smaller capacitance impedance. As a result, there is also small ratio of current pass through the high R layer to yield phase retardation.

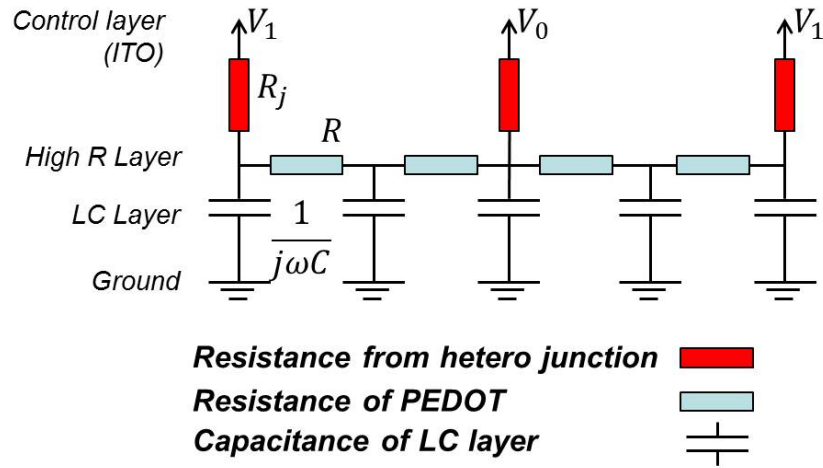


Figure 4-9 The R-C circuit utilized to model GD-LC lens.

4.3 Experimental Results

For investigation of focusing profile of GD-LC Lens in convex mode, the device with 2mm lens aperture was setup in front of GENTEC Beamage Series CCD sensor at a distance of corresponding focal length. The incident light source was 632.8nm polarized Hi-Ne LASER. The marginal controlling electrodes were driven at 2.4 kHz, and the central electrode was grounded and connected to the ground electrode. As the operating voltage was at $V=0$, the incident light passed through the device directly without focusing, as Figure 4-10 (a) shows. The top and bottom figures of Figure 4-10 indicate the top-view and cross-section of the measured beam profile. At $V=2.35V_{rms}$, which the phase retardation was driven in the convex mode, the incident light was converged, and showed a focusing result, as Figure 4-10 (b) illustrated. The results showed the structure of GD-LC Lens is feasible for lens applications. Although the 60um thickness of LC layer is tested, the operating voltage was low as 2.35Vrms for 5cm focal length.

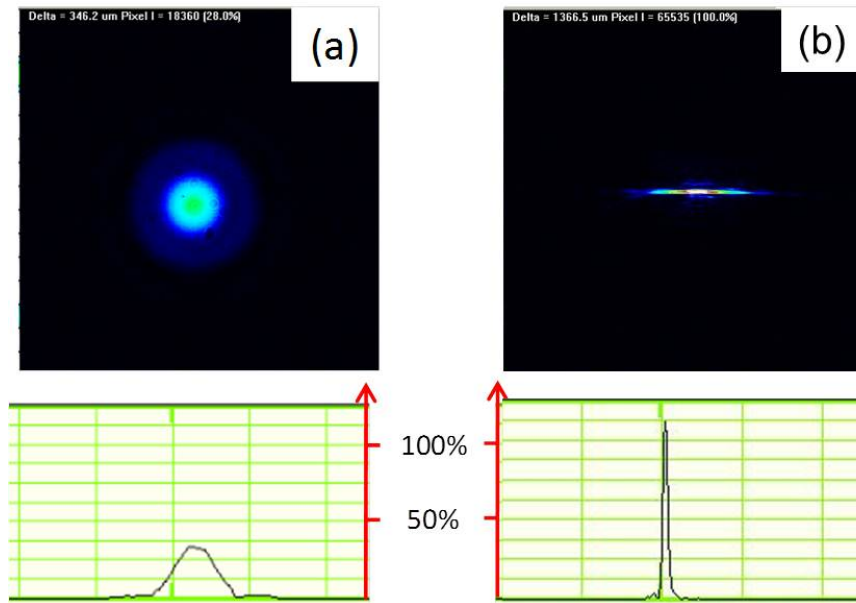


Figure 4-10 The focusing profile of GD-LC Lens driven at (a) $V=0$, and (b) $V=2.35V_{rms}@2.4kHz$ for 5cm focal length.

The focal length of GD-LC Lens is voltage and frequency dependent. As operating voltage and frequency increased, the focal length became gradually shorter. Figure 4-11 shows the relationship between focal length to operating voltage and frequency. In this study, the LC cell gap was designed as $60\mu m$ and the operating voltage was generally lower than $3V_{rms}$. The shortest focal length was 2.5cm which was not be further estimated due to the limitation of the experimental setup and the CCD sensor's structure. As Figure 4-11 shows, the range of driving voltage was from $1.9V_{rms}$ to $2.7V_{rms}$ to yield the focal length from 2.5cm to 10cm. By controlling the driving frequency, the focusing profile can be further modified, as shown in Figure 4-12. Through the result, the focusing profiles could be superior by the two control freedom, voltage and frequency. Although the profiles at the shortest and longest focal length cannot be as well as that of the middle range, these voltage-frequency control can yield wider range of focusing than that of external and internal structure in Figure 3-6. To achieve higher control freedom, the multi-electrode concept should be combined with GD-LC lens.

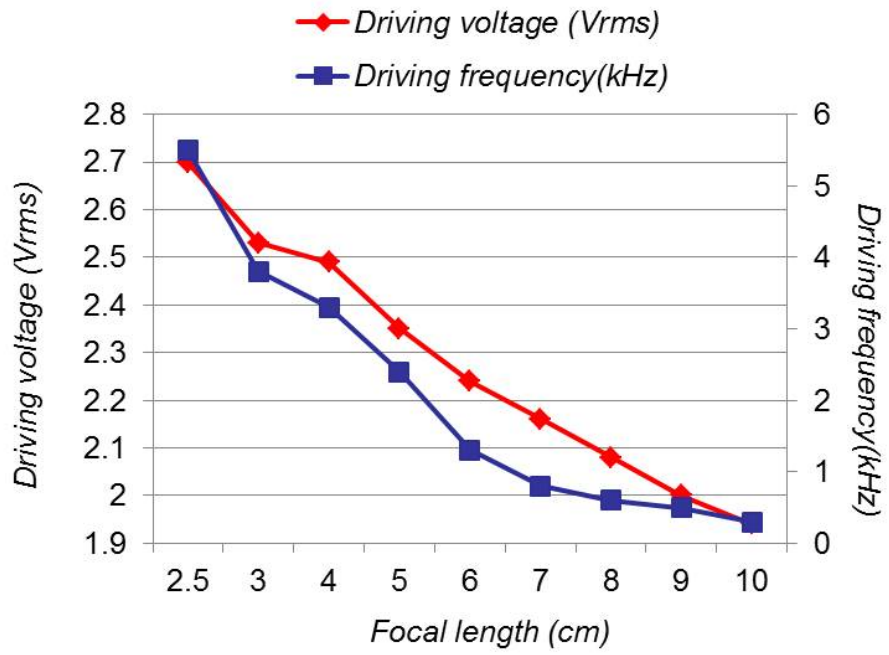
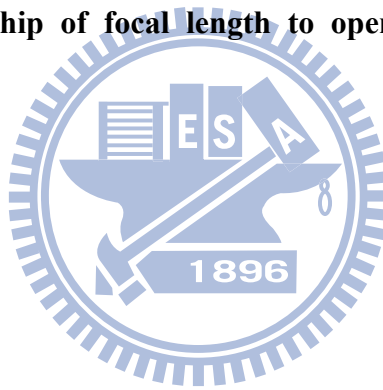


Figure 4-11 The relationship of focal length to operating voltage and frequency of GD-LC Lens.



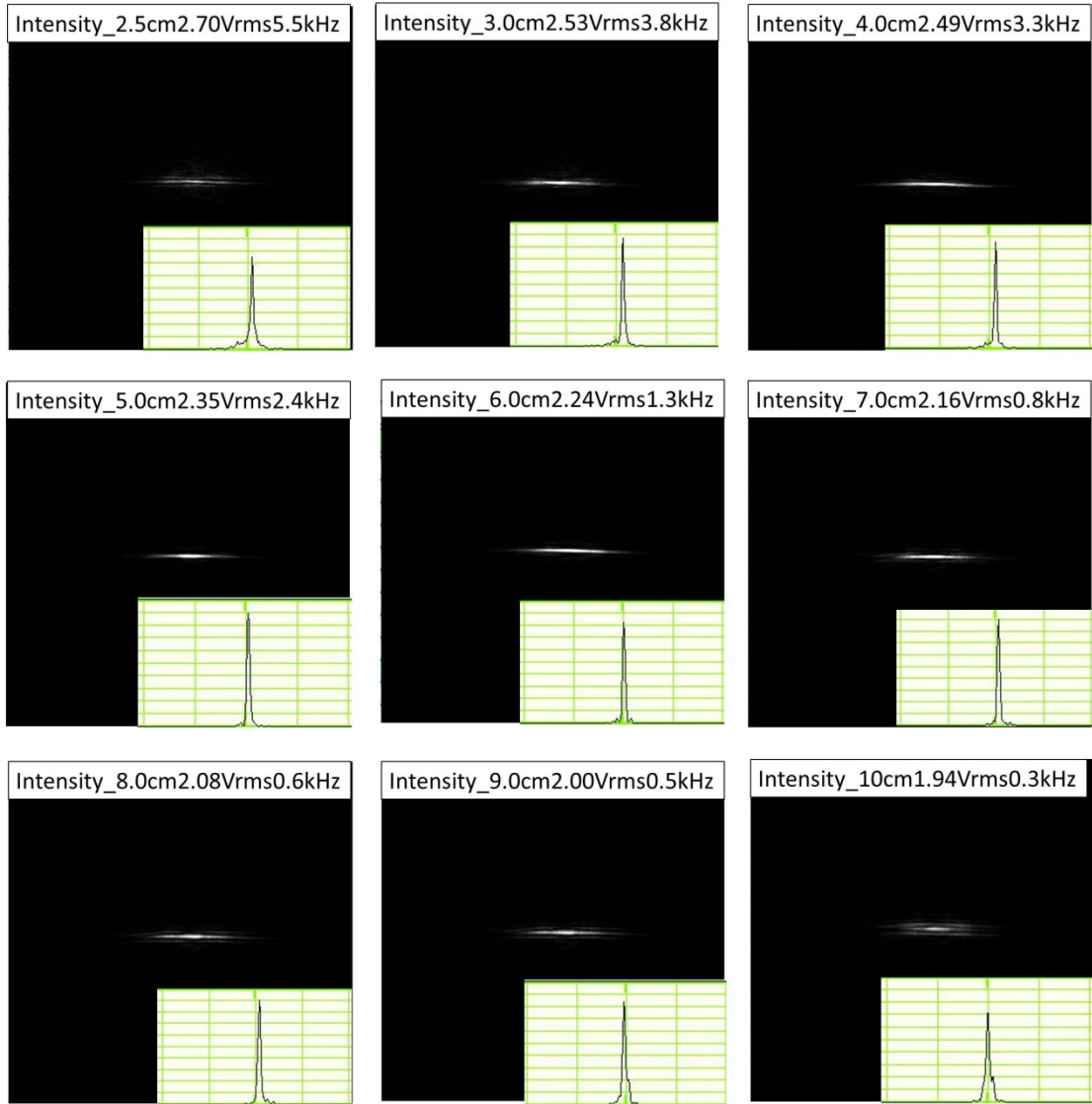


Figure 4-12 The focusing profiles of GD-LC lens at different focal length from 2.5cm to 10cm controlled by voltage and frequency.

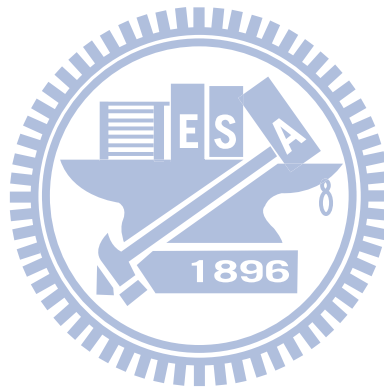
4.4 Phase Retardation of Convex and Concave Modes

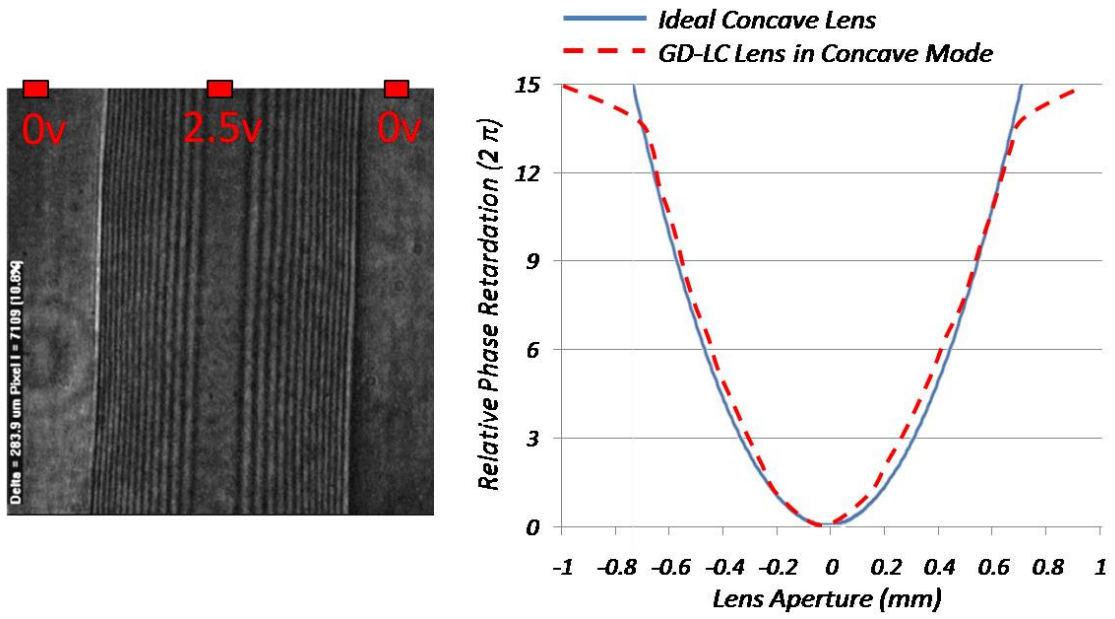
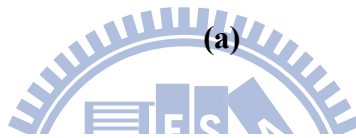
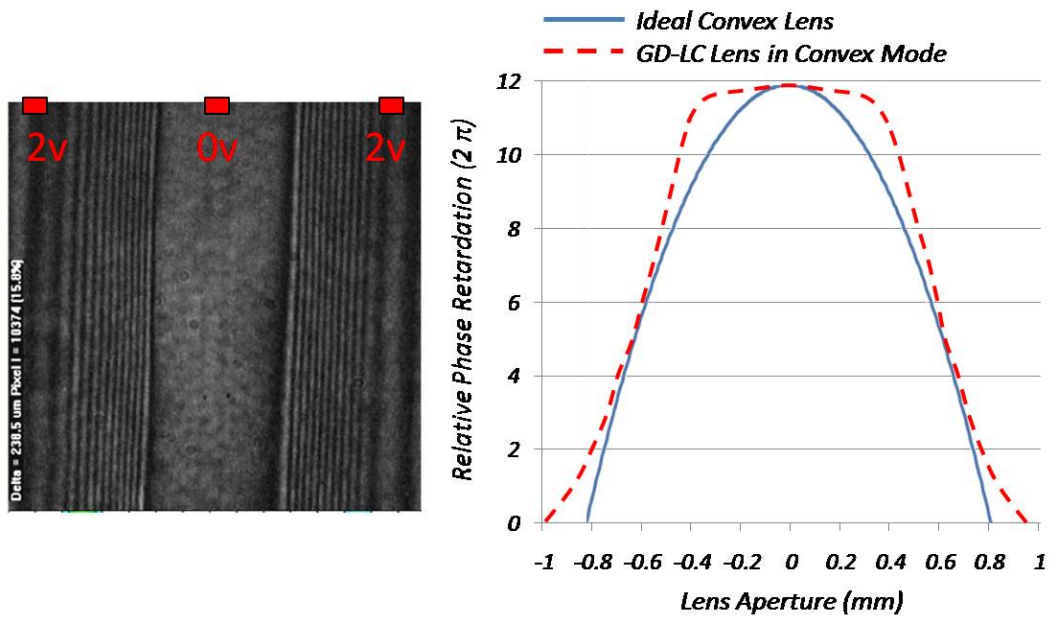
The interference pattern is one of the mostly used methods to measure the phase retardation of LC cells. To evaluate the optical properties of GD-LC Lens, we investigated the phase retardation by observing the interference pattern between the ordinary and extraordinary rays passed through the lens cell under crossed polarizers. The rubbing direction of the lens cell is oriented at 45° with respect to the fast axis of the linear polarizer. Two images of GD-LC Lens driven in convex and concave modes are shown in Figure 4-13 (a) and (b) respectively. In convex mode, as shown in Figure 4-13 (a), GD-LC Lens yielded a phase retardation

approximating to that of ideal lens with 1.6mm effective lens aperture. This result was coherent to that as shown in Figure 4-13, according to the following relation:

$$f \cong n_0 \cdot \frac{r^2}{2\Delta n \cdot d} \quad (4-8)$$

where r , and f donate the aperture radius, and focal length respectively. The central grounded electrode with two marginal controlling voltages drives GD-LC Lens in concave mode. The results presented the phase retardation is much closer to that of an effective ideal lens, as Figure 4-13 (b) illustrated.





(b)

Figure 4-13 The phase retardation of GD-LC Lens operated in (a) convex, and (b) concave modes. By the different operating arrangement, both convex and concave lenses were achieved.

Table 5 shows the summary of comparison between GD-LC Lens and conventional LC lens with internal electrodes. Through the result, GD-LC Lens dramatically improved 86.0 % operating voltage and can be only driven by less than 5V_{rms} which has been within the range of normal driver IC.

Table 5 The comparison of focusing time and corresponding operating voltage. The result shows GD-LC Lens significantly improved driving voltage and only can be only driven by less than 5V_{rms}.

Comparison	LC cell Gap	Operating Voltage
GD-LC Lens	60 μm (E7)	2.35 V _{rms}
Conventional LC Lens with Internal Electrodes	60 μm (E7)	~25V _{rms}

4.5 Conclusion

GD-LC Lens was proposed exhibiting ultra-low operating voltage for the structure with 60um LC cell gap and 2mm lens aperture. The focal length was voltage and frequency tunable driven by less than 5V_{rms}. Compare to the conventional result, which usually requires extremely high driving voltages, GD-LC Lens brought the applications utilizing LC lenses to be feasible and practical. Furthermore, both convex and concave effective lenses were achieved by the structure of GD-LC Lens with different operating voltage. Therefore, not only the structure of GD-LC Lens intrinsically solved the issue of high driving voltage in the applications of LC lenses but also the concept of gradient driven would be potentially used for future form of LC lenses.

Chapter 5.

Over-drive Method for Fast Focusing Liquid Crystal Lens

5.1 Introduction

As mentioned in previous sections, Liquid crystal (LC) is widely used in many optical applications because of the properties of high sensitivity to electric field and easy control. For lens applications, LC lens owns a very unique property that the focal length is electrically tunable without mechanical moving and shape changing. This advantage made applications for focal length tunable and switchable system slimmer and more compact. However, for lens application, optical power of LC lenses is relatively smaller than that of conventional lenses. Thus, thickness of the LC layer is usually required few tens or over hundreds of micrometers to generate high optical power rather than that of few micrometers in LCDs. The large thickness results in slow focusing time. For example, as the relation of optical power, P , shows

$$P = f^{-1} = \frac{2\Delta n(r)d}{r^2} \quad (5-1)$$

P is dependent on the difference of refractive index between that at border and center, $\Delta n(r)$, cell gap, d , and radius of aperture radius, r . The optical power is difficult to achieve 25m^{-1} , as the LC lens has 1mm aperture radius and 60um LC cell gap (Merck nematic E7), whose $F/\#$ is large as 20. As $\Delta n(r)$ is constrained by the index of material and only has a small region of variation due to structures of LC lenses, the cell gap is usually designed much thicker. According to rising time, τ_{rise} of LC devices, larger cell gap results in slow focusing time which is proportional to d^2 from relaxing state to focusing state, as Equation (5-2) shows.

$$\tau_{rise} = \frac{\gamma_1 d^2 / K \pi^2}{(V/V_{th})^2 - 1} \quad (5-2)$$

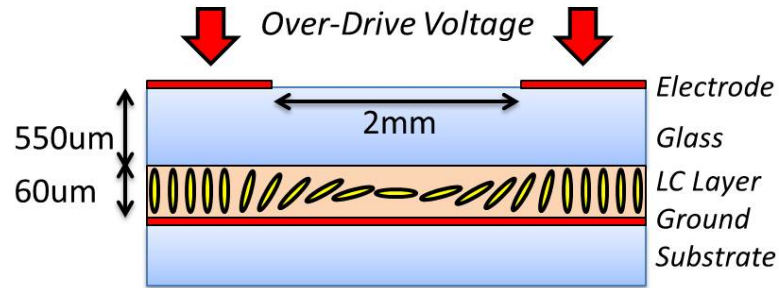
where τ_{rise} is the function of cell gap d , rotational viscosity γ_1 , elastic constant K , threshold voltage V_{th} , and applied voltage V . The slow focusing time makes applications unfeasible and unpractical, such as lens head in mobile devices which is requesting very fast auto-focusing or zoom functions, and 3D switchable displays having large numbers of viewing zones. To overcome slow response of LC cells, over-drive is employed for accelerating the response times in LCD industry. By optimized the over driving voltages and switching to target operation, the LC response time can be much reduced.

5.2 Over-drive Method for LC Lens

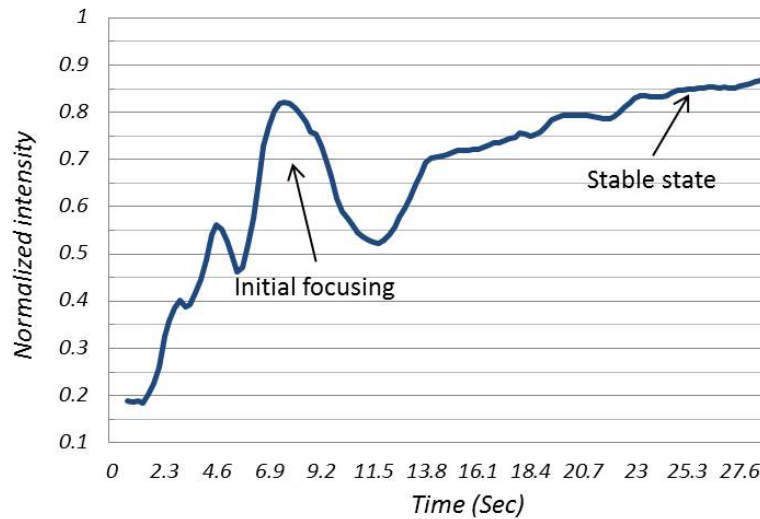
In this chapter, we propose Over-drive (OD) method for reducing the focusing time of LC lenses. Different from that for LCDs, the OD method investigated focusing behavior of LC lenses to determine the timing for switching. The appropriate operation can significantly reduce the focusing time.

For a test sample, we prepared a homogeneous LC lens structure with external driving electrodes which were patterned upon the glass, as shown in Figure 5-1(a). The electrodes were driven by OD voltage ($\sim 65V_{rms}$) which was higher than that for particular focal length ($\sim 45V_{rms}$ for 5cm). The variation of normalized focusing intensity with time which was used to indicate the variation of focusing performance, as illustrated in Figure 5-1 (b), was measured by GENTEC Beamage Series CCD sensor placed at the focal length of the LC lens illuminated by a laser source ($\lambda = 632.8nm$). The initial focusing shows the OD voltage generated an instantaneous but unstable focus. The following focus ability was immediately decay and went to a stable state. This phenomenon was investigated by Fluorescence Confocal Polarizing Microscopy (FCPM) method [67] to analyze the exact director of LC molecules rotated with time, whose details investigations of FCPM for LC lens will be discussed in following section. The analysis showed gradient electric field by the OD voltage deformed the LC directors to generate a phase retardation which modulated the incident light to have instantaneous focusing in the beginning of response. After the initial focusing, the LC

molecules rapidly and continually rotated to form another phase retardation that generated the focus in the stable state which had similar focusing intensity with the initial focusing, although the two forms of LC directors were totally different.



(a)



(b)

Figure 5-1 (a) General structure of homogeneous LC Lens driven by marginal over-drive voltages, and (b) The curve of focusing response time to normalized intensity on CCD sensor for a particular focal length. The over-drive voltages yielded a initial focusing as shown the first peak.

To perform the process of OD method, the switching operation was examined. In the experiment, the same test sample was driven by the OD voltage (~65Vrms) and then switched to 45Vrms for 5cm focal length while the focusing intensity was almost achieving that of the initial focusing. The variation of intensity is shown by the solid curve in Figure 5-2. From the result, the intensity curve was maintained and further increased to around 90% starting from

the position of the initial focusing instead of intensity decay, although there was tiny variation at the beginning of the switching. This result indicated the initial OD voltage rapidly forced the LC molecules to form a distribution which was approximate to that for optimized focusing. The switching operation, at this time, can further deform the LC orientations, and finally keep to stable focusing. Comparing with general operation which is shown by the double-line in Figure 5-2, the directly applying $\sim 45\text{V}_{\text{rms}}$ to the electrodes for 5cm exhibited a very slow increasing of focusing intensity. To achieve the same focusing performance, applying OD method can significantly improve the focusing time from around 25.3sec to 7.1sec in this experiment, as we defined the focusing time was when the intensity stably achieved 90%.

As mentioned previously, the director of LC molecules was rapidly rotated by the OD voltage. In fact, the timing of switching affected the result of focusing behavior. As the OD voltage was switched before the time of the initial focusing, meanwhile the LC directors have not at the orientations for optimized focusing; the maximum focusing intensity was achieved slowly due to the driving voltage was reduced. The similar situation was also occurred if the switching was performed after the initial focusing. The LC directors exceeded the orientations for maintaining the focusing instead rotating back due to the reduced driving voltage. The results are shown in Figure 5-3. The most improved result was obtained when the switching was performed at the time approximated to the initial focusing.

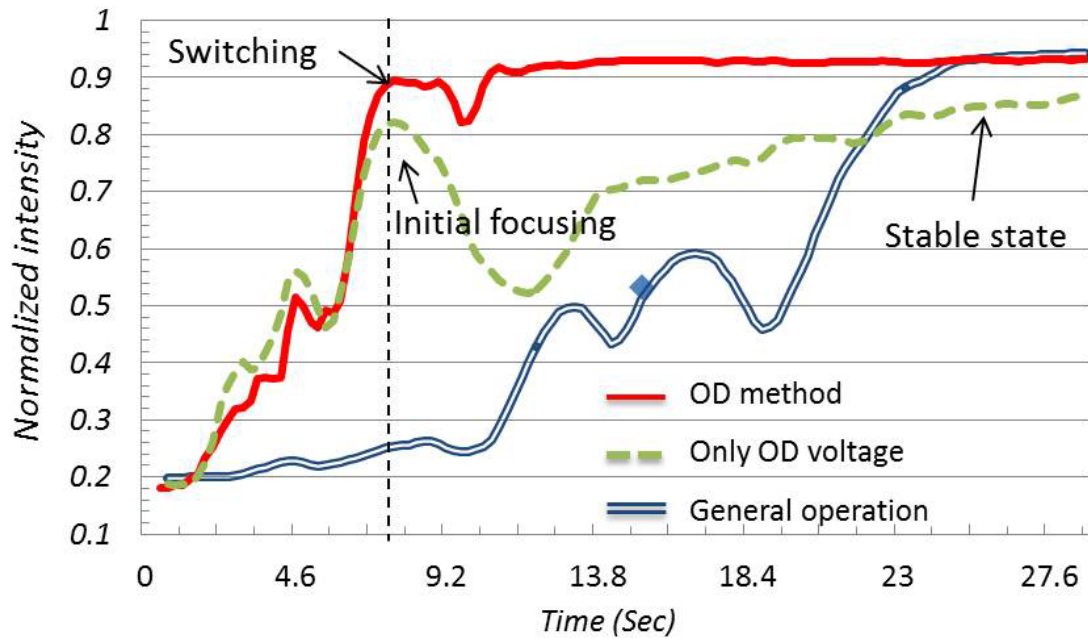


Figure 5-2 The variation of focusing intensity with time driven by OD method and general driving was measured by CCD sensor.

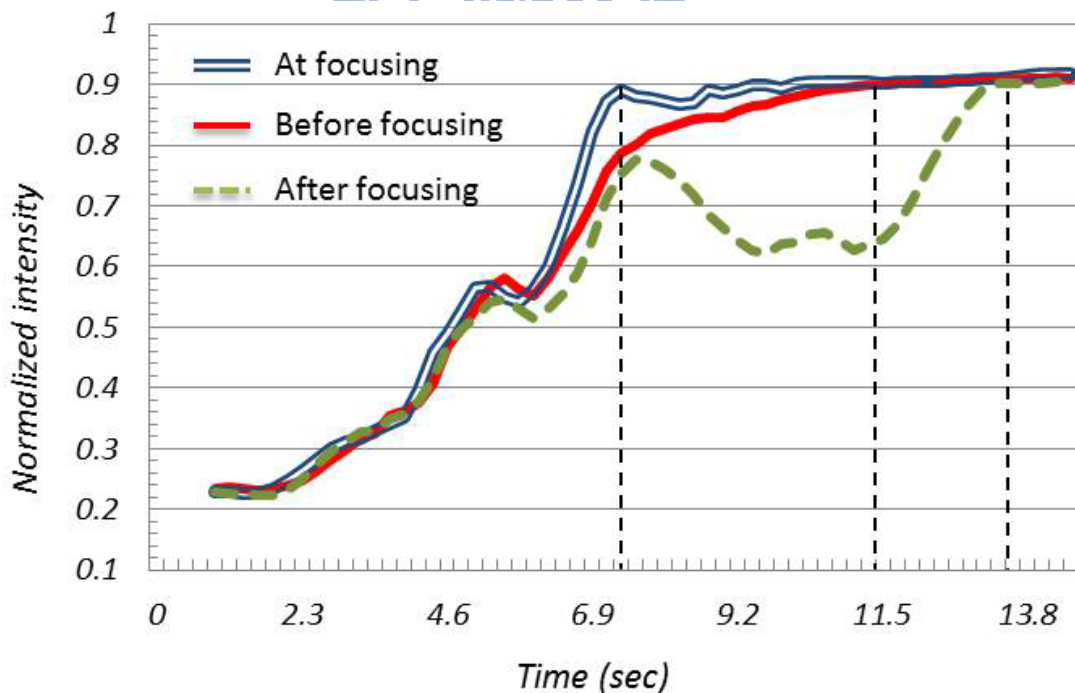


Figure 5-3 The results of OD method by different switching time. The switching at the time approximated to the initial focusing can obtained the shortest focusing time.

5.3 3-Dimensional Imaging and Analysis for LC Lenses by Fluorescence

Confocal Polarizing Microscopy

Fluorescence Confocal Polarizing Microscopy is a confocal microscopy system, whose photo detector would detect the fluorescent light intensity emitted from the dye molecules doped in the LC cell [68]. The transition dipole of the dye molecule is along the direction of the rod-shaped LC molecules, which means the tilt angles of the LC molecules are along the adjacent dye molecules. As shown in Figure 5-4, while the FCPM emits a laser with a linear polarization, \hat{P} , the probability of the photon absorption is proportional to $\cos^2(\alpha)$, where α is the angle between the transition dipole of the dye molecule and the polarization \hat{P} of the laser. The probability of the fluorescent photon reaches to the detector through almost the same polarization is proportional to $\cos^2(\alpha)$ if we assume the time of emission is much shorter than that of rotation of LC molecules [69]. The function of the pinhole is to filter out the fluorescence emitted from the dyes out of the region of focus. Therefore, the LC cell can be layer-by-layer scanned. The relation between the incident light intensity and the fluorescent light intensity of each scanning is

To investigate the phenomenon of instantaneously focus, FCPM was utilized to reconstruct the 3D orientation of LC layer. According to the fluorescent intensity of each LC layer, the orientation distribution was derived, and scales of fluorescent intensity, IFCPM, to LC tilt angle, α , is shown as follows:

$$I_{flu} = I_0 \cos^4(\alpha) \quad (5-3)$$

where I_0 is the intensity of laser light source, and I_{flu} is the intensity of detected fluorescence emitted from the excited dye molecule. By the calculation of Equation (5-3), the tilt angle of LC molecules in LC cell can be observed.

Through the focusing response time, optical path of the LC layer was calculated. The initial focusing indicated that the OD voltage generated a parabolic approximated phase distribution at the moment of the peak and the stable state. At the time before and after the

first peak, the phase retardation cannot yield a superior focusing on the CCD sensor. The curves of initial focusing and stable state also matched the corresponding focal length.

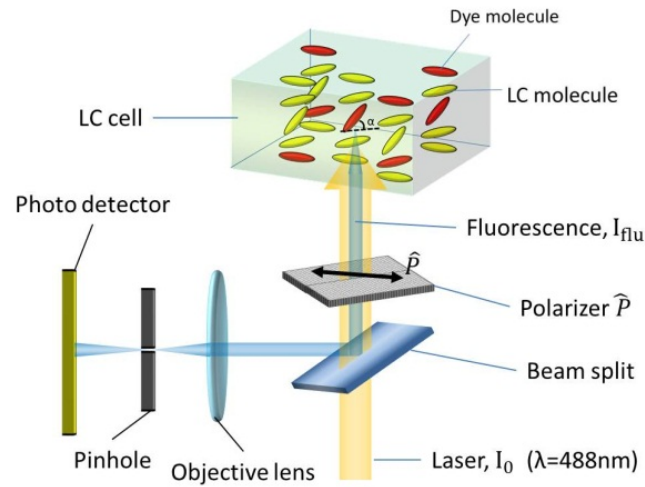


Figure 5-4 The diagram of the fluorescence confocal polarizing microscopy system.

5.3.1 3-D Imaging of LC lenses

To observe the 3-D image of LC orientations, a circle-electrode LC lens with 60 μm LC layer was prepared. The LC material used in the device were Merck nematic LC (E7) whose extraordinary refractive index $n_e = 1.7472$ and ordinary refractive index $n_o = 1.5271$. The alignment of the LC lens was anti-parallel rubbing and placed along the polarization of incident laser, whose wavelength is $\lambda = 488\text{nm}$, as Figure 5-5 shows. The laser light source scanned the LC cell from the 0 μm layer to the 60 μm layer with 5- μm vertical resolution, and the scanning area was 1.4 $\text{mm} \times 1.4\text{mm}$ when utilizing 10X objective. The detected intensity of excited fluorescence was used to represent the tilt angle of LC molecules. The scanned result before applying driving voltage is shown in Figure 5-6(a). The fluorescence intensity detected was uniform indicates almost the same director of LC molecules of the layer. The uniform result also shows the phase retardation was not different over the layer. After applying 20V $_{\text{rms}}$ on the electrode, the LC profile started to be deformed and the fluorescence intensity became central symmetrically darker at the border due to the larger tilt angle of LC molecules. We choose three of the layers to illustrate this, as shown in Figure 5-6(b-d).

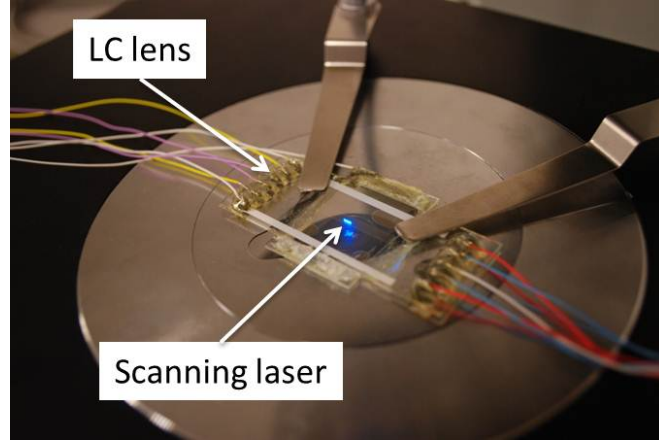


Figure 5-5 The setup of measure by FCPM.

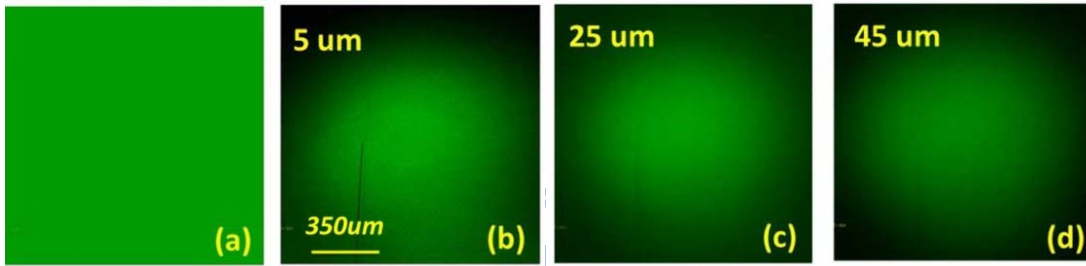


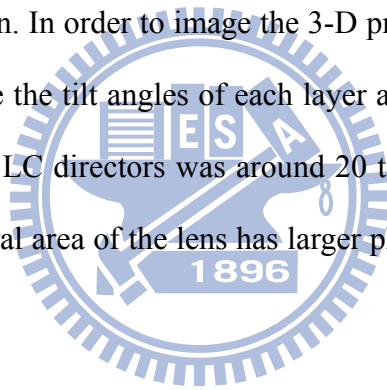
Figure 5-6 (a) The scanned result before applying driving voltage, and (b) ~ (d) that of scanned layers after driving.

In Figure 5-6 (b-d), we can notice the distributions of fluorescence intensity far away from bottom layer were more spherical that is because the different structure of top and bottom electrodes. However, the centers of the bright part are not coaxial, as shown in Figure 5-6 (c-d). This result not only indicates defect of fabrication but also the errors of measurement. The errors may be caused by non-horizontal scanning due to the placing of samples and the non-uniform of the doped dyes. According to Equation (5-3), the ratio of the intensity with and without driving voltage is equal to $\cos^4(\alpha)$, as following:

$$\frac{I_{voltage}}{I_{no\ voltage}} = \frac{I_0 \cos^4(\alpha)}{I_0 \cos^4(0)} = \cos^4(\alpha) \quad (5-4)$$

To calculate tilt angle, α , Equation (5-4) was more useful rather than Equation (5-3) due to limitation of dynamic range of the FCPM. The low dynamic range resulted in the initial intensity was need to be adjusted for observing the information of low brightness when the tilt angle of LC molecules became too large. Once the spatial distribution tilt angles, $\alpha(x, y, z)$,

of the LC lens is known, we can calculate the effective index $n_{eff}(\alpha)$ of each layer by Equation (2-8). By digital image processing, contours were plotted to indicate refractive index and tilt angle, as shown in Figure 5-7. As the contour shows, the index distribution of each layer was around 1.58 to 1.68, and Δn was only 0.1, which was not achieving the maximum $\Delta n_{max} = n_e - n_o \cong 0.22$ of E7 material due to the deformation of the LCs at the lens center and not vertical tilt angle of LCs at the border. Actually, in many structures designed for LC lenses, the Δn_{max} is difficult to be achieved. Therefore, the cell gap of LC layer is usually thicker, assuming the high optical power is required. In Figure 5-7, we can find the lens profile is not symmetrical, as mentioned previously. The contours are more broken in the top and bottom layers which were closed to the boundaries, while the layers near the middle layer had more smooth distribution. In order to image the 3-D profile of LC molecules, rod-like LC modal were used to simulate the tilt angles of each layer according the contours, as shown in Figure 5-8. The variance of LC directors was around 20 to 80 degree. The smaller degree at the center indicates the central area of the lens has larger phase retardation which resulted in a convex lens effect.



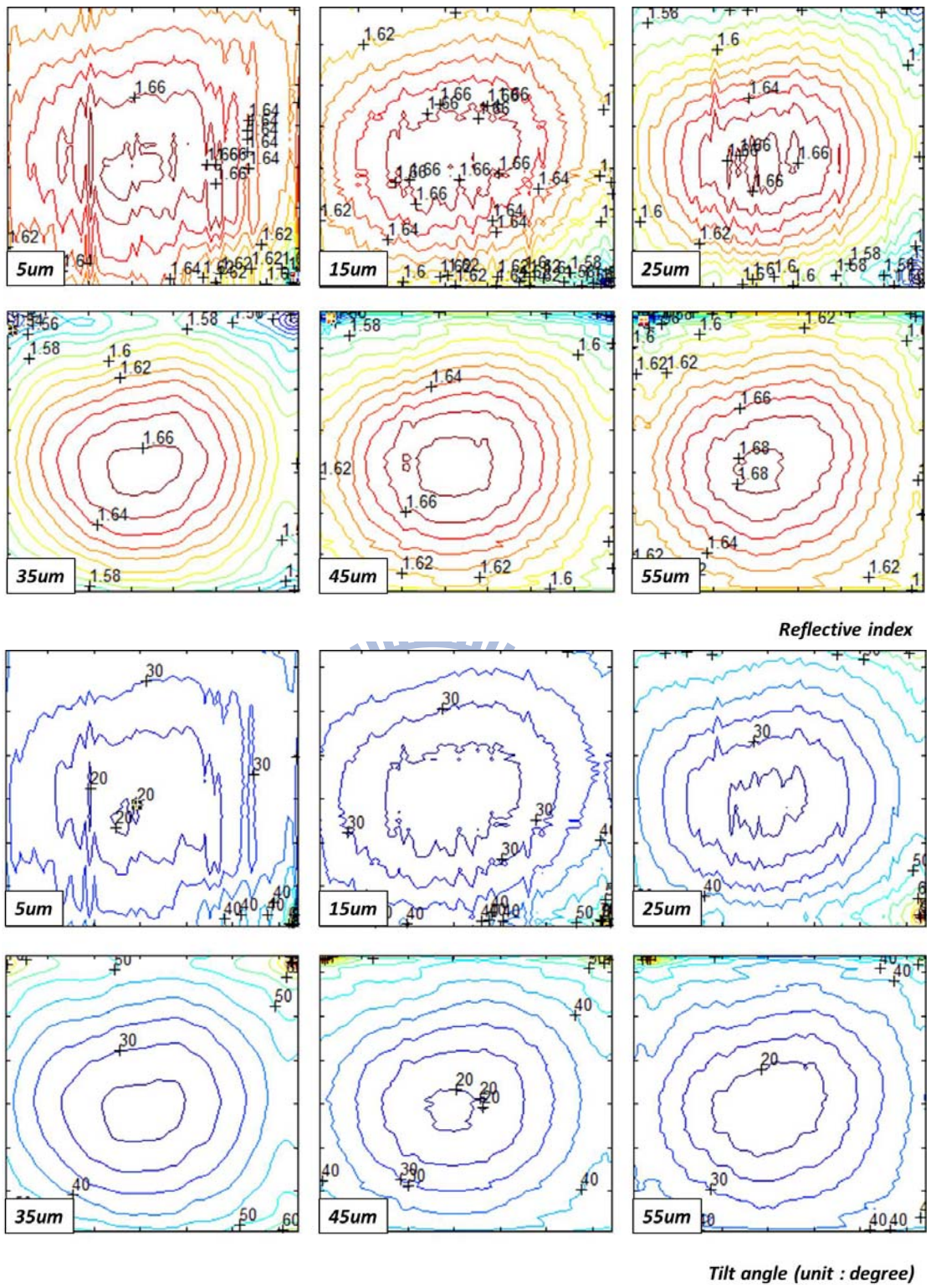


Figure 5-7 The contours indicating the refractive index and LC tilt angle of each layer.

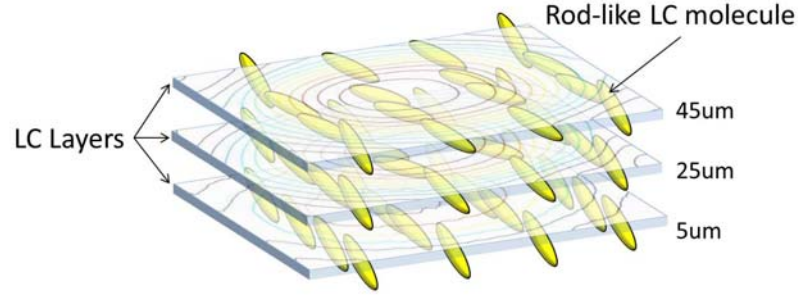


Figure 5-8 The 3D diagram of LC profile.

5.3.2 Phase retardation

To verify the optical properties of the scanning results, the scanning layers were used to calculate phase retardation. Typically, f-number ($F/\#$) of LC lenses is relative large compared to conventional lenses. Thus, paraxial approximation can be employed for the propagation of rays in LC lenses to calculate the phase. If we assume light traveling straightly through the LC lens, the phase retardation of the LC lens can be approximated to

$$\varphi = \frac{2\pi}{\lambda} \cdot \int n(\vec{r}) ds = \frac{2\pi}{\lambda} \cdot \int_0^d n_{eff}(x, y, z) dz \quad (5-5)$$

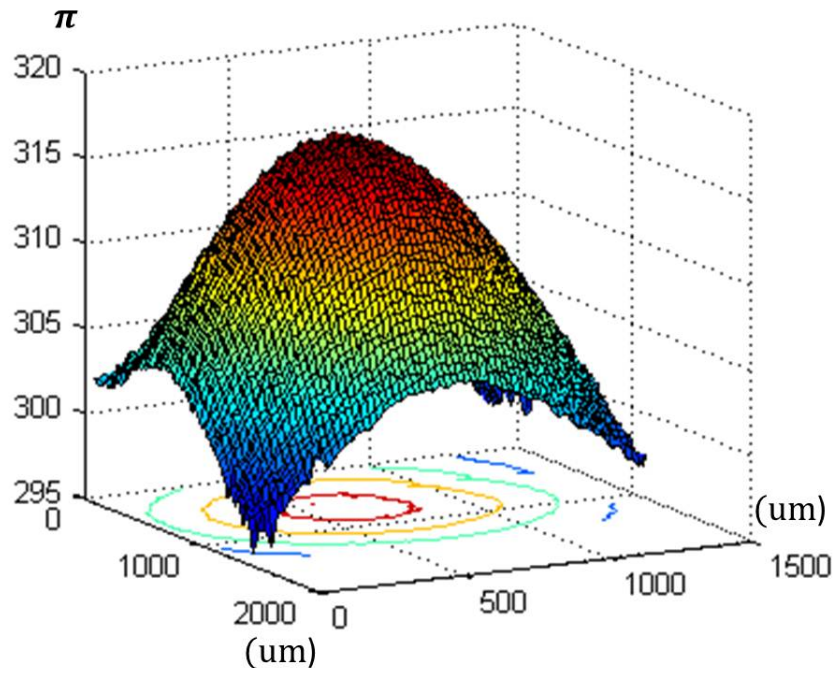
where d is thickness of the LC layer, and λ is wavelength of the laser. Optic axis of the lens was set to be along z-axis. From Equation (5-5), the integral result of phase retardation, φ , from layer 0-um to 60-um was calculated, as shown in Figure 5-9 (a). Figure 5-9 (a) clearly indicated the absolute phase retardation at the center of the lens was around 371π , and OPD between the center and border was around $+12 \pi$. The phase retardation was also measured by fringing pattern method, as shown in Figure 5-9 (b). Within the scanning area, the relative phase was also around 12π , but the signs cannot be directly evaluate.

To compare the accuracy of measured results, focal length corresponding to the phase retardations was investigated. Under the 20 Vrms driving voltage, the LC lens had maximum focal intensity at 5cm distance away from the lens when illuminated by a laser source ($\lambda = 632.8\text{nm}$). The focal intensity was measured by GENTEC Beamage Series CCD sensor placed at the focal length in back of the LC lens. The ideal distribution of phase retardation, $\Delta\phi$, for lenses with focal length, f , can be represented by following equation:

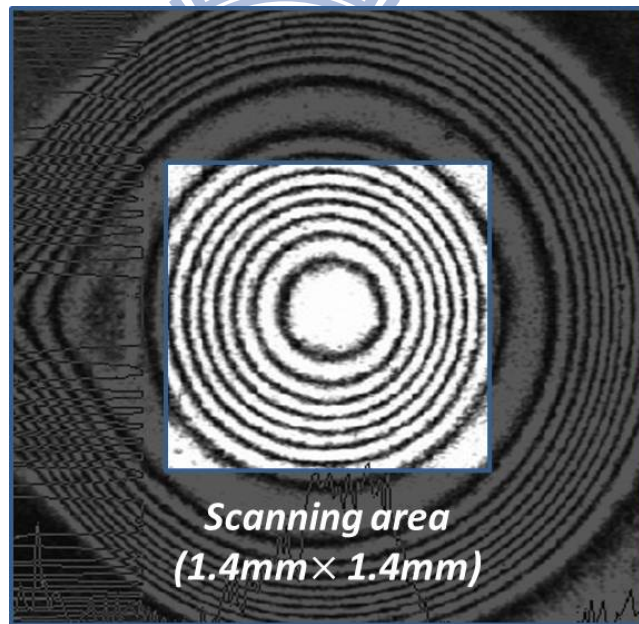
$$\Delta\phi(r) = -\frac{2\pi}{\lambda} \left(\frac{r^2}{2f} \right) \quad (5-6)$$

where r is aperture ray height in cylindrical coordinate system. Equation (5-6) indicates the form of the phase retardation, $\Delta\phi(r)$, is a parabolic curve if no spherical aberration occurs and light focus at a single point. Compare the results by capturing the cross section of profiles in Figure 5-9 (a) and Figure 5-9 (b), the curves, as well as the ideal parabolic curve for 5cm focal length, are shown in Figure 5-10. These three curves are almost matched indicates the measured results of FCPM method and fringing pattern were coherent, and also matched with the measurement of focal length.





(a)



(b)

Figure 5-9 The phase retardation calculated by (a) FCPM method and (b) measured by fringing pattern approach.

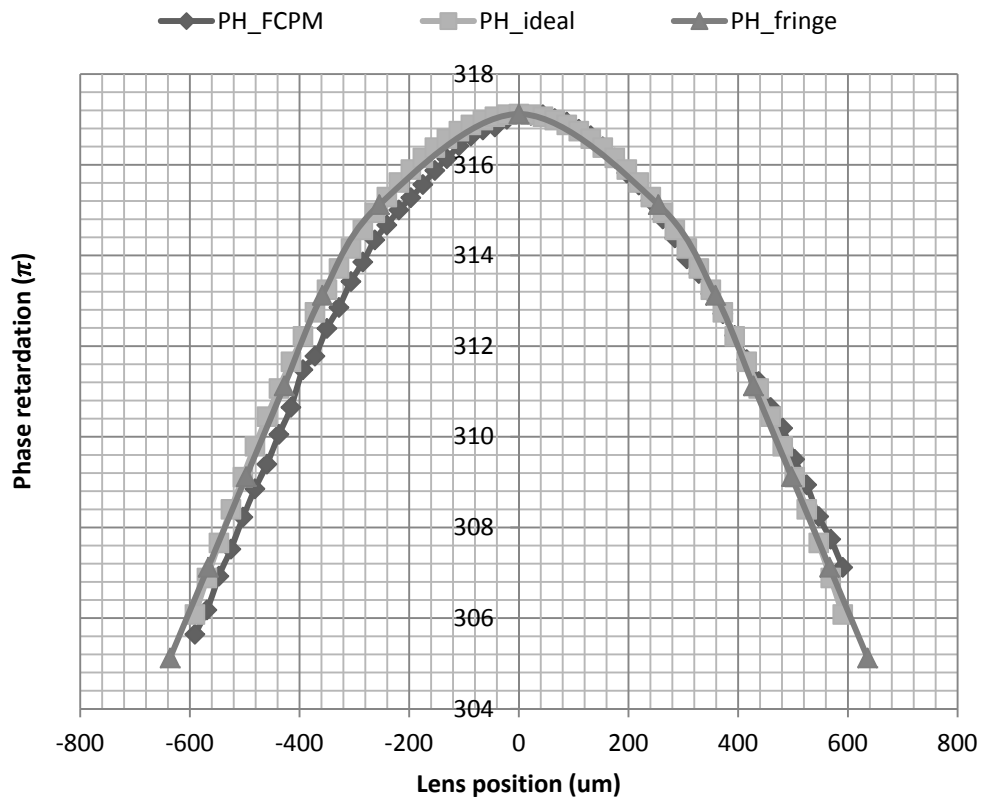


Figure 5-10 The cross sections of phase retardation for 5 cm focal length by FCPM method and fringing pattern approach, as well as the ideal curve.

5.4 Experiments and Optimization of Over-Driving Voltages

Not only the switching time but also the values of OD voltage affected the result. Optimization for OD voltages was analyzed by applying different OD voltages to the electrodes. Typically, the focusing time was improved when the OD voltage was increased, as Figure 5-11 shows. The dash line shown in the result indicates directly applying the 45Vrms without OD method which yielded 25sec focusing time, as illustrated in Figure 5-2. As we applied OD method and increased the OD voltage to exceed 45Vrms, the focusing time started to be improved. Of course, the improvement cannot be obtained if the OD voltage is lower than that of general operation. In this experiment, the improvement was saturated as the over-drive voltage was increased to exceed 65Vrms, which means the extremely high over-drive voltage did not increase focusing time proportionally.

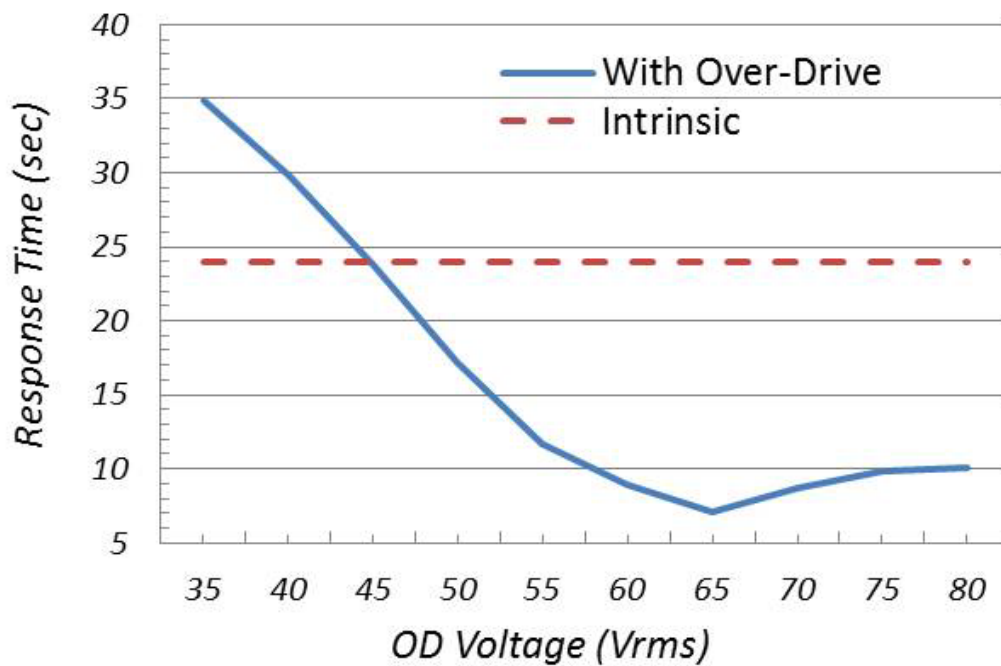
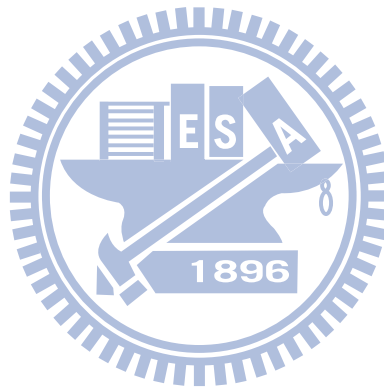


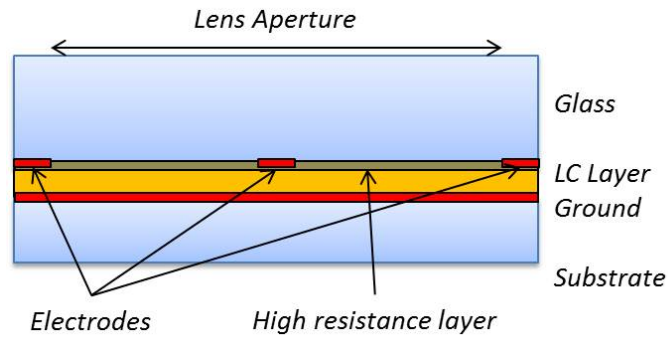
Figure 5-11 The result of relation between focusing time and OD voltages. Improvement was saturated as the voltage was larger than 65Vrms.

In this experiment, GD-LC Lens was examined, as structure shown in Figure 5-12(a). The focusing time was dramatically reduced down to 0.2sec by operating 15Vrms OD voltage. Figure 5-12 (b) shows the relation of OD voltages to focusing time. This result also showed OD method is necessary for different structures if the fast focusing was required. A comparison of focusing response time, over-drive voltage, and stable driving voltage are listed in Table 6. Two main LC lens structures mentioned above driven by Over-drive Method with 2mm aperture size and 60um LC cell gap were discussed. The LC model was Merck nematic LC (E7). Although the external structure had slower focusing time due to insertion of high K glass, by Over-drive Method, the focusing time was effectively improved from 23.5sec to 7.1 sec. For GD-LC lens, the focusing time was significantly reduced down to 0.2sec with only 15Vrms over-drive voltage.

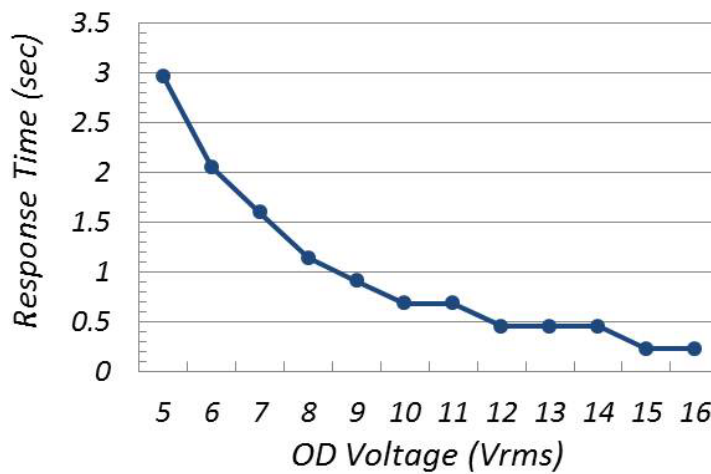
Table 6 The results and comparisons of two main structures of LC lenses driven by OD method. In the internal structure part, focusing response time was reduced to 0.2sec by 15Vrms over-drive voltage.

	<i>External Electrodes</i>	<i>GD-LC Lens</i>
<i>Over-drive Voltage (OD)</i>	<i>65Vrms</i>	<i>15Vrms</i>
<i>Stable driving Voltage</i>	<i>45Vrms</i>	<i><5Vrms</i>
<i>Initial focusing time</i>	<i>23.5sec</i>	<i>12.5sec</i>
<i>Focusing time with OD method</i>	<i>7.1sec</i>	<i>0.2sec</i>





(a)



(b)

Figure 5-12 (a)The structure of GD LC lens with multi-electrically control, and (b) the relation of response time to over-drive voltages.

5.5 Conclusion

In summary, we proposed Over-drive (OD) method for fast focusing LC lenses. By initial OD driving, fast and instantaneous initial focusing was generated. A switching operation following the OD voltage at the time of the initial focusing can significantly improve the focusing time. By optimizing the OD voltages and the timing for the switching, the focusing response time of LC lens of two structures, external electrodes and GDLC lens, was improved from 25.3sec to 7.1sec and 12.5sec to 0.2sec with each optimized OD voltage and stable driving. This result showed Over-drive Method for LC lenses was effective and feasible, which also indicated the significance for fast focusing applications.

Chapter 6.

AF Imaging with Spherical GD-LC Lens

6.1 Introduction

In previous chapters, we proposed two kinds of structures, MeDLC lens and GD-LC lens to exhibit the different features. In MeDLC lens, the multi-electrode can finely control the lens profile to yield a wide range of focusing, although the structure is complicated for achieving spherical structure. On the other hand, GD-LC lens employed a high resistant layer as the control layer connected with the center and border electrode, and used the electrodes to initially generate the voltage difference. This new structure benefits us to significantly improve the driving voltage and focusing time while we combine the OD method for LC lenses, as discussed in Chapter 5. Furthermore, the simpler structure of GD-LC lens was easy for us to construct a spherical GD-LC lens (sGD-LC lens), because there were only two control electrodes, at the center and border. For imaging applications, spherical lens is suggested as imaging and aberration theory were developed for hundred years.

In this chapter, fabrication of sGD-LC lens and its imaging system will be discussed. AF performed with GD-LC lens was also examined its optical performance, driving voltage and focusing time. It was noteworthy that GD-LC lens can exhibit an instantaneous focusing with lower driving voltage and provided superior image quality.

6.2 Fabrication

The difference between cylindrical and spherical GD-LC lens is the pattern of electrodes, as shown in Figure 6-1. The spherical structure has a central electrode without horizontal connection line because the connection line will distort the distribution of voltages after the high resistant layer coated. This situation will result in asymmetrical optical properties which are unfeasible for imaging system.

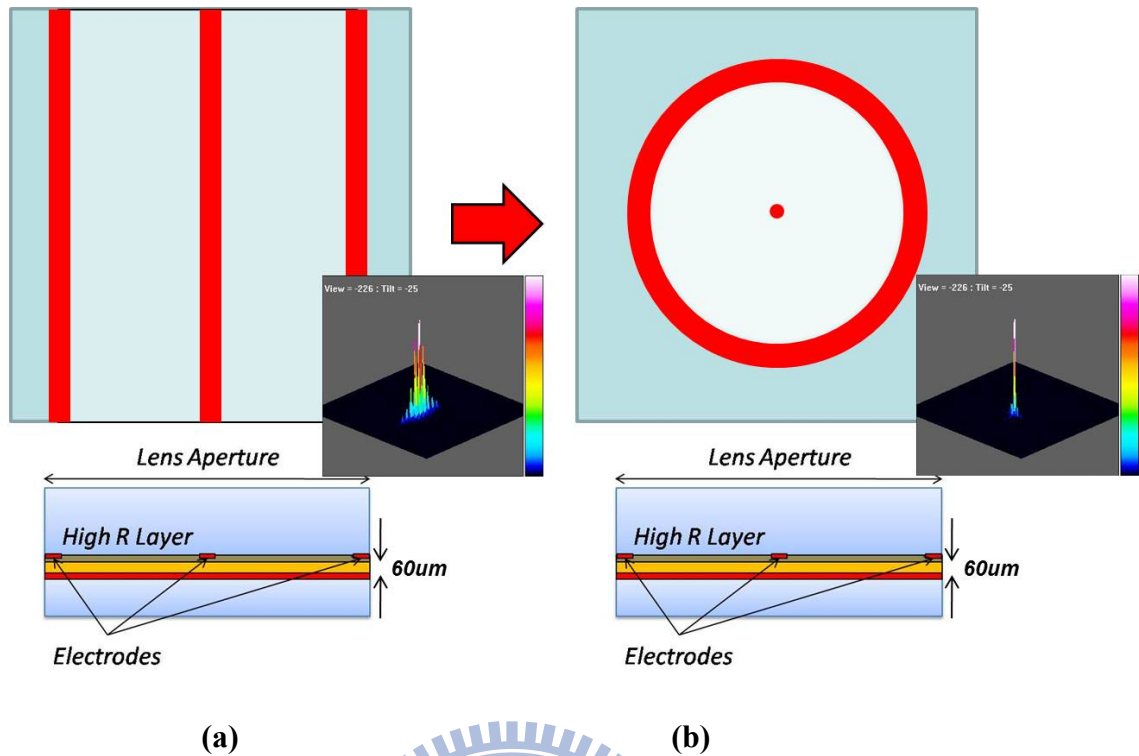


Figure 6-1 The electrode patterns of (a) cylindrical and (b) spherical GD-LC lens.

To fabricate the electrode pattern of spherical GD-LC lens, as shown in Figure 6-1 (b), a double-layer electrode structure was chosen, as shown in Figure 6-2. The electrode layers on different horizontal height were separated by an insulator layer. The material of the insulation was recommended to use SiO_2 , SiN_x , Su8, and so on. The different materials of insulator exhibit different compactness which may cause connection of two electrode layers in the overlap area, as Figure 6-2 shows. This connection will make the structure unworkable due to no voltage difference between two electrodes after applying the driving voltage. Limited by the process, we finally chose SiN_x as the insulator, although SiN_x still cannot 100 percent to insulate two electrode layers. Similar to cylindrical GD-LC lens, the final structure of spherical one is shown in Figure 6-3. The lens aperture was designed as 2mm with a 60um central electrode. The LC cell gap was also chosen to 60um sandwiched by two 550um glass substrates.

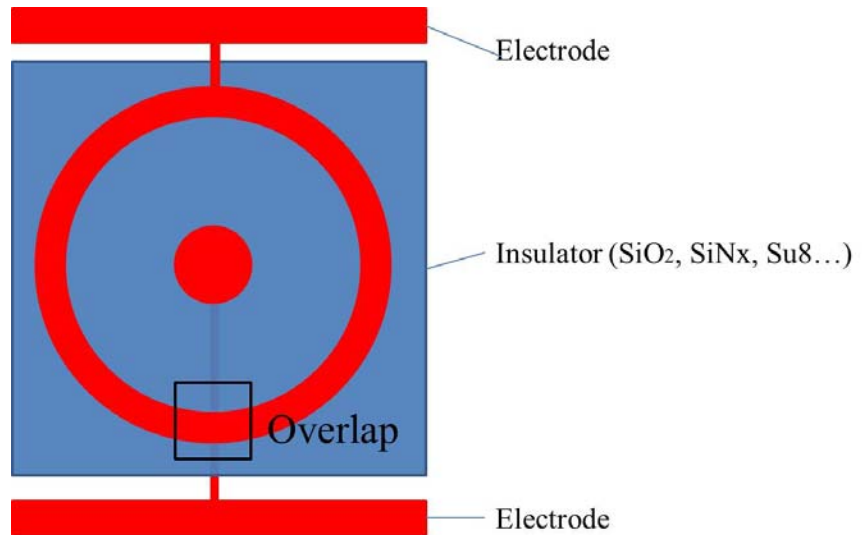


Figure 6-2 The double-layer electrode structure of sGD-LC lens employing an insulator to separate the electrode layers.

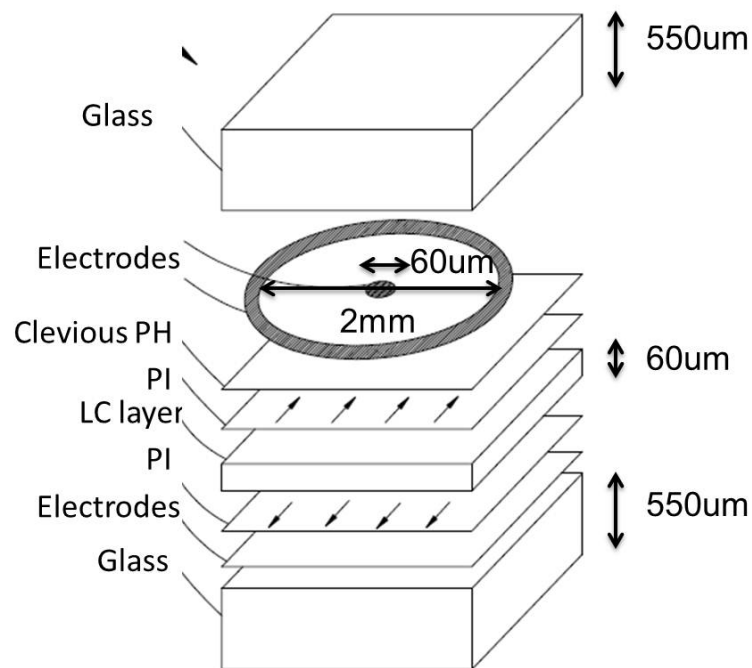


Figure 6-3 The structure of GD-LC lens.

6.3 Optical Properties of sGD-LC Lens

To investigate the focusing profile of sGD-LC lens, the experimental setup was the same as cylindrical GD-LC lens (cGD-LC lens). The difference is that the exposure time of CCD was reduced to 20ms to avoid intensity saturation because the focusing profile was axially symmetrical whose light intensity was much higher than that of the line focusing of cGD-LC

lens. The focusing profile driven by $3.3V_{rms}$ at 4.22 kHz is shown in Figure 6-4. The left side is the top view of the focusing which obviously shows the focusing profile was different from line focusing of cGD-LC lens. The left bottom and the right side figures are cross-section and 3-D profile of the focusing. The focusing profile cannot be symmetry due to the defects of fabrication. This issue could be suppressed by improving cleanliness of the process. For different focal length, the focusing profiles of sGD-LC lens were also modulated by driving optimized voltages and frequencies, as the cross sections shown in Figure 6-5. The profiles of focal length from 7 to 15 cm can be maintained to higher focusing ability by the voltage-frequency driven. As the focal length was out of the range, the focusing profiles started to decrease. This not only means there were defects but also higher control freedom was required, as mentioned in Chapter 3. Figure 6-6 also shows the relationship between focal length to operating voltage and frequency. The results was coherent to cGD-LC lens that the decreased operating voltage and frequency generated longer focal length. Although the driving range was different from that of cGD-LC lens due to the coated resistance of high R layer, the results still shows low operating voltages which were feasible for mobile devices.

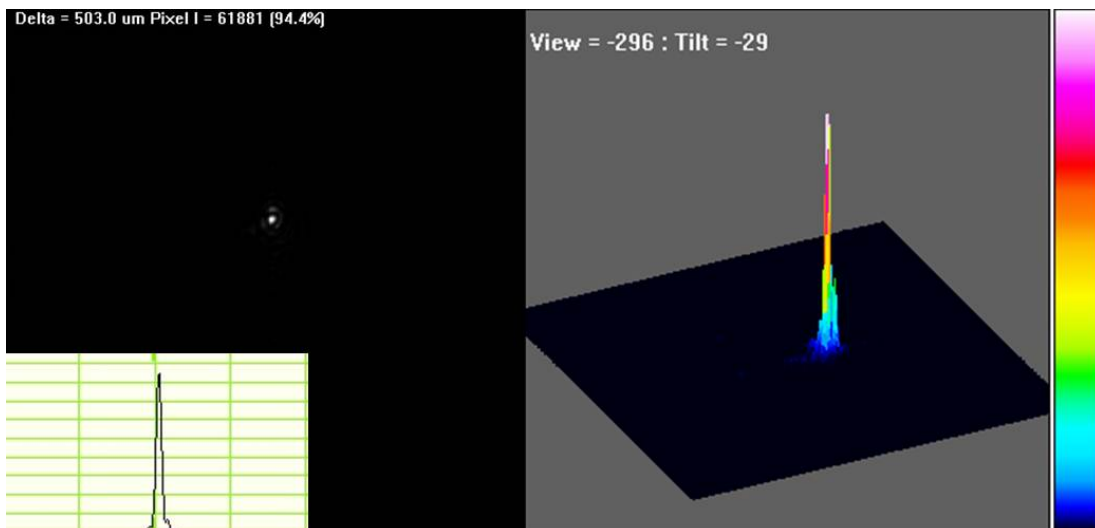


Figure 6-4 The focusing profile of sGD-LC lens driven by $3.3V_{rms}$ at 4.22 kHz.

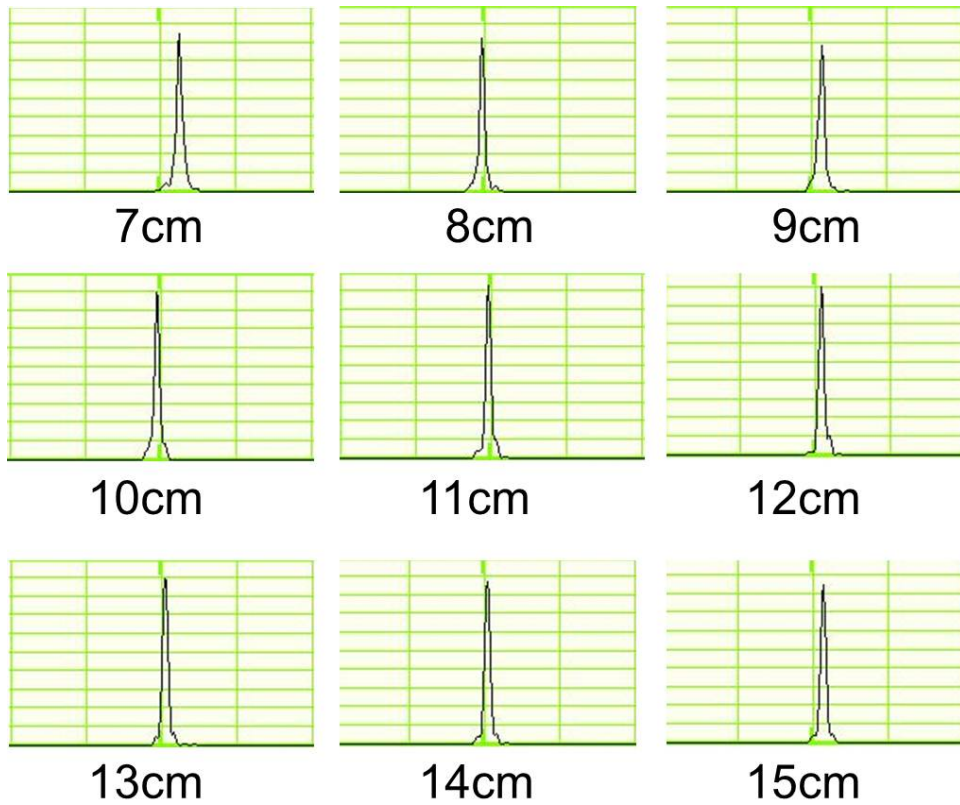


Figure 6-5 The focusing profiles of sGD-LC lens from focal length, 7cm~15cm.

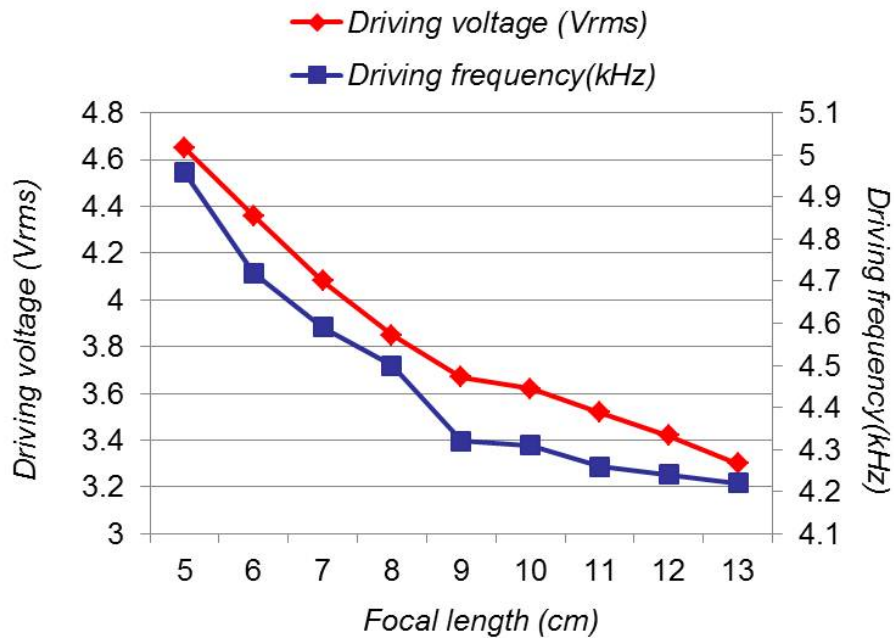


Figure 6-6 The relationship between of focal length to operating voltage and frequency of sGD-LC Lens.

6.4 AF Experiment with sGD-LC lens

6.4.1 Experimental Principle

The AF by LC lens can be performed with a conventional lens-head and a LC lens. The lens-head was used to provide the most ratio of lens power and to correct aberrations. Combining with the LC lens in front of the lens-head, the lens system can change the total lens-power by operating voltages (and frequencies) to focus the near objects, as mentioned in previous sections. The structure is shown in Figure 1-9. To simplify the analysis, parallel light, which was used to describe object light source at infinity, was input to the lens-head in both case of with and without LC lens, as shown in Figure 6-7. In the LC lens case, the light source from a near object point was converged to the parallel light for the lens-head. This was assumed the LC lens has diffraction-limit performance to converge a parallel light to an image point. The benefit of the arrangement is because the lens-head was optimized for infinity object. By Gaussion and Lens makers' formula, the relations of object distance (S), image distance (S'), focal length of LC lens and lens-head (f_{LC} and f_C), and separation of LC lens with lens-head (d) can be represented by

$$\frac{1}{f} = \frac{1}{f_{LC}} + \frac{1}{f_C} - \frac{d}{f_{LC} \cdot f_C} \quad (6-1)$$

$$\frac{1}{S'} = \frac{1}{f} + \frac{1}{S} \quad (6-2)$$

as the assumption above, f_{LC} and f_C are equal to

$$f_C = S' \quad (6-3)$$

$$f_{LC} = -S \quad (6-4)$$

which simplified Equation (6-1) to

$$\frac{1}{f} = \frac{1}{f_{LC}} + \frac{1}{f_C} \quad (6-5)$$

and the optical power was independent to d . From Equation (6-3) to (6-5), the f_{LC} is directly corresponding to the object distance (S) and the system lens power is equal to the sum of two lenses. In the structure of Figure 6-7, the back principle plane of the lens-head is stationary

and consistent with the system back principle plane. The image distance therefore was the same as that of non-LC-lens system.

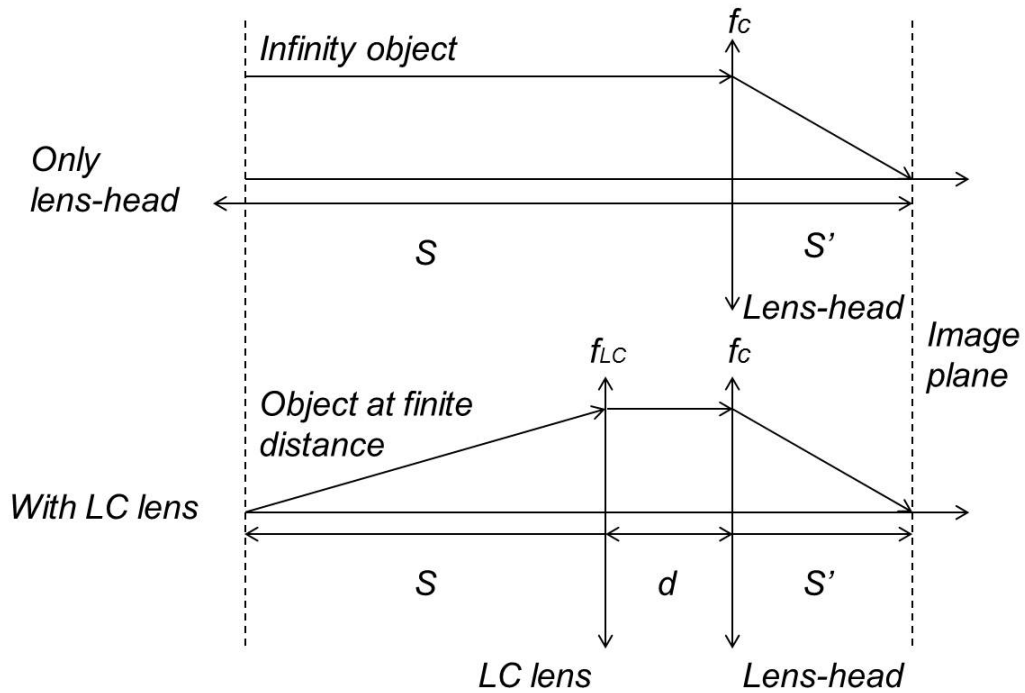
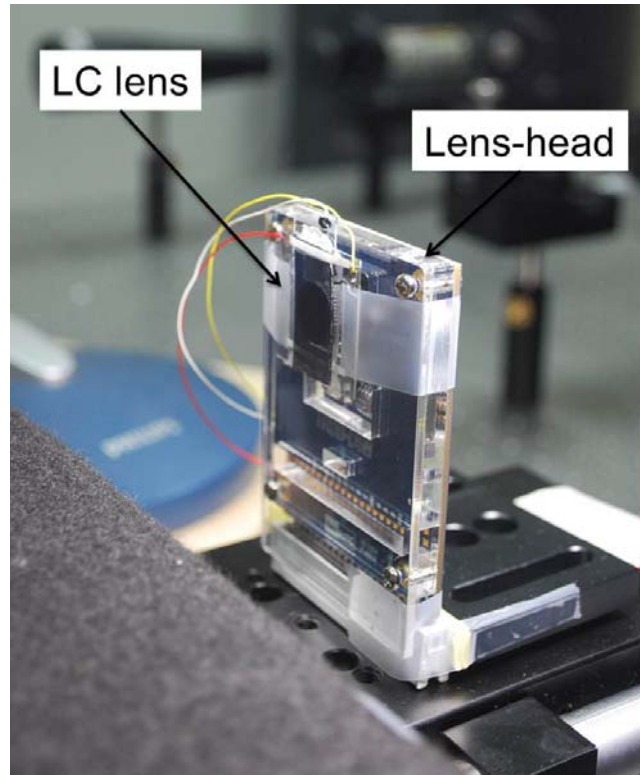
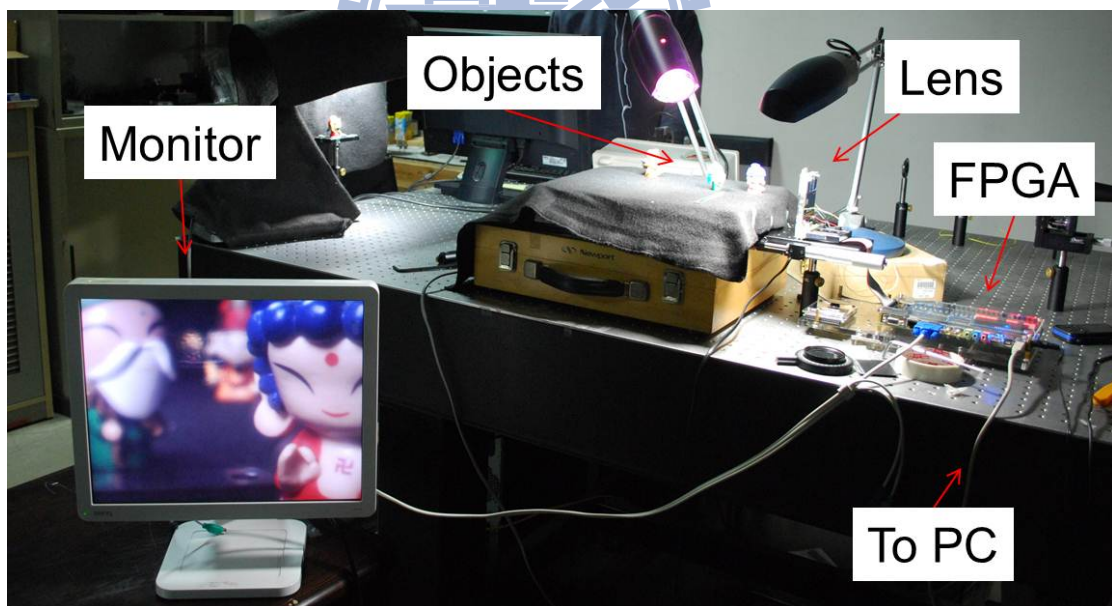


Figure 6-7 The schematic of lens-system with and without LC lens.

In the experimental setup, sGD-LC lens and a 5-mega-pixel lens-head were prepared as shown in Figure 6-8 (a). An FPGA board was used to deliver the captured images to PC and monitor, as shown in Figure 6-8 (b). The test objects including I3A/ISO Resolution Test Chart-1X (NT56-074, Edmund) and toys were setup at different distances. The lens-head originally was tuned to focus on infinity, and utilized the sGD-LC lens to focus objects at finite distance. A control signal used to perform OD method for sGD-LC lens was connected. The signal consisted of three channels which were zero state, OD state and stable state, and the channels were selected by another control board. The width of the OD state can be modified by coding of the board which can significantly affect the focusing time. The function and equipment are shown in Figure 6-9.

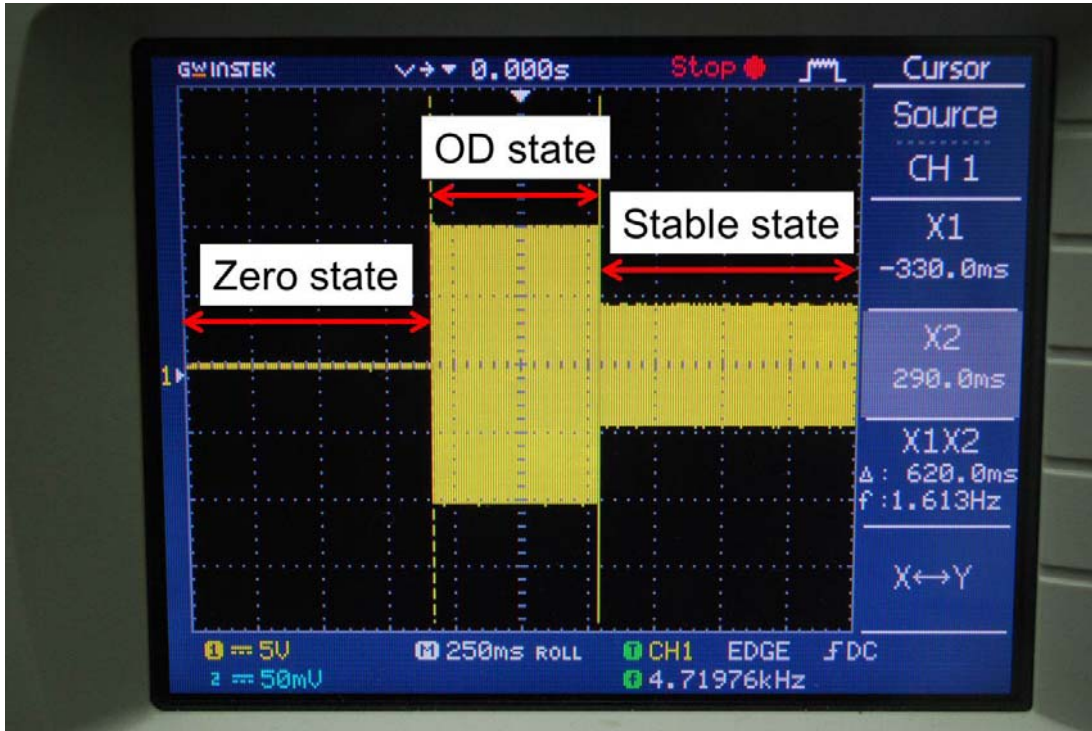


(a)

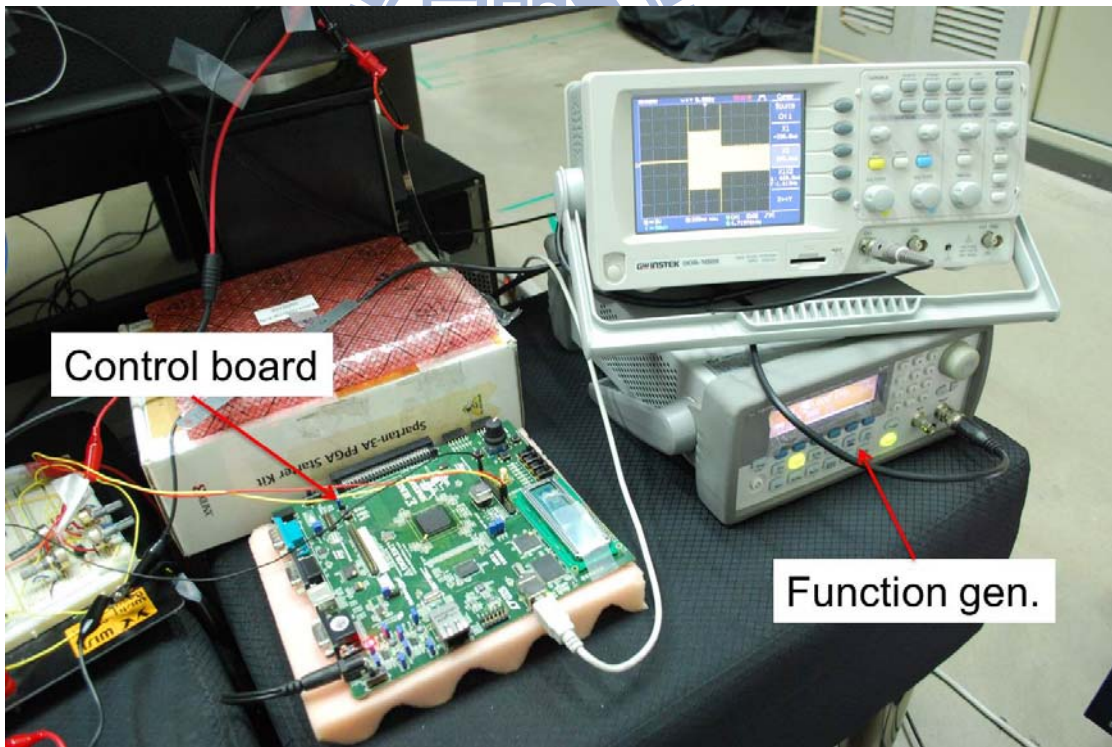


(b)

Figure 6-8 (a)The setup of lens-system and (b) the experimental arrangement.



(a)



(b)

Figure 6-9 (a)The function of control signal and (b) the equipmet.

6.4.2 Results

Resolution Test Chart for different focal length

The first test object was I3A/ISO Resolution Test Chart-1X (NT56-074, Edmund) which was used to test the resolution of sGD-LC lens combined with the lens-head. The test chart was placed at the distance corresponding to the focal length of sGD-LC lens and captured by the system, as shown in Figure 6-10. The captured results of the magnified part indicated in Figure 6-10 are shown in Figure 6-11. The test resolution was chosen from 6 to 20 line-pairs/mm. From the results, the low resolution range can be easily distinguished. Even in the range from 18 to 20 line-pairs/mm, some of the focal length also can provide acceptable contrast. The ghost image appears on the black-white edge was due to the misalignment of LC directors to the direction of polarizer. Therefore, there was always a minimum ghost image due to the ordinary rays. This issue can be suppressed by DIP approach, and the relative works is under the research.

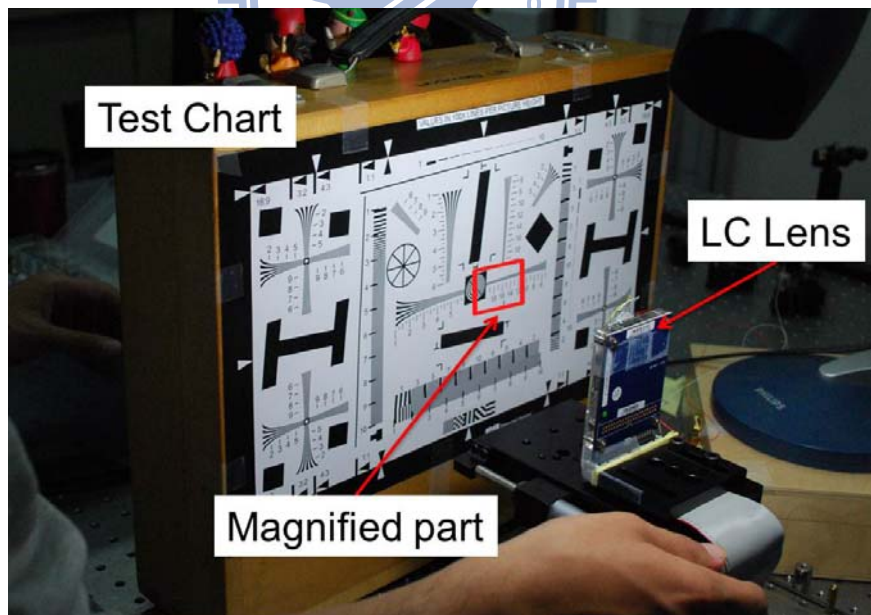


Figure 6-10 The test chart placed in front of sGD-LC lens at the distance corresponding to the focal length.

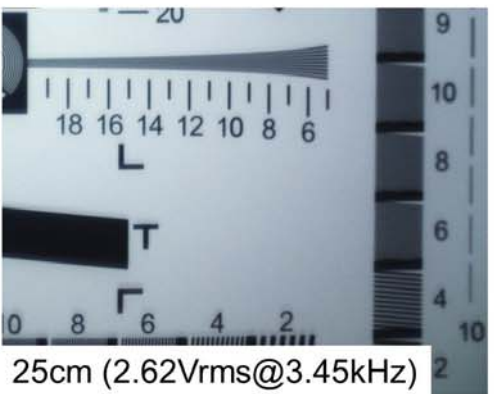
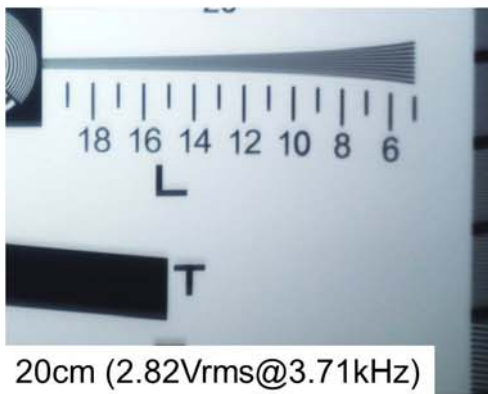
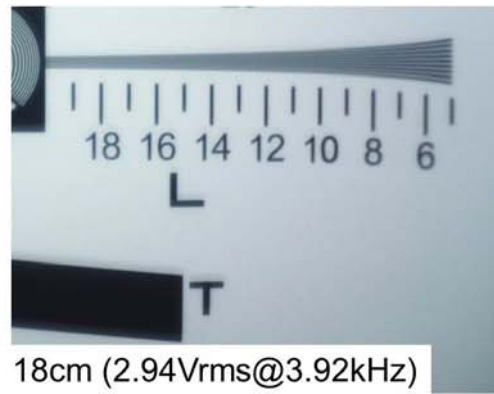
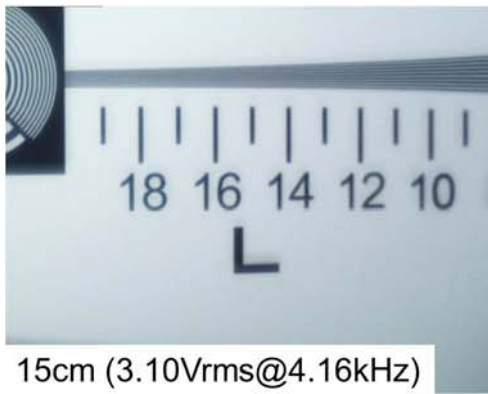
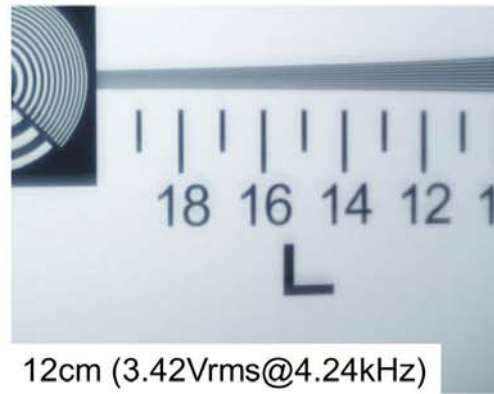
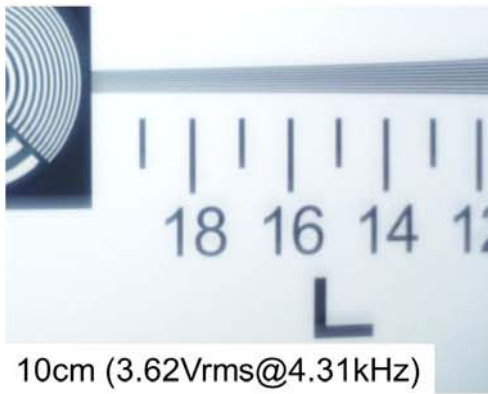
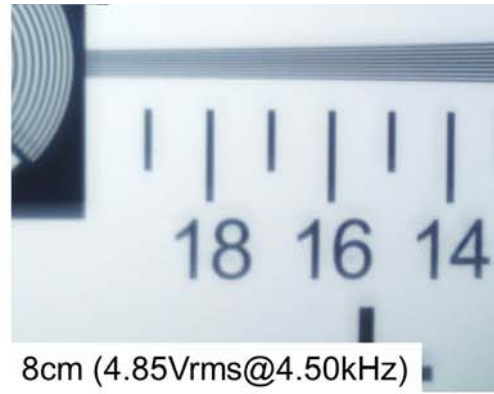
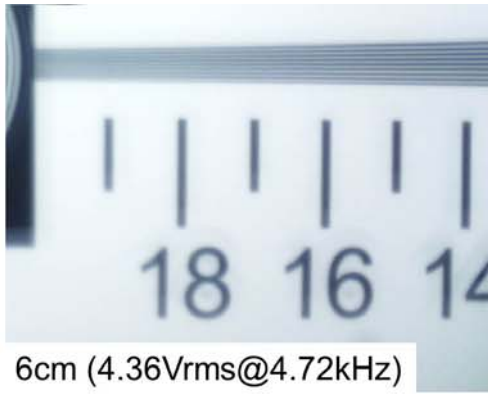


Figure 6-11 The results of test chart for different focal length

AF test

To perform AF with sGD-LC lens, four toys were placed in front of the lens with different distances, as shown in Figure 6-12. Each of the toys was separated to out of its depth of field. By different operation for each focal length, the toys can be individually focused, as Figure 6-13 shows. Through the result of Figure 6-13, the objects were obviously focused by operating corresponding driving voltage and frequency. As the operation changed, the toys out of the depth of field started to be blurred. The OD method used to increase the focusing time was also perform for focusing from the toys at the 90cm to the 6cm. The OD voltage was $10V_{rms}$ with 500m sec OD state and then switched stable state for focusing on the 6cm toy. The focusing time was around 1sec.

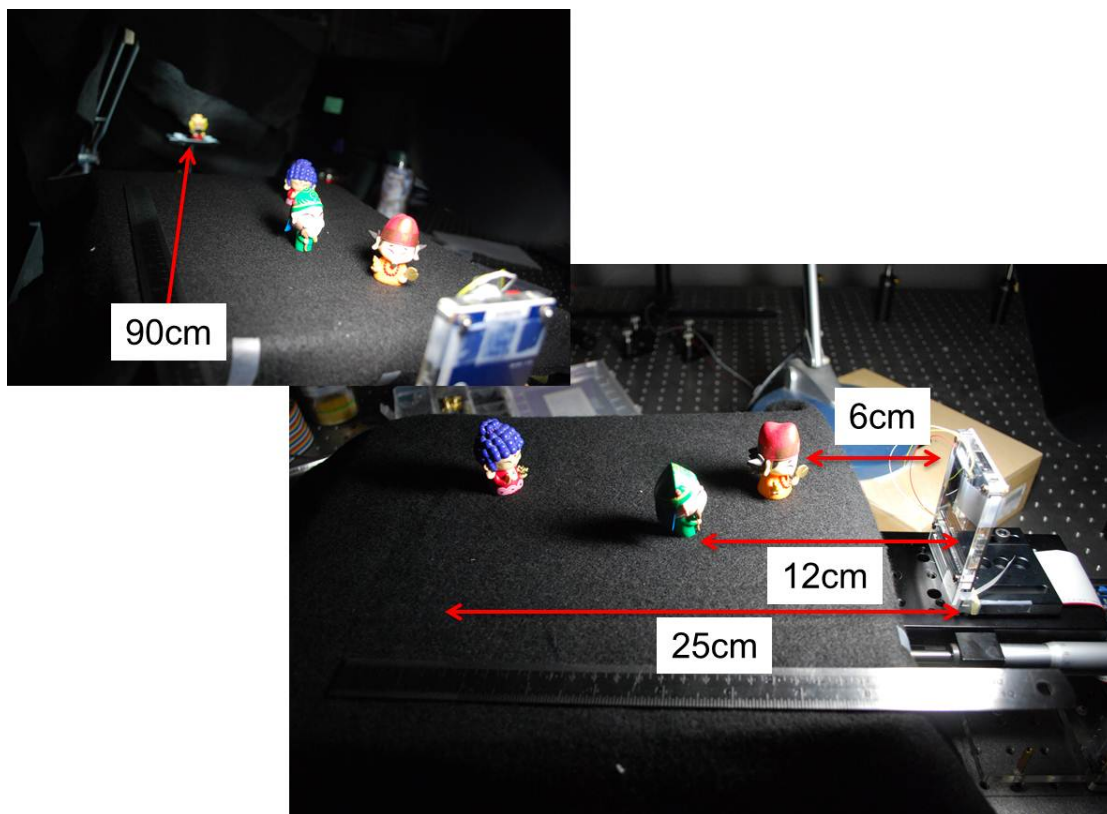


Figure 6-12 The AF experiment and the toys placed at different distances.

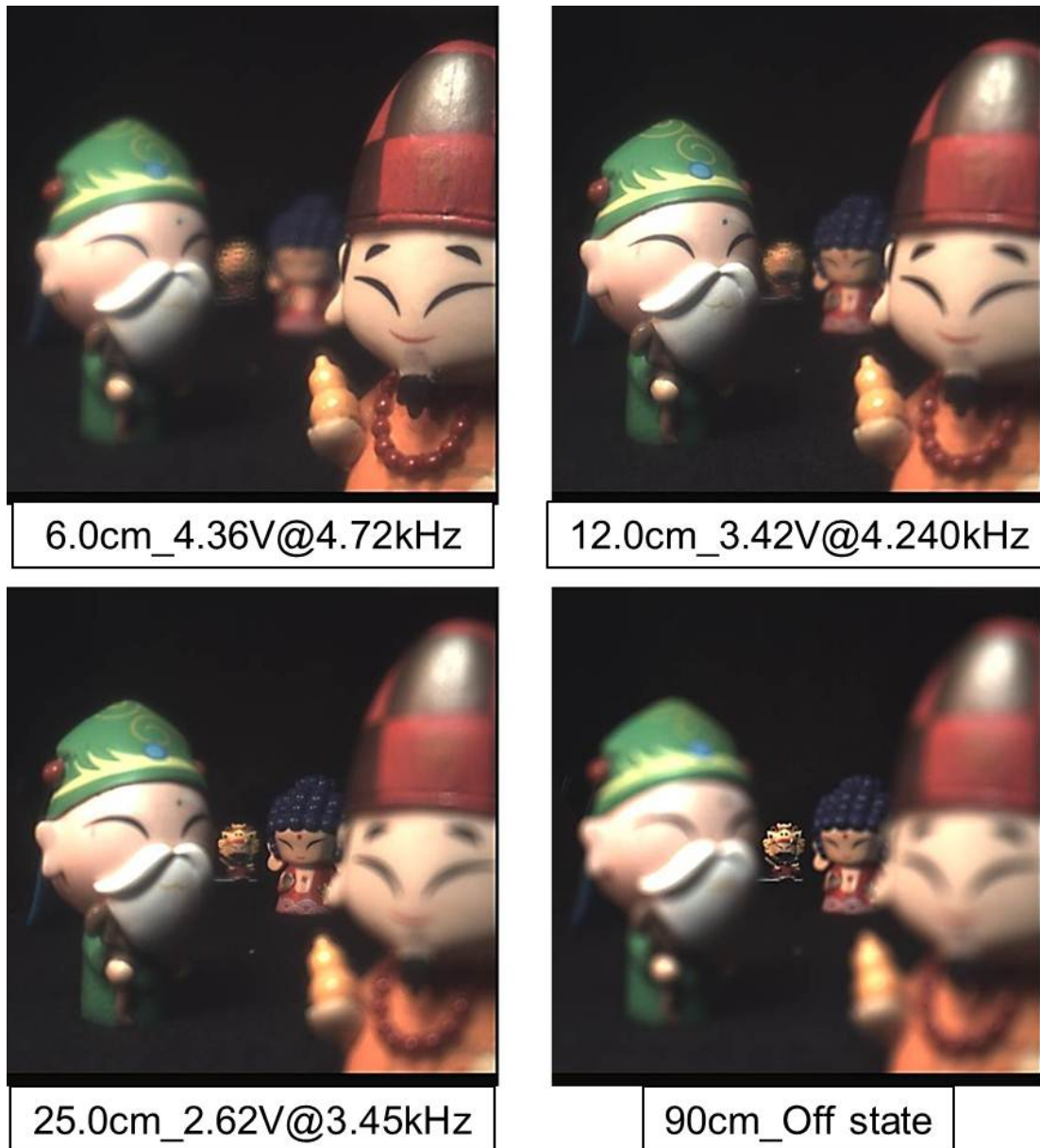


Figure 6-13 (Video) The AF result of four toys at different distances, and OD result focusing from the farthest toy to the nearest one.

MTF measurement

Figure 6-14 shows MTF of sGD-LC lens focusing at 10cm measured by ImageMaster® HR, Trioptics [70]. From the result, we can find this lens can provide 90% contrast at 10lp/deg and larger than 50% for 25lp/deg. This result is similar to that of liquid lens reported by Philips Research Eindhoven in 2004 [71] which has around 70% at 25lp/deg. However, compare with conventional lens-head, for a typical 5-MP lens module, the contrast

is required to higher than 30% at 280lp/mm for center (0.0 field), not to mention the requirement for corner (0.8 field) which is higher than 30% at 140lp/mm. Moreover, MTF of the LC lens in the different field was also measured, as shown in Figure 6-15. As the result shows, as the field of view increased, the contrast was decreased rapidly. At the area of large field, there was almost no signal be measured due to the undetectable focusing signal. This shows not only the image quality for the MTF at central area has to be improved, but also the large field, which requires more compensation for the image quality at the border. This is a major challenge for LC lenses to improve its image quality if we really considered its applications in consumer products.

To improve this issue, the optical design of conventional lens for LC lens can be take into consideration. In the first step, the focusing performance of LC lens should be optimized, and then utilize solid lens to correct the image quality, image aberrations, and enhance MTF. The role of the solid lens is to obtain a balance solution for focusing at infinity and close objects.

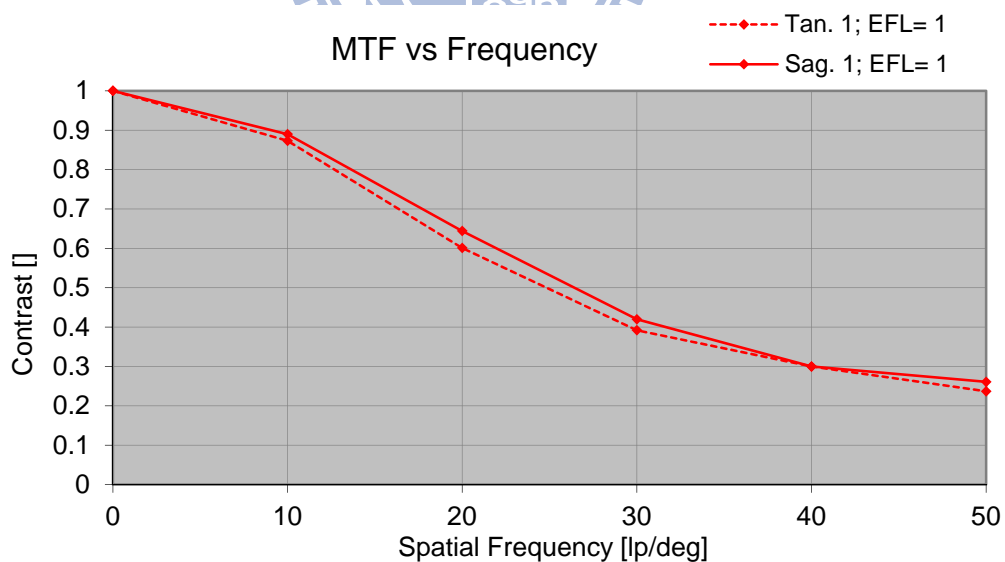


Figure 6-14 MTF of sGD-LC lens measured by ImageMaster® HR, Trioptics.

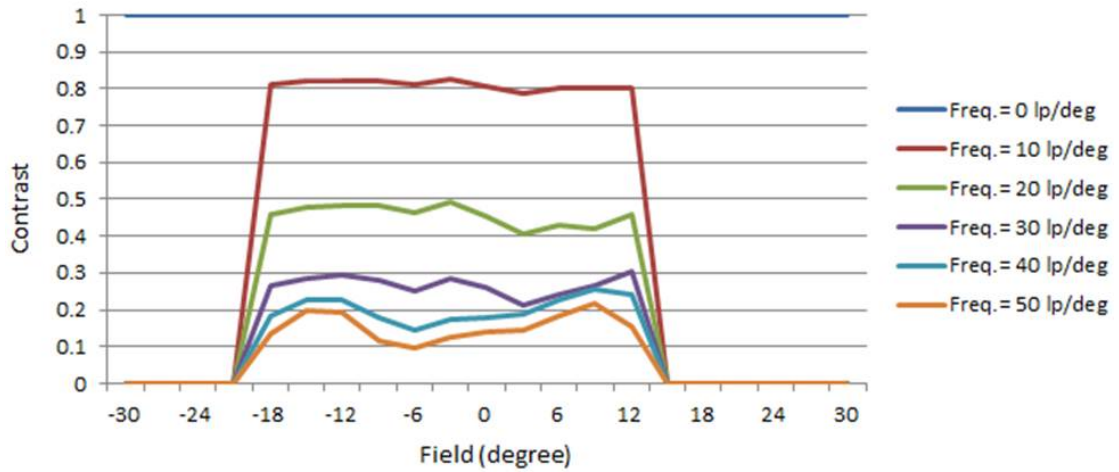


Figure 6-15 Global MTF of the LC lens with field of views from 0 to 30 degree.

6.5 Conclusion

In this chapter, we fabricated spherical GD-LC lens (sGD-LC lens) and investigated its optical properties. The AF system with sGD-LC lens was also setup. The sGD-LC lens was placed in front of a 5-mega-pixel lens-head which was connected to a FPGA board to capture the output images. OD method was also coded by a control board to demonstrate the fast focusing. As the result shows, the objects within different depth of field can be focused individually by different operating. The focusing time was also achieved in 1sec.

Chapter 7.

Conclusion and Future Work

7.1 Conclusion

Liquid Crystal Lens (LC lens) exhibits the ultimate features, such as its focal length is electrical tunable without any mechanical movement or surface shape changing and its tiny volume is suitable for employing in mobile devices. However, the major issues, inferior optical quality, slow focusing time, and high driving voltage, result in the unpractical and unfeasible applications of LC lenses. To overcome these issues, we have reported three main topics, MeDLC Lens, Over-driving Method, and GD-LC lens. The relations of the topics for each issue are shown in Figure 7-1. Finally, combine the features of the proposed topic, all the issues were suppressed.

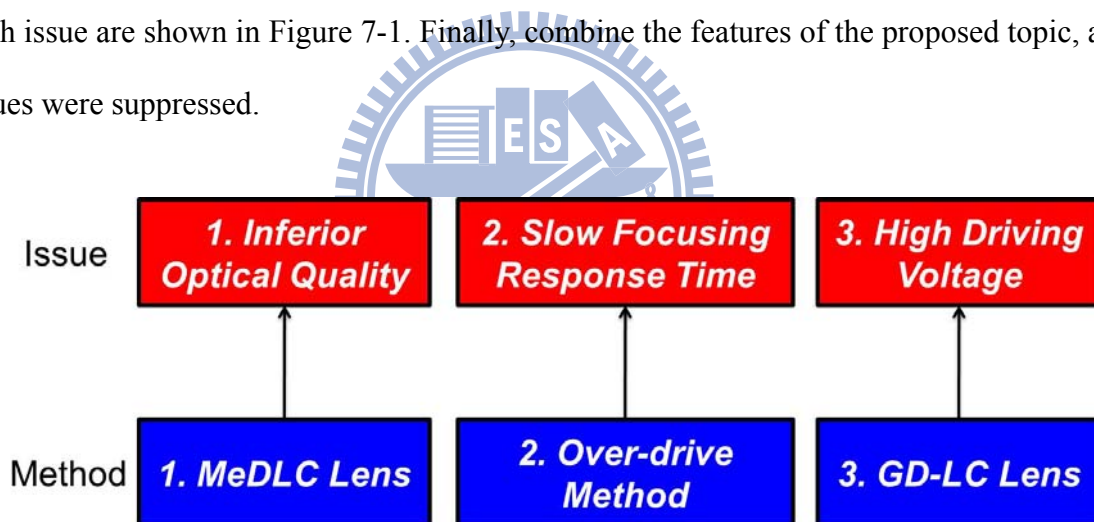


Figure 7-1 The relations of the topics for each issue

7.1.1 Multi-electrode Driven LC Lens (MeDLC Lens)

The first one is Multi-electrode Driven LC Lens (MeDLC Lens) which utilized multi-electrode to finely control the orientations of LC molecules for each focal length to have superior focusing profiles. In this stage, we changed the structures of LC lenses and utilized multi-electrode rather than the single control freedom of conventional structures, as Figure 7-2 shows.

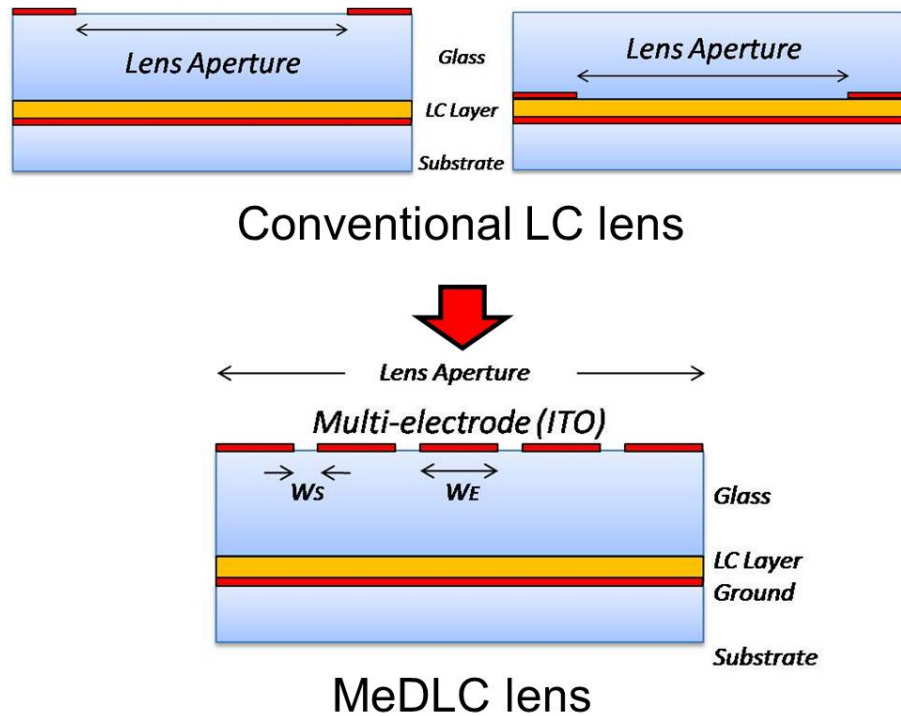
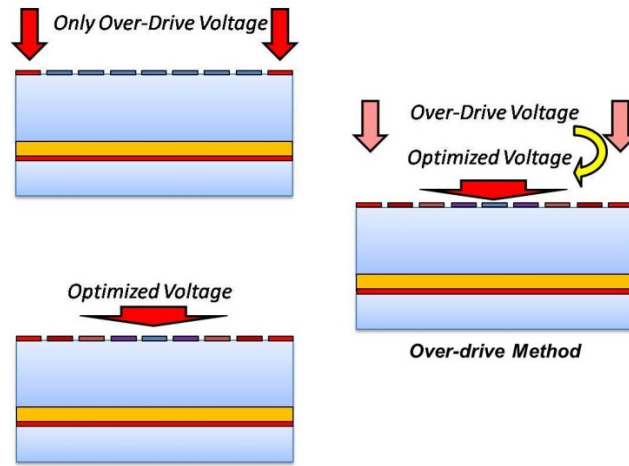


Figure 7-2 The change of LC lens structure from conventional single control to multi-control freedom.

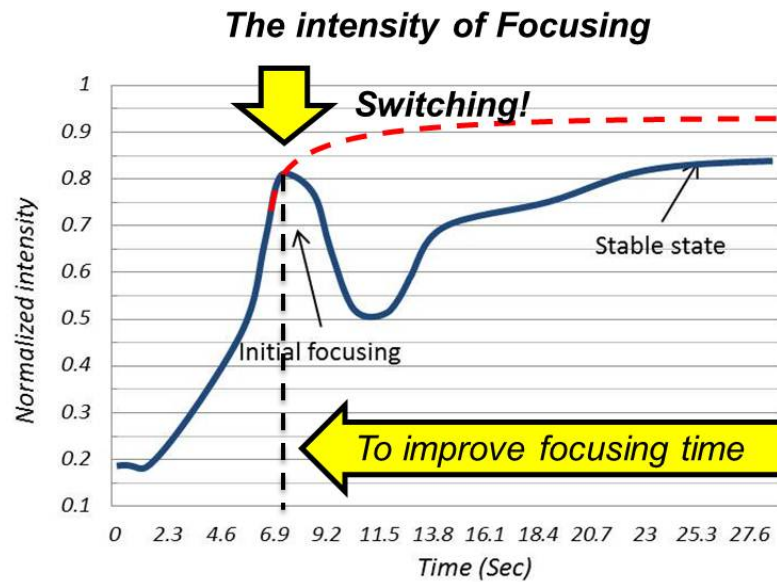
In the experiments, we demonstrated the high control freedom of MeDLC lens can yield similar focusing profile at each focal length and minimize the spot size of these focusing. To obtain superior image quality, the multi-control was necessary to optimize the focusing.

7.1.2 Over-driving (OD) Method for LC lenses

The second topic is Over-driving (OD) Method for LC lenses which utilized an initial OD voltage to increase the deformation of LC molecules and switch the OD voltage according to the focusing profile to an optimized driving to significantly reduce the focusing time, as Figure 7-3 illustrates. Different from the OD technology widely employed in Liquid Crystal Display (LCD) industry, OD method for LC lens was investigated according to transition of the focusing profile. In this stage, we also demonstrated the timing for switching the driving voltage was optimized at the initial focusing peak by the OD voltage.



(a)



(b)

Figure 7-3 (a) The operation of OD method and (b) the focusing transition by OD method.

7.1.3 Gradient Driven Liquid Crystal Lens (GD-LC lens)

The most important topic, the third one: Gradient Driven Liquid Crystal Lens (GD-LC lens), was proposed to intrinsically solve the issue of high driving voltage. Compare to previous papers or the newly reports, we demonstrated a dramatic improvement for reducing the driving voltage from tens voltages or even higher than hundred voltages down to less than 5 V_{rms} for focal length from 6cm to infinity. The structure of GD-LC lens utilized a resistant

layer connected by tree electrodes as the control electrode. The first one benefit of this structure is that the applied electric field can be conserved inside the LC cell to be effectively employed the without leaking out. The second one is that the resistance layer controlled by these tree electrodes can initially produce gradient voltage distribution for yielding lens profile. Furthermore, the structure also can be controlled by operating voltage and frequency to achieve the concept of multi-control. In our experiment, the focusing profiles of each focal length can be optimized by this dual-control which has benefited the image quality in our auto-focusing (AF) experiments. The most important breakthrough was that the focusing time has been improved from the typical larger than 10 sec or over 1 min down to less than 1sec (~600ms) for focusing from infinity to 6cm closed object, as Figure 7-4 illustrates.



***6cm macro shoot with < 5Vrms!!
& AF performed within 600ms!!***

Figure 7-4 The dramatic improvement in driving voltage and focusing time with GD-LC lens combined with the volt. & freq. dual-control and OD method.

To compare with results of the world's leading groups, as shown in Table 7, not only the driving voltage was reduced to a reasonable range that the normal IC could drive but also the focusing time was improved to perform AF within 600ms. We also made a comparison with

other solutions for AF mentioned in section 1.4.1 after the improvement of our group. As mentioned, the issues of driving and focusing time have almost been solved, although the image quality still cannot compete with conventional lens-head.

Table 7 The comparisons of single tunable lenses.

	Liquid Lens (Philips 2004)	LC Lens (Sato 2009)	LC Lens (S.T.Wu 2006)	LC Lens (Other 2010)	sGD-LC Lens (Our group)
LC cell	--	MLC6080 ($\Delta n=0.25$) d=60um	BL-038 ($\Delta n=0.27$) d=25um	MLC-2070 ($\Delta n=0.26$) d=25um	Merck E7($\Delta n=0.21$) d= 60um
Driving Volt.	120Volt. (2cm)	90Vrms (14cm)	140Vrms (96cm)	90Vrms (10cm)	<5Vrms (6cm)
Focusing time	--	~30sec In our test		261ms	600ms
MTF	70%@25lp/deg	--	--	--	60%@20lp/deg 30%@40lp/deg

Table 8 The comparison of the AF solutions after the improvements of our group for LC lens.

	Size	Integration	Driving	Speed	Image Quality
Voice Coil Motor (VCM)	✗	✗	△	○	○
Extend Depth of Focus (EDoF)	○	○	△	△	✗
Liquid Crystal Lens (LC Lens)	○	○	○	○	△

○ :Better △ :Adequate ✗ :Worse

7.2 Future work

7.2.1 Optical design for LC lens

In current status, we significantly improve the issues of LC lenses, especially the slow focusing time and high driving voltage. In the optical quality part, however, although the

concept of multi-control can be used to optimize the focusing profiles of each focal length, the spot size still cannot be competed with that of conventional lens-heads, as well as its aberration values also cannot be corrected by this single-lens system. For camera industry, diffraction-limit performance is usually required even for the use in mobile phones. To improve this issue, the optical design of conventional lens for LC lens can be take into consideration. In the first step, the focusing performance of LC lens should be optimized, and then utilize solid lens to correct the image quality, image aberrations, and enhance MTF. The role of the solid lens is to obtain a balance solution for focusing at infinity and close objects. Finally, the simulation tools for lens design, such as CodeV and Zemax, and LC cells, such as 2Dimos and ExpertLCD, should be linked to simulate the imaging result of LC lens and to analysis items such as aberrations, MTF, imaging result, and tolerance. Optimization is also importance for the lens modifying. The relation of the link is shown in Figure 7-5.

Simulation tool linked for LC lens design

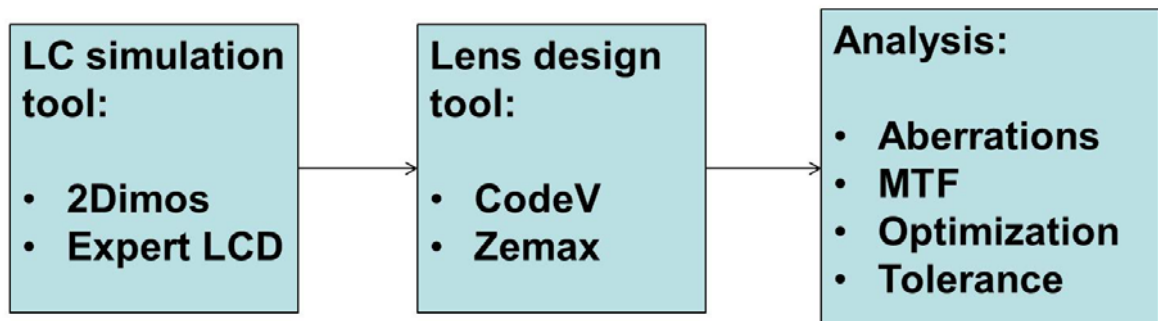


Figure 7-5 The relation of lens design tool for LC lens design

7.2.2 Polarizer free LC lens

In the application of lens with LCs, polarized light is necessary to distinct the ordinary-rays and extraordinary-rays. However, this property results in a half of incoming light losing due to the usage of polarizer. To make the application of LC lens more feasible, polarizer free LC lens is required. The general method for polarizer free LC lens is to use two crossed LC lenses with perpendicular rubbing direction. Each of the lens is used to deal with one polarization. However, this method would increase cost due to the double piece of LC layers for one lens.

Therefore, our group would use DIP to compute the imaging result without employing polarizer. In such a LC lens without polarizer, it can be used for the hyper distance shooting without losing gathering light. For AF usage, the lens system firstly takes an original image before AF which includes information from ordinary-rays and extraordinary-rays, and takes another one after AF ready. The difference of these two images is that the extraordinary-rays in the second image were focused. By DIP, the information coming from ordinary-rays can be eliminated, and according to the original luminance to restore the AF image in the second image with proper intensity, as shown in Figure 7-6.

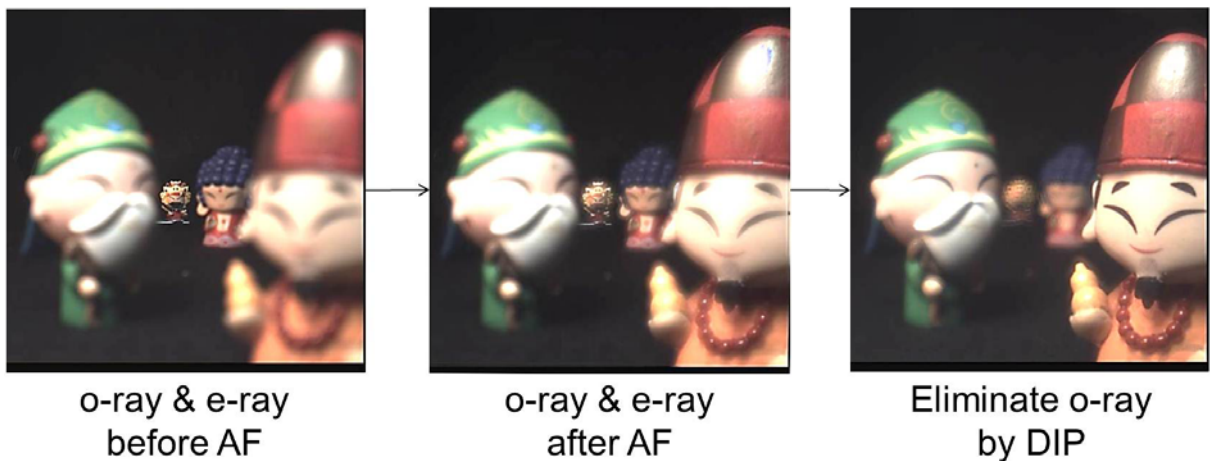


Figure 7-6 The concept of DIP for polarizer free LC lens.

7.2.3 Optical Zoom

As discussed in section 4.4, GD-LC lens can be easily performed in convex and concave mode. This feature is benefit for the application in LC optical zoom lens because zoom lens usually requires a convex and a concave lens group as the variator and compensator. Therefore, we add another LC lens in front of the LC AF system, as shown in Figure 7-7. The structure consist of two LC lenses To achieve the concept of zoom lens, Equation (7-1) and Equation (7-2) can be used to obtain the optical power of the zoom system and fix the imaging plane on position of image sensor.

$$K = K_1 + K_2 + K_3 - D_{12}(K_1K_2 + K_2K_3) - D_{23}(K_1K_3 + K_2K_3) + D_{12}D_{23}K_1K_2K_3$$

$$\Rightarrow K = AK_1 + BK_2 + CK_1K_2 + D \quad (7-1)$$

$$BFL = \frac{(1 - D_{12}K_1)}{(K_1 + K_2 - D_{12}K_1K_2)} \quad (7-2)$$

K_1 and K_2 are the lens power of two LC lens, and other parameters are the spacing and fix optical power. As we utilize K_1 and K_2 as the variator and compensator respectively. The lens power of the system was simulated, as Figure 7-8 shows. In the simulation result, although lens power of the system, K , can be varied, but the lens power of LC lenses were limited within $\pm 0.03(\text{mm}^{-1})$. Therefore, the zoom ratio, as shown in Equation (7-3)

$$\text{Zoom Ratio} \equiv \frac{EFL_{Tele}}{EFL_{Wide}} = \frac{K_{Wide}}{K_{Tele}} \quad (7-3)$$

is only around 1.5X. The next step is to demonstrate the feasibility of the LC zoom lens concept and to improve the zoom ratio.

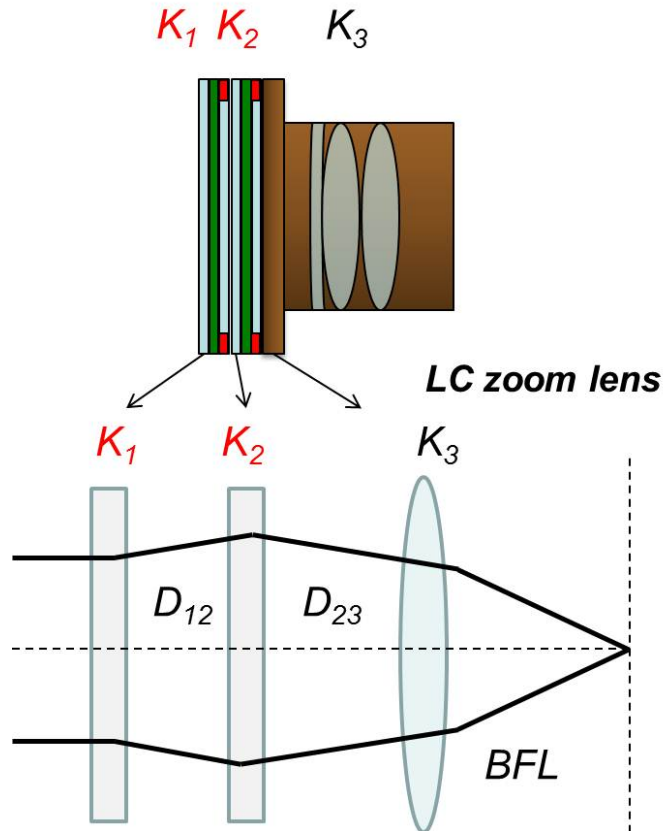


Figure 7-7 The schematic of LC zoom lens

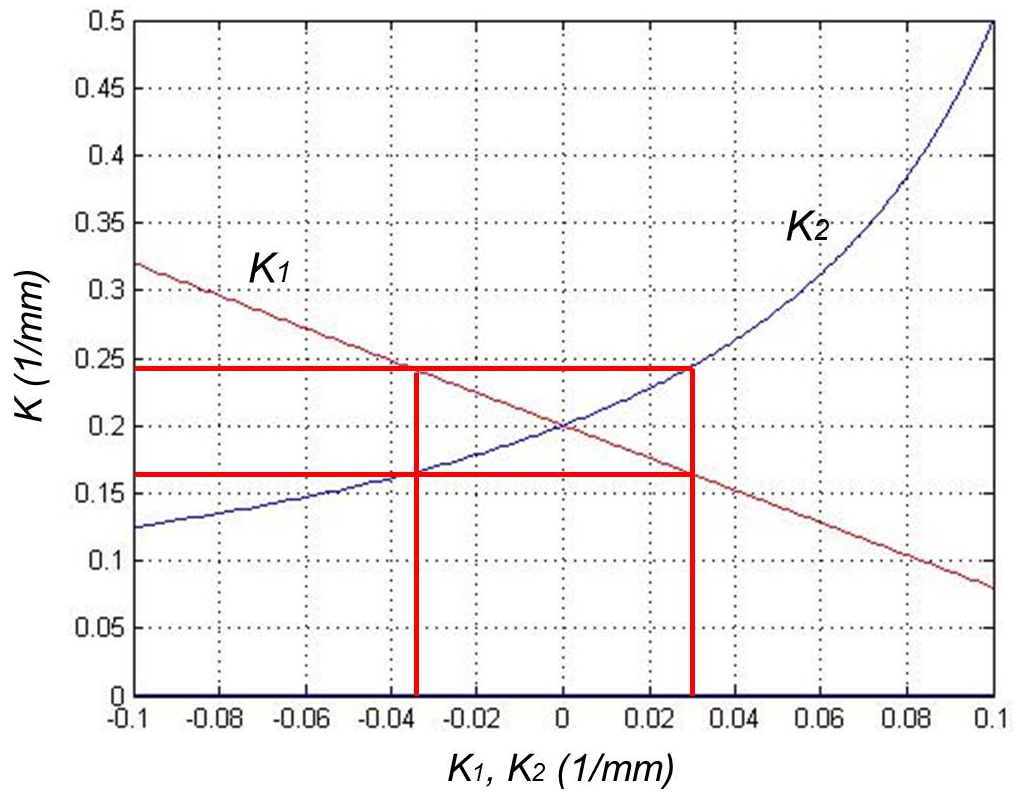
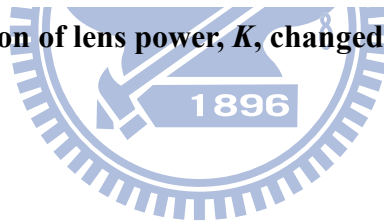


Figure 7-8 The variation of lens power, K , changed by LC lens power, K_1 and K_2



Reference

- [1] B. Y. Song, *et al.*, "Auto-focusing actuator and camera module including flexible diaphragm for mobile phone camera and wireless capsule endoscope," *Microsystem Technologies-Micro-and Nanosystems-Information Storage and Processing Systems*, vol. 16, pp. 149-159, 2010.
- [2] P. C. P. Chao, *et al.*, "Robust dual-stage and repetitive control designs for an optical pickup with parallel cantilever beams powered by piezo-actuation," *Microsystem Technologies-Micro-and Nanosystems-Information Storage and Processing Systems*, vol. 16, pp. 317-331, 2010.
- [3] K. Kyung-Ho, *et al.*, "A mobile auto-focus actuator based on a rotary VCM with the zero holding current," *Optics Express*, pp. 5891-6, 2009.
- [4] J. S. Choi, *et al.*, "Small form factor actuator design for camera phone lens systems," *Microsystem Technologies-Micro-and Nanosystems-Information Storage and Processing Systems*, vol. 15, pp. 1489-1497, 2009.
- [5] L. Chien-Sheng and L. Psang Dain, "Miniaturized auto-focusing VCM actuator with zero holding current," *Optics Express*, pp. 9754-63, 2009.
- [6] E. Simon, *et al.*, "Liquid lens enabling real-time focus and tilt compensation for optical image stabilization in camera modules," *Micro-Optics 2010*, vol. 7716, 2010.
- [7] N. Olivier, *et al.*, "Liquid lens approaches for simultaneous standard and extended depth of field imaging," *2010 Conference on Lasers and Electro-Optics (CLEO)*, p. 2 pp., 2010.
- [8] H. Oku and M. Ishikawa, "High-speed liquid lens with 2-ms response and 80.3-nm root-mean-square wavefront error," *Moems and Miniaturized Systems Ix*, vol. 7594, 2010.
- [9] H. Oku and M. Ishikawa, "High-Speed Liquid Lens for Computer Vision," *2010 Ieee International Conference on Robotics and Automation (Icra)*, pp. 2643-2648, 2010.
- [10] D. W. Lee and Y. H. Cho, "A 4 bit digital liquid lens for variable focal length," *Journal of Micromechanics and Microengineering*, vol. 20, 2010.
- [11] K. Jingran, *et al.*, "A tunable liquid lens with extended depth of focus," *2010 International Conference on Optical MEMS & Nanophotonics*, pp. 89-90, 2010.
- [12] A. Jae Yong, *et al.*, "Eye-shaped coplanar variable liquid lens using spherical polymer encapsulation," *2010 International Conference on Optical MEMS & Nanophotonics*, pp. 17-18, 2010.
- [13] Y. Hsiharn, *et al.*, "Low Voltage Piezoelectricity Actuating Variable Focus Plano-convex Liquid Lens Module Fabrication," *2010 Symposium on Design, Test, Integration and Packaging of MEMS/MOEMS (DTIP 2010)*, p. 5 pp., 2010.

- [14] H. L. Guo, *et al.*, "Optical Manipulation of Microparticles in an SU-8/PDMS Hybrid Microfluidic Chip Incorporating a Monolithically Integrated On-Chip Lens Set," *Ieee Journal of Selected Topics in Quantum Electronics*, vol. 16, pp. 919-926, 2010.
- [15] L. Tae-Rin, *et al.*, "Numerical Simulation of a Nanoparticle Focusing Lens in a Microfluidic Channel by Using Immersed Finite Element Method," *Journal of Nanoscience and Nanotechnology*, pp. 7407-11, 2009.
- [16] S. K. Y. Tang, *et al.*, "Dynamically reconfigurable liquid-core liquid-cladding lens in a microfluidic channel," *Lab on a Chip*, vol. 8, pp. 395-401, 2008.
- [17] T. Kamei and T. Wada, "Contact-lens type of micromachined hydrogenated amorphous Si fluorescence detector coupled with microfluidic electrophoresis devices," *Applied Physics Letters*, vol. 89, 2006.
- [18] A. L. Birkbeck, *et al.*, "Laser-tweezer-controlled solid immersion lens for high-resolution imaging in microfluidic and biological samples," *Proceedings of the SPIE - The International Society for Optical Engineering*, vol. 5275, pp. 76-84, 2004.
- [19] H. W. Ren and S. T. Wu, "Variable-focus liquid lens," *Optics Express*, vol. 15, pp. 5931-5936, 2007.
- [20] H. W. Ren, *et al.*, "Tunable-focus liquid lens controlled using a servo motor," *Optics Express*, vol. 14, pp. 8031-8036, 2006.
- [21] H. Ren and S. T. Wu, "Variable-focus liquid lens by changing aperture," *Applied Physics Letters*, vol. 86, 2005.
- [22] B. Berge and J. Peseux, "Variable focal lens controlled by an external voltage: An application of electrowetting," *European Physical Journal E*, vol. 3, pp. 159-163, 2000.
- [23] L. Dong, *et al.*, "Adaptive liquid microlenses activated by stimuli-responsive hydrogels," *Nature*, vol. 442, pp. 551-554, 2006.
- [24] C. C. Cheng and J. A. Yeh, "Dielectrically actuated liquid lens," *Optics Express*, vol. 15, pp. 7140-7145, 2007.
- [25] B. R. Boruah, "Zonal wavefront sensing using a liquid crystal spatial light modulator," *Practical Holography Xxiv: Materials and Applications*, vol. 7619, 2010.
- [26] M. Ares, *et al.*, "Active optics null test system based on a liquid crystal programmable spatial light modulator," *Applied Optics*, vol. 49, pp. 6201-6206, 2010.
- [27] Z. L. Cao, *et al.*, "Diffractive characteristics of the liquid crystal spatial light modulator," *Chinese Physics*, vol. 16, pp. 1665-1671, 2007.
- [28] S.-h. Yan, *et al.*, "Manufacturing system for gray-scale masks based on the spatial light modulator," *Chinese Journal of Lasers*, vol. A31, pp. 45-7, 2004.
- [29] H. T. Dai, *et al.*, "Characteristics of LCoS Phase-only spatial light modulator and its applications," *Optics Communications*, vol. 238, pp. 269-276, 2004.
- [30] H. T. Dai, *et al.*, "Characteristics of LCoS Phase-only spatial light modulator and its

- application," *Apoc 2003: Asia-Pacific Optical and Wireless Communications; Materials, Active Devices, and Optical Amplifiers, Pts 1 and 2*, vol. 5280, pp. 270-277, 2004.
- [31] L. N. Thibos, *et al.*, "Vision through a liquid-crystal spatial light modulator," *Proceedings of 2nd International Workshop on Adaptive Optics for Industry and Medicine|Proceedings of 2nd International Workshop on Adaptive Optics for Industry and Medicine*, pp. 57-62|xvii+398, 2000.
- [32] H. Toyoda, *et al.*, "Optical design of associative memory using a bistable spatial light modulator," *Progress in Connectionist-Based Information Systems, Vols 1 and 2*, pp. 745-748, 1998.
- [33] C. Chatwin, *et al.*, "UV microstereolithography system that uses spatial light modulator technology," *Applied Optics*, vol. 37, pp. 7514-7522, 1998.
- [34] V. A. Berenberg, *et al.*, "Correcting the aberrations of an objective in a wide spectral range by means of a liquid-crystal light-controlled spatial light modulator," *Journal of Optical Technology*, vol. 64, pp. 863-864, 1997.
- [35] T. Yamada and T. Kawashi, "Liquid crystal display devices," *Journal of the Institute of Electronics and Communication Engineers of Japan|Journal of the Institute of Electronics and Communication Engineers of Japan*, vol. 53, pp. 469-72, 1970.
- [36] Heilmieie.Gh, "LIQUID-CRYSTAL DISPLAY DEVICES," *Scientific American*, vol. 222, pp. 100-&, 1970.
- [37] S. Sato, "Liquid-crystal Lens-cells with Variable Focal Length," *Japanese Journal of Applied Physics*, vol. 18, pp. 1679-1684, 1979.
- [38] H. W. Ren and S. T. Wu, "Getting in Tune : Electronically controlled liquid crystal yields tunable-focal-length lenses," *SPIE's oemagazie*, pp. 24-27, 2004.
- [39] R. Hongwen, *et al.*, "Tunable-focus flat liquid crystal spherical lens," *Applied Physics Letters*, vol. 84, pp. 4789-91, 2004.
- [40] R. Hongwen, *et al.*, "Liquid crystal lens with large focal length tunability and low operating voltage," *Optics Express*, pp. 11328-35, 2007.
- [41] H. W. Ren and S. T. Wu, "Adaptive liquid crystal lens with large focal length tunability," *Optics Express*, vol. 14, pp. 11292-11298, 2006.
- [42] B. Wang, *et al.*, "Lens of electrically controllable focal length made by a glass lens and liquid-crystal layers," *Applied Optics*, vol. 43, pp. 3420-3425, 2004.
- [43] H. Nemati, *et al.*, "A simple holographic technique for fabricating a LC/polymer switchable Fresnel lens," *Europhysics Letters*, p. 64001 (4 pp.), 2009.
- [44] H. Nemati, *et al.*, "A simple holographic technic for fabricating a LC/polymer switchable Fresnel lens," *Epl*, vol. 87, 2009.
- [45] V. Y. Reshetnyak, *et al.*, "Theoretical modeling of heterogeneous LC systems: nano-suspensions and polymer stabilized LC lens - art. no. 658709," *Liquid Crystals*

- and Applications in Optics*, vol. 6587, pp. 58709-58709, 2007.
- [46] C. R. Lee, *et al.*, "Electrically switchable Fresnel lens based on a liquid crystal film with a polymer relief pattern," *Japanese Journal of Applied Physics Part 1-Regular Papers Brief Communications & Review Papers*, vol. 46, pp. 4144-4147, 2007.
- [47] H. W. Ren, *et al.*, "Liquid-crystal microlens arrays using patterned polymer networks," *Optics Letters*, vol. 29, pp. 1608-1610, 2004.
- [48] Y. H. Fan, *et al.*, "Electrically controlled lens and prism using nanoscale polymer-dispersed and polymer-networked liquid crystals," *Liquid Crystal Materials, Devices, and Applications X and Projection Displays X*, vol. 5289, pp. 63-73, 2004.
- [49] G. M. Davis, "Liquid crystal polymer thin film anisotropic optical components," *Sharp Technical Journal*, pp. 22-25, 1995.
- [50] M. Yuki, "LOW-TEMPERATURE POLY SI TFT AND LIQUID-CRYSTAL POLYMER COMPOSITE FOR BRIGHTER VIDEO PROJECTION SYSTEM," *Ieice Transactions on Electronics*, vol. E76C, pp. 86-89, 1993.
- [51] H. Chi-Yen, *et al.*, "Dual-operation-mode liquid crystal lens," *Optics Express*, pp. 20860-5, 2009.
- [52] Y. H. Lin, *et al.*, "Tunable-focus cylindrical liquid crystal lenses," *Japanese Journal of Applied Physics Part 1-Regular Papers Short Notes & Review Papers*, vol. 44, pp. 243-244, 2005.
- [53] <http://www.tdk.com.cn/product10.html>.
- [54] S. Kuthirummal, *et al.*, "Flexible Depth of Field Photography," *Ieee Transactions on Pattern Analysis and Machine Intelligence*, vol. 33, pp. 58-71, 2011.
- [55] P. Chao, *et al.*, "Study on depth of field of wavefront coding imaging system," *Proceedings of the SPIE - The International Society for Optical Engineering*, p. 70732C (8 pp.), 2008.
- [56] Q. G. Yang, *et al.*, "Optimized phase pupil masks for extended depths of field," *Optics Communications*, vol. 272, pp. 56-66, 2007.
- [57] Y. Frauel and A. Castro, "Increasing the depth of field of imaging systems with numerically optimized phase masks - art. no. 673611," *Unmanned/Unattended Sensors and Sensor Networks Iv*, vol. 6736, pp. 73611-73611, 2007.
- [58] E. Ben-Eliezer, *et al.*, "Experimental realization of an imaging system with an extended depth of field," *Applied Optics*, vol. 44, pp. 2792-2798, 2005.
- [59] R. Porras, *et al.*, "Wavefront coding technology in the optical design of astronomical instruments," *Riao/Optilas 2004: 5th Iberoamerican Meeting on Optics and 8th Latin American Meeting on Optics, Lasers, and Their Applications, Pts 1-3*, vol. 5622, pp. 796-800, 2004.
- [60] R. Raskar, "Computational Photography: Epsilon to Coded Photography," in *Emerging Trends in Visual Computing*. vol. 5416, F. Nielsen, Ed., ed Berlin: Springer-Verlag

- Berlin, 2009, pp. 238-253.
- [61] M. A. Newhouse and D. B. Keck, "EFFECT OF AXIAL PERTURBATION OF GRIN LENS PERFORMANCE," *Applied Optics*, vol. 21, pp. 990-992, 1982.
- [62] A. F. Naumov, *et al.*, "Control optimization of spherical modal liquid crystal lenses," *Optics Express*, vol. 4, pp. 344-352, 1999.
- [63] M. Loktev, *et al.*, "Liquid crystal wavefront corrector with modal response based on spreading of the electric field in a dielectric material," *Optics Express*, vol. 15, pp. 2770-2778, 2007.
- [64] I. Guralnik, *et al.*, "Modal control principle: a new way to the design of liquid crystal adaptive optics devices," *Wave propagation in the atmosphere and adaptive optics. Selected research papers|Wave propagation in the atmosphere and adaptive optics. Selected research papers*, pp. 171-81|v+216, 2000.
- [65] P. J. W. Hands, *et al.*, "Adaptive modally addressed liquid crystal lenses," *Liquid Crystals VIII*, vol. 5518, pp. 136-143, 2004.
- [66] A. F. Naumov, *et al.*, "Liquid-crystal adaptive lenses with modal control," *Optics Letters*, vol. 23, pp. 992-994, 1998.
- [67] O. D. Lavrentovich, "Fluorescence confocal polarizing microscopy: Three-dimensional imaging of the director," *Pramana-Journal of Physics*, vol. 61, pp. 373-384, 2003.
- [68] S. Camou, *et al.*, "PDMS 2D optical lens integrated with microfluidic channels: principle and characterization," *Lab on a Chip*, vol. 3, pp. 40-45, 2003.
- [69] I. Dierking, "Fluorescence confocal polarizing microscopy: Imaging liquid crystal director fields in three dimensions," *Chemphyschem*, vol. 2, pp. 663-+, 2001.
- [70] <http://www.trioptics.com/imagemaster/description.php>.
- [71] S. Kuiper and B. H. W. Hendriks, "Variable-focus liquid lens for miniature cameras," *Applied Physics Letters*, vol. 85, pp. 1128-1130, 2004.

LIN-YAO LIAO

• National Chiao Tung University • Rm.502 CPT Building, 1001 Ta Hsueh Road, Hsinchu, Taiwan 300,

• Tel: +886-3-5712121 ext 59210 • Fax: +886-3-5737681

• E-mail: finalhome.eo95g@nctu.edu.tw

PERSONAL PROFILE

- The 1st in Ph.D. qualify exam of optics in Institute of Electro-Optical Engineering, National Chiao Tung University (NCTU).
- Led national scale project relative to Liquid Crystal Lens design for 3 years and acquired breakthrough in performance.
- Experienced in lens design for consumer mobile devices as well as programming of optimized designs in doublet and triplet lens for initial lens designs.
- Experienced in design of Liquid Crystal Displays with dynamic backlights, and led projects for the purpose of contrast ratio enhancement and motion blur suppression during period of master study.
- Won the Excellent Project Award for project, High Dynamic Rang LCDs, during intern in AU Optronics Corp.

EDUCATION

Ph.D., Institute of Electro-Optical Engineering, National Chiao Tung University, Hsinchu, Taiwan **2007/9 ~ present**

* *Research Topic* – “Liquid Crystal Lens Design”

* *Advisors* – Prof. Yi-Pai Huang

M.S., Institute of Electro-Optical Engineering, National Chiao Tung University, Hsinchu, Taiwan **2006/9 ~ 2007/7**

* *Research Topic* – “High Image Quality with Low Power Consumption LCDs”

* *Advisors* – Prof. Yi-Pai Huang

B.S., Electric Engineering, National Sun Yat-sen University, Kaohsiung, Taiwan **2002/9 ~ 2006/7**

Courses taken included:

- Geometrical Optics
- Physical Optics
- Fourier Optics
- Display Optics
- Advanced Optical Design
- Classical Electrodynamics
- Digital Signal Process
- Digital Image Process
- Statistical Optics and Image Formation
- Thin Film Optics
- Advanced Geometrical Optics
- Quantum Mechanics

EXPERIENCE

Liquid Crystal Lens Design Project with National Science Council 2008/9 ~ present

* *The study of a novel heterogeneous integrated compact camera module*

Project number: NSC 98-2220-E-009-019

- Joined the national scale project and cooperate with several groups in other fields, and led a group to develop high efficient Liquid Crystal Lens module for mobile devices.
- Realized fast-focusing Liquid Crystal Lens exhibiting 0.2sec focusing time, only driven by 3~5 Vrms. Compare to that of the other world leading groups, which require around 30~60sec focusing time and usually driven by 50~100Vrms.

Technology transfers of patents with companies for the Liquid Crystal Lens developments were done.

Internship in Large-size Panel EE Dep., AU Optronics Corporation, 2007/7 ~ 2007/9
Hsinchu , Taiwan

* *Project – “High Dynamic Range LCDs”*

- Won the Excellent Project Award.

High Dynamic Range LC Display Project with AU Optronics 2006/7 ~ 2007/6
Corporation, Hsinchu, Taiwan

- Led project, High Dynamic Range LCDs, to design a display with the benefits of high image quality, and low power consumption.
- Published 3 journal papers in *Journal of Display Technology* and *Journal of Society of Information Display*, 4 conference papers in *Society of Information Display* 2007 ~ 2010 (SID 07 ~ 10), and 3 patent packages in Taiwan, United States, and People’s Republic of China.

ACADAMIC HONORS AND AWARDS

Ranked 1st in Ph.D. qualify exam of optics 2006/7

Institute of Electro-Optical Engineering Scholarship 2006/9 ~ 2007/6

Awarded to 5 out of 150 PhD students in Institute of Electro-Optical Engineering, NCTU

Pre-Ph.D. Scholarship 2006/9 ~ 2009/6

Awarded to Ph.D. students for being Teaching Assistant in NCTU

AU Optronics Corporation Excellent Project Award 2007 2007/8

The best project during the internship in AU Optronics Corp.

OPT '07 (Optics & Photonics Taiwan 2007) Student Paper Award 2007/5

Paper Subject – “High Dynamic Range LCDs”

PUBLICATIONS

Journal Paper

1. Yi-Pai Huang, Lin-Yao Liao, and Chih-Wei Chen, ” 2D/3D Switchable Autostereoscopic Display with Multi-electrically Driven Liquid Crystal (MeD-LC) Lenses,” *accepted by J. Soc. Inf. Display* (2010)
2. Lin-Yao Liao, Yu-Min Lin, Yi-Pai Haung, and Han-Pin David Shieh, “Gradient Driven Liquid

Crystal Lens Exhibiting Ultra-fast Focusing by Low Operating Voltages,” submitted to *Optics Express*.

3. Lin-Yao Liao, Po-Yuan, Shieh, and Yi-Pai Huang, “3-Dimensional Imaging and Analysis for Liquid Crystal Lenses by Fluorescence Confocal Polarizing Microscopy,” submitted to *Optics Express*.
4. Lin-Yao Liao, Po-Yuan, Shieh, and Yi-Pai Huang, “Over-drive Method for Fast Focusing Liquid Crystal Lens Applications,” is under writing.
5. Lin-Yao Liao, and Yi-Pai Huang, ” Blur-Mask Approach for Real-Time Calculation of Light Spreading Function (LSF) on Spatial Modulated High Dynamic Range LCDs,” *J. of Display Technology*, vol. 6, issue 4, pp. 121-127, 2010.
6. Lin-Yao Liao, Chih-Wei Chen, and Yi-Pai Huang, “Local Blinking HDR LCD Systems for Fast MPRT with High Brightness LCDs.” *J. of Display Technology*, vol. 6, issue 5, pp. 178-183, 2010.
7. Fang-Cheng Lin, Yi-Pai Huang, Lin-Yao Liao, Cheng-Yumr Liao, and Han-Ping D. Shieh, "Dynamic Backlight Gamma on High Dynamic Range LCD TVs," *J. of Display Technology*, vol. 4, no. 2, pp.139-146, 2008.

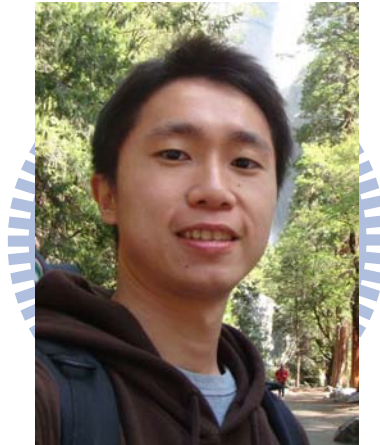
Conference Paper

[International Conference]

1. Lin-Yao Liao, Po-Yuan Shieh, and Yi-Pai Huang, “Marginal Electrodes with Over-drive Method for Fast Response Liquid Crystal Lens Applications,” 2010 SID, P-134.
2. Lin-Yao Liao, Chih-Wei Chen, and Yi-Pai Huang, ” Fast MPRT with High Brightness LCD by 120Hz Local Blinking HDR Systems,” 2009 SID, pp. 862-865
3. **(Invited paper)** Yi-Pai Huang, Han-Ping D. Shieh, Kuo-Gzen Wang, Lin-Yao Liao, Fang-Cheng Lin, Yu-Kuo Cheng, “Backlight Adjustment, Image Compensation, and Color Model Mapping for High Dynamic Range(HDR) Spatial Modulated Display System”, 2009 IDW .
4. Lin-Yao Liao, and Yi-Pai Huang, ”A Real-Time Image Compensation for High Dynamic Range LCDs,” 2008 SID, pp. 764-767.
5. Lin-Yao Liao, Fang-Cheng Lin, Yi-Pai Huang, and Han-Ping D. Shieh, "A Real-Time Liquid Crystal Signal Compensation Method for High Dynamic Range LCD," 2007 IDW, pp. 1433-1434.
6. Fang-Cheng Lin, Cheng-Yu Liao, Lin-Yao Liao, Yi-Pai Huang, Han-Ping D. Shieh, Po-Jen Tsai, Te-Mei Wang, Yao-Jen Hsieh, “Inverse of Mapping Function (IMF) Method for Image Quality Enhancement of High Dynamic Range LCD TVs”, 2007 SID, pp 1343~1346.
7. **(Invited paper)** Yi-Pai Huang, Fang-Cheng Lin, Cheng-Yumr Liao, Ya-Ting Hsu, Wei-Kai Huang, Cheng-Han Tsao, Lin-Yao Liao, Chun-Ho Chen, Han-Ping D. Shieh, “Advanced Technologies for High Quality LC Display”, 2007 AOE, Shanghai, China.

[Domestic Conference]

8. Yu-Min Lin, **Lin-Yao Liao**, Yi-Pai Haung, Han-Pin David Shieh, and Jih-Fon Huang
“Tunable-Focus Cylindrical Liquid Crystal GRIN Lens Exhibiting Fast Response and Low
Operating Voltage,” Taiwan Display Conference 2010, D011.
9. Po-Yuan Hsieh, **Lin-Yao Liao**, and Yi-Pai Huang, “Over-Drive Method for Fast Response
Liquid Crystal Lens Applications,” Taiwan Display Conference 2010, D024.
10. **[Best Students Paper Award]** **Lin-Yao Liao**, Fang-Cheng Lin, Yi-Pai Huang, Han-Ping
D.Shieh, Szu-Che Yeh, and Julienne Lyu, “A Liquid Crystal Signal Compensation Method with
Lower Computational Complexity for Dynamic Range LCD,” OPT 2007, GO-006 .
11. **(Invited paper)** Yi-Pai Huang, Fang-Cheng Lin, Cheng-Yumr Liao, Ya-Ting Hsu, Wei-Kai
Huang, Cheng-Han Tsao, **Lin-Yao Liao**, Chun-Ho Chen, Han-Ping D. Shieh, “Advanced
Technologies for High Quality LC Display”, accepted by AOE’07, Shanghai, China.
12. Fang-Cheng Lin, **Lin-Yao Liao**, Cheng-Yumr Liao, Yi-Pai Huang, and Han-Ping D. Shieh,
“Backlight Determination of High Dynamic Range LCDs,” OPT 2007.



Lin-Yao Liao